The University of Dublin, Trinity College

On the Performance and Design Tradeoffs of Low Altitude UAV Small Cells in Urban Environments

Author:
Boris Galkin

Supervisors:
Prof. Luiz A. DaSilva
Dr. Jacek Kibiłda

This thesis is submitted for the degree of
Doctor of Philosophy

11th April 2019

Declaration

I declare that this thesis has not been submitted as an exercise for a degree at this or any other university and is entirely my own work.

I agree to deposit this thesis in the University's open access institutional repository or allow the Library to do so on my behalf, subject to Irish Copyright Legislation and Trinity College Library conditions of use and acknowledgement.

Signed:

Boris Galkin,
11th April 2019

Summary

Cellular data demand continues to increase from year to year, and to manage this rising demand network operators adopt new technologies and designs for their cellular networks. Among these, network densification is seen as a viable method of increasing network capacity in dense urban environments. This densification will consist of network operators deploying miniaturised base stations (referred to as small cells or picocells) at areas of particularly high user traffic (which we refer to as hotspots). These small cells have very small coverage areas compared to conventional base stations, and would supplement the existing base station networks in providing cellular service to users.

The recent proliferation of Unmanned Aerial Vehicles (UAVs) in hobbyist and commercial fields has attracted the attention of network operators, and UAVs are beginning to see integration into cellular networks for covering low-density areas, as well as for emergency applications. In this thesis we explore the possibility of using small, quadcopter-style UAVs which carry small cells to deliver wireless service to users in urban environments, for dealing with demand hotspots. Because of their airborne nature and their ability to intelligently move in three-dimensional space, UAV small cells will achieve very different coverage and capacity performance, when compared to static terrestrial infrastructure. A review of the existing state-of-the-art from the wireless community on UAV operation shows that certain important aspects of UAV networks have not been adequately explored. These aspects include: the impact of inter-cell UAV interference, the impact of the wireless backhaul infrastructure design, and the impact of UAV recharging techniques. While the wireless community has adopted stochastic geometry for analysing the performance of terrestrial networks, there is currently a lack of UAV network models which capture all of the unique features of UAV networks.

The purpose of this work is to analyse the performance of UAV small cell networks when they are used to serve users in dense urban environments, and to explore how the various design parameters of the UAV network impact this performance. We consider both the user access as well as the wireless backhaul links in our analysis. Our contributions are as follows:

We provide a stochastic geometry model for UAV small cells in interference-limited

urban environments, when positioned above user hotspots. This model captures the impact of several UAV network and environmental parameters, such as the height of the UAVs above ground, their density per unit area, their antenna directionality, the geometry of the buildings in the area, as well as the size of user hotspots.

Using our model we demonstrate that there exists an optimum height that the UAVs should operate at, to maximise the achieveable performance. This height mitigates the impact of both signal blockage due to buildings, as well as interference from other UAVs. The value of the optimum height is shown to be a function of the other network parameters.

We also demonstrate that, for sufficiently large densities of UAVs in the network, the UAVs should be spaced out in a regular grid to mitigate interference and improve network performance, rather than be positioned above the hotspots to minimise distance to the users.

For the wireless backhaul link we consider a dedicated network of Ground Stations (GSs) which are deployed exclusively for UAV backhaul connectivity. We compare the backhaul performance of the dedicated GS network against the performance when UAVs backhaul through the existing terrestrial base station network. We demonstrate how the GS network is necessary for providing wireless backhaul connectivity unless the UAVs are equipped with high-performance antennas.

We consider sub-6GHz and millimeter-wave technologies and demonstrate that both have their strengths and weaknesses when used for the wireless backhaul. The sub-6GHz technology can allow for simpler GS deployment, as existing base station sites may be reused. The millimeter-wave backhaul, on the other hand, provides for superior performance due to larger bandwidths and active beam steering, which mitigates interference.

We model the battery consumption behaviour of the UAVs and demonstrate several methods that can be used to recharge UAV batteries while ensuring that the UAV network continues to provide service to user hotspots. We demonstrate how these methods impact the network performance in different ways, whether it is capital expenditure, downtime, or restrictions on the range of acceptable UAV heights. We also review several upcoming developments in the field of battery technology, and demonstrate how UAV small cells may be able to operate for longer when the technologies enter use.

We conclude with a discussion of the legal restrictions on UAV flight, and how they are being gradually relaxed to accommodate commercial adoption of UAVs. We then discuss possible research directions for our future work.

Acknowledgements

All research work, no matter the field, can be described as dwarves standing on the shoulders of giants. Behind each of us there is a crowd of people who support our work and allow us to succeed. In this section I would like to acknowledge all of the people who have made my work possible. This thesis is dedicated to the people (the giants) below.

I want to begin by first acknowledging my family and their role in my work. In many ways, my research interest in flying devices is the continuation of a family tradition. My late grandfather was a test pilot during the post-war years in the USSR. His son, my father, would go on to work as an electronics engineer at TsAGI, the leading aviation research institute of the USSR. My mother, in turn, was involved in the Soviet space program, designing gas spectrometer equipment for the probes sent to Venus as part of the Venera program. With a family history such as this it is not surprising that I would have a lifelong interest in aviation, and that it would inform my own research interests in the area of telecommunications. Even my surname is flight-related, as it refers to the jackdaw bird in Russian. Although my grandfather would not live to see the results of my research work, both of my parents have supported me immensely over the course of this PhD, and I would like to thank them both for it.

I will give special thanks to my secondary school engineering teacher, Philip Devereux. His classes are one of the big reasons I took engineering in university to begin with.

I would like to thank all of the people of CONNECT for their support and motivation. Both of my supervisors, Prof. Luiz DaSilva and Dr. Jacek Kibiłda, have been invaluable over the course of this thesis, I could not have achieved the work without them. I would also like to acknowledge the postdocs Jonathan, Nick, Neill, Danny, Francisco and Pedro for their advice over the course of this thesis. I thank the other students in our department for their support and for creating a fantastic office culture in our building, in no particular order: Jernej, Alan, Andrea, Connor, Harleen, Nima, Erika, Fadhil, Parna, Merim, Joao, the other Joao, and Marcello. I want to extend a special thank you to Andrew and Stefan for their work in promoting my research to the public.

Outside of CONNECT I want to thank my friends John, Cian, Declan, Eoghan, Patrick, Craig, Tiernan, and Marina for all their support.

Contents

List of Figures

List of Tables

List of Acronyms

3GPP	3rd Generation Partnership Project
ATC	Air Traffic Control
BS	Base Station
BPP	Binomial Point Process
C&C	Command & Control
EASA	European Aviation Safety Agency
FAA	Federal Aviation Administration
FSO	Free-Space Optical
GPS	Global Positioning System
GS	Ground Station
IoT	Internet of Things
KPI	Key Performance Indicator
LOS	Line-of-Sight
LTE	Long Term Evolution
MCP	Matern Cluster Process
MC	Monte Carlo
MIMO	Multiple Input Multiple Output
MNO	Mobile Network Operator
NLOS	non-Line-of-Sight

OTT Over-The-Top

pdf Probability Density Function

PCP Poisson Cluster Process

PPP Poisson Point Process

PV photo-voltaic

QoS Quality of Service

RC Remote Control

SE Spectral Efficiency

SIR Signal-to-Interference Ratio

SINR Signal-to-Interference-and-Noise Ratio

SNR Signal-to-Noise Ratio

UAV Unmanned Aerial Vehicle

UE User Equipment

1 Introduction

In this introductory chapter we outline the motivation for our research and state the main contributions of our work. The chapter is structured as follows. We begin by discussing the growing need for network densification in next-generation cellular systems and justify the choice of Unmanned Aerial Vehicle (UAV) small cells as a viable alternative to fixed, terrestrial picocells. We then describe the envisioned architecture of the UAV small cell network, and outline a typical use case for such a network. We then describe the main contributions of our work, and list the publications associated with our research.

1.1 Motivation

In 2017 the number of unique mobile subscribers worldwide exceeded five billion, with a further nine hundred million expected to connect to cellular networks by 2025 [1]. As Internet of Things (IoT) devices become more used in industrial applications the number of IoT connections is expected to triple by 2025, from 7.5 billion to 25 billion. In addition to this, the total cellular data traffic exhibits a compound growth rate of 42% every year, and given this growth rate the cellular traffic in 2023 is forecasted to be almost eight times greater than the traffic experienced by networks in 2018 [2]. The continuing growth of data demand and the resulting increase in wireless traffic rates in modern cellular networks call for new technologies and designs for commercial telecommunication services. Among other innovations future cellular networks will rely much more heavily on a dense deployment of low-power, short-range access points to deliver adequate data rates to the consumer [3]. These devices are commonly referred to as small cells or picocells [1], to reflect their small size compared to conventional macrocell Base Stations (BSs). This cell densification will ultimately result in higher data rates due to higher spectrum efficiency. Picocell access points are typically deployed as part

[1]To avoid confusion, in this thesis we use the term "picocell" to refer to a small cell which is statically mounted in a terrestrial position, as opposed to flying overhead.

of a two-tier heterogeneous network and positioned in hotspots of user activity inside the coverage areas of existing macrocells [4]. The deployment process requires time, manpower and additional expenses on the part of the Mobile Network Operator (MNO), as deploying conventional picocells in a hotspot area typically involves trained personnel mounting and configuring the access points one by one. Obtaining access to the picocell sites and the authorisation to deploy the picocells at those sites can also be a major hurdle for deploying picocells, particularly outdoors.

An alternative to using fixed picocells mounted around a hotspot area is to use UAVs carrying radio equipment, acting as flying small cells [5]. In recent years, the popularity of UAVs has exploded as both hobbyist devices, and as valuable tools that can be used in a variety of commercial applications [6–9]. The number of UAVs in the consumer market is increasing exponentially, with global revenue steadily growing from year to year, as shown in Fig. 1.1. UAVs have become recognised by the wireless community as an attractive solution for providing basic connectivity to environments where fixed infrastructure is either too difficult to deploy, or where fixed infrastructure cannot be justified economically. As of the time of writing, UAV-mounted infrastructure is already beginning to see real-world adoption in cellular networks. In 2017 Puerto Rico was devastated by Hurricane Maria, with significant damage done to its cellular network. In response, telecommunications company AT&T deployed a prototype UAV around parts of the country to provide basic Long Term Evolution (LTE) service [10]. The UAV consisted of a small helicopter design carrying an LTE BS, hovering 60 m above ground, while tethered to a Ground Station (GS). Although the UAV deployment was very limited in scope the company reported that the UAV trials were a success [11]. Google's Project Loon balloons [12] were also used for providing basic connectivity, and the company reported that in excess of 200,000 people were being served with basic LTE functionality by their platforms [13]. In the United Kingdom MNO EE is deploying blimp and tethered multi-rotor UAVs in rural areas to provide basic coverage as well as for disaster recovery [14]: the tethered blimp is for long-term deployments and the multi-rotor is for deployments where coverage needs to be provided quickly. MNOs such as AT&T and EE have expressed interest in deploying small cells mounted on UAVs as alternatives to fixed picocells at public events such as sporting events or music festivals [15].

UAV small cells are an attractive alternative to fixed picocells because they can offer several benefits over conventional, terrestrial infrastructure:

1. Flexible Positioning. As network densification causes individual cells to become smaller in size the mismatch between the location of the cell and the location of

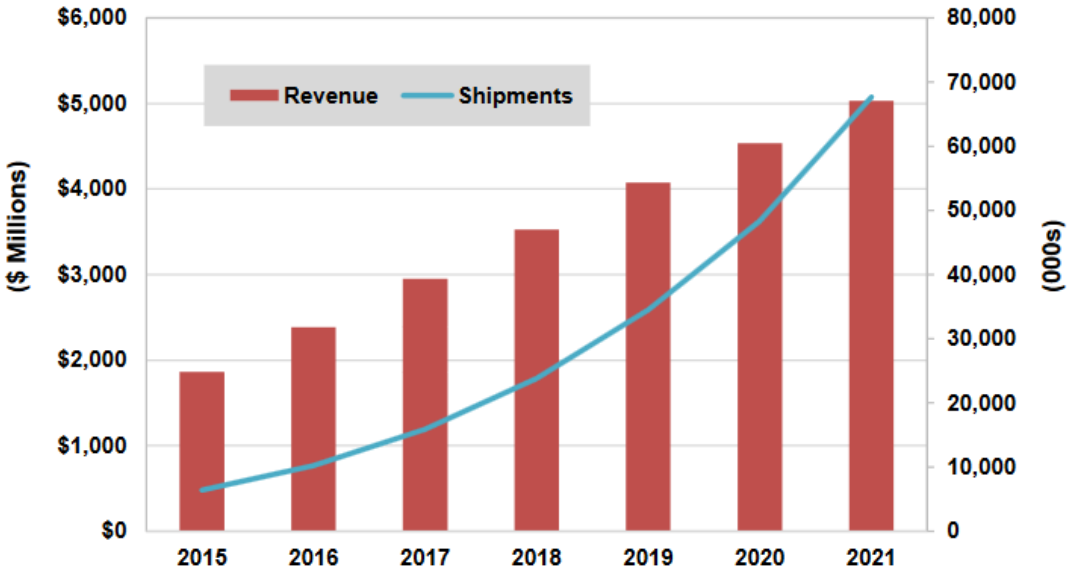

Figure 1.1: Forecast of global consumer UAV revenue and shipments. Source: [7]

the traffic demand will cause increased performance degradation [5]. UAVs are a viable solution to this issue: because the UAVs are rapidly deployed and fully mobile they may be positioned around actual User Equipment (UE) locations in real-time, unlike fixed picocells which are deployed around expected concentrations of UEs. Additionally, because of their aerial vantage point the UAVs are more likely to establish Line-of-Sight (LOS) on the UEs than the picocells[2].

2. Reduction of Service Overheads. The streamlined deployment process suggests that the UAVs are suitable for deployment in flash demand scenarios where temporary UE hotspots form. In contrast, a fixed picocell deployed to service a temporary hotspot would remain underutilised once the hotspot moved to a different location or disappeared [16]. A mobile UAV, on the other hand, can be reassigned to another hotspot, thus servicing multiple hotspots at different times rather than remaining underutilised.

3. Reduction of Cost. Unlike fixed picocells the UAVs do not require manpower to be mounted: these devices will instead hover over an area specified by a control unit. As this control can be largely automated we predict a reduction in cost for deployment compared to the fixed alternative.

[2]This aerial vantage point may also harm network performance under some UAV deployment conditions, see Chapter 3

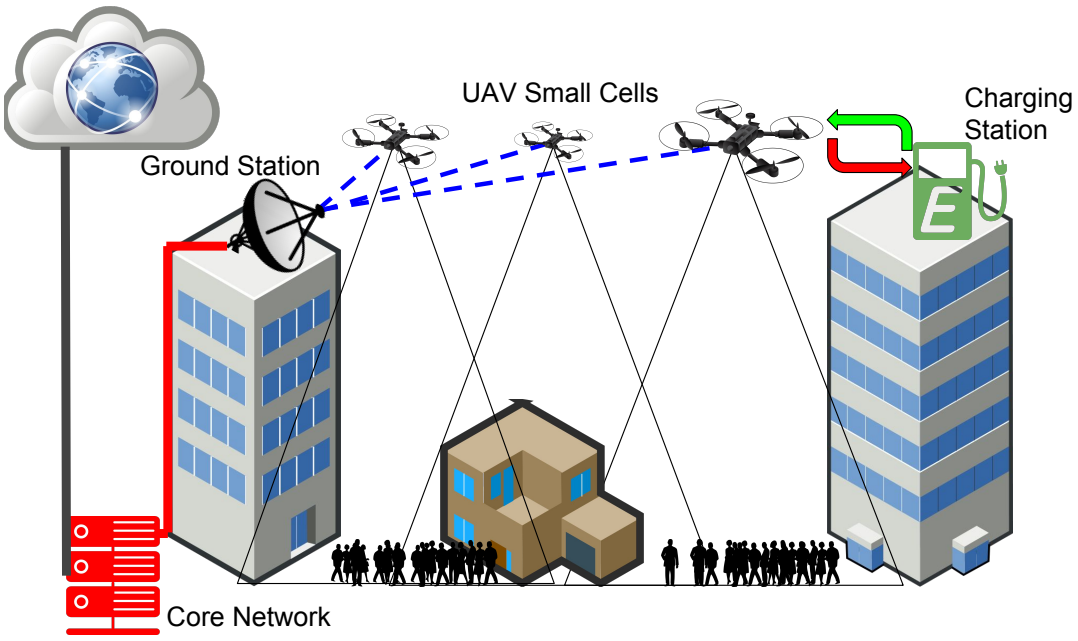

Figure 1.2: The envisioned architecture of the UAV small cell network in an urban area.

1.2 Envisioned Architecture

The UAV small cell network that we envision for our urban use case will consist of three separate components, as shown in Fig. 1.2: the UAV small cells themselves, the GSs that the UAVs use to wirelessly backhaul into the core network, and the charging stations which the UAVs use to recharge or replace their batteries.

1.2.1 The UAV Small Cells

A typical UAV in the network consists of a multi-rotor[3] flying platform carrying radio equipment such as antennas and signal processing electronics necessary to fulfill the functions of a small cell access point, in addition to equipment such as Global Positioning System (GPS) and infrared obstacle sensors which are required to allow the UAV to safely fly in the environment. The UAV is assumed to operate wirelessly, with no mechanical tethers to any ground devices as in [14], and therefore it relies on an on-board power

[3]The advantage of the multi-rotor UAV design over a fixed-wing (airplane) or an aerostatic (balloon) design [17] is superior maneuverability and the ability to vertically take-off, which is necessary to enable UAVs to safely fly in a dense urban environment and land on their charging stations.

supply for power and uses wireless connections for data tranmission. The UAV is equipped with two sets of antennas, one for communicating with terrestrial UEs in the cellular bands, and another for the wireless backhaul to the network of GSs. We assume that the communications payload has a total weight in the order of 1-2 kg [18], although lighter hardware designs may be possible [19]. There are a variety of commercial quad- and hexcopters available on the market from manufacturers such as DJI [20] which can be used given this payload weight range, an example is shown in Fig. 1.3. The UAVs in the network are assumed to be controlled by a central controller which receives information about UEs and traffic demand locations, and generates UAV deployment solutions which meet the Quality of Service (QoS) requirements of the UEs. We assume that the UAVs operate exclusively at heights which fall inside unregulated airspace, as this ensures that the UAVs will not interfere with manned aircraft (a discussion of UAV flight rules and regulations is provided in Section 6.2). Typically this corresponds to maximum UAV flight ceilings in the order of 120-150 m.

1.2.2 The UAV Ground Stations

The UAVs backhaul into the core network using GSs which a MNO rolls out in an area where UAVs are expected to operate. These GSs are deployed on elevated sites such as rooftops in the urban environment. They may make use of existing terrestrial BS sites, or they may have their own dedicated sites. To avoid interference with the underlying cellular networks the GSs use dedicated frequency bands for providing a wireless backhaul to the UAV small cells. Two types of data are transmitted on the backhaul link, the payload data related to the terrestrial UEs and Command & Control (C&C) data related to the flight of the UAV itself. The exact type of antenna the GS will have will be determined by the technology used for the backhaul; however, the antennas will be tilted (either mechanically or electronically) towards the sky to ensure better beam alignment with the aerial UAVs which operate at greater heights than the GSs.

1.2.3 The UAV Charging Stations

When not in use the UAVs are docked at special stations designed to keep the UAVs in a state of preparedness for rapid deployment, while also protecting them from adverse weather conditions. These stations keep the UAV batteries charged so that the UAVs can be rapidly deployed in response to sudden surges of traffic demand. As the UAV battery life is limited the UAVs will eventually need to be recharged by the charging stations. There are a number of techniques that can be used to recharge or otherwise keep the

Figure 1.3: A variety of off-the-shelf UAVs are available for carrying light payloads with a high degree of precision and safety. Image: [20]

UAVs operational for longer periods: these will determine the precise configuration of the charging stations and their impact on the UAV network. As an example of a real-world charging station configuration we can consider the design presented in [21], where the charging station consists of a box with battery charging components. A UAV is housed inside the box until it needs to be deployed, at which point the box unfolds and the UAV takes off. The box then closes to protect the circuits from exposure to moisture.

1.2.4 Example of a Typical Use Case Scenario

We consider the following example use case: a number of UEs aggregate in an urban area due to an atypical event, such as a public gathering, traffic congestion or an emergency situation. The increased number of UEs creates a spatially localised spike in data demand, which puts an increased load on the underlying cellular BS network. If the load is significant enough that the underlying BS network is no longer able to deliver service while meeting the QoS requirements, a decision is made by the MNO to deploy a UAV network to supplement the BS network in the affected area. The central UAV controller is provided information about the affected area (such as the location and type of UEs, number and locations of available UAVs, obstacles in the environment, and safety restrictions that may apply in the area). The controller uses this information to select which UAVs to deploy and where to deploy them. The selected UAVs are awoken from their standby state by the flight controller and are issued deployment instructions. After carrying out a pre-flight safety check (ie, checking that components such as the motors and the sensors are working correctly) the UAVs take off from their charging stations. Using a

combination of flight instructions sent by the controller and their own internal collision avoidance sensors the UAVs arrive to their pre-determined deployment locations: at this point they activate their radio components and begin serving UEs below them while hovering in place. The controller continues monitoring the traffic demand in the area; as the demand changes the UAVs are issued new commands to reposition or return back to their charging stations. The controller also monitors the UAV battery life and instructs the UAVs to recharge as necessary.

1.3 Our Contribution

The UAV small cell network is a fundamentally new way to deliver wireless service to UEs. Even though UAVs are starting to be adopted by MNOs in real-world applications the full impact of employing flying small cells is not well understood. UAVs offer a completely unprecedented level of control and performance optimisation in a cellular network due to their inherent mobility, and the adjustable UAV height offers an entirely new degree of freedom in network QoS optimisation that is absent in terrestrial networks.

Our contribution in this thesis is to investigate the impact that the UAV small cell design parameters and flexible mobility can have on the achievable physical layer performance of a cellular network. Point-by-point, our contributions are:

1. We provide a three dimensional stochastic geometry model which captures the coverage probability of a UAV small cell network in a scenario where the UAVs are positioned above the centers of UE hotspots, and which captures the effect of LOS blocking buildings, inter-cell interference, UAV antenna directionality, and the hotspot size on the performance. We compare the performance of this model against a case where UAVs are positioned around UE locations via a heuristic optimisation algorithm, and demonstrate how our stochastic model can accurately capture the performance of the optimised UAV placement.

2. Using our stochastic geometry model we demonstrate that there exists an optimum height for the UAV network to operate at, to maximise the coverage probability of the UEs on the ground. This height represents the trade-off between the negative impact of LOS blockage from buildings and the negative impact of interference from neighbouring UAVs. The value of the optimum height is shown to vary for different UE hotspot sizes, UAV densities and UAV antenna beamwidths.

3. We demonstrate that, for sufficiently high densities of UAVs, the achieveable performance is maximised when the UAVs are positioned with respect to one another in

a regular grid, rather than above UE hotspots. Using simulations we demonstrate how the UAV density threshold which causes this phenomenon varies for different UAV operating heights.

4. We provide a stochastic model for analysing the performance of a network of dedicated GSs that is providing the UAVs with wireless backhaul connectivity, using either sub-6GHz or millimeter-wave technology, and given different UAV antenna configurations. For the sub-6GHz case we verify the performance of the model against a pathloss model proposed by the 3rd Generation Partnership Project (3GPP) and demonstrate that there is a good fit given larger UAV heights.

5. Using our stochastic geometry model and simulations we compare the performance of the dedicated GS network and a typical terrestrial BS network at providing the UAVs with a backhaul, demonstrating how the GS network can deliver superior performance.

6. We compare the performance of a sub-6GHz and a millimeter-wave backhaul, demonstrating that the two technologies require different GS network deployment strategies to provide optimal backhaul performance.

7. We analyse several battery management techniques that a network can implement to compensate for the limited flight time of the UAVs. We model the performance of the UAV network with these battery management techniques, and compare their strengths and weaknesses.

1.4 Thesis Outline

The remainder of the thesis is organised as follows:

Chapter 2 – A Review of Existing Literature In this chapter we review the existing work that has been published by the wireless community on the topic of UAV networks which are relevant to our UAV use case. We provide an overview of the work that has been published under several different categories, and we summarise the observed research trends. This allows us to identify a number of areas in the existing art where we can provide contributions.

Chapter 3 – The UAV Access Link In this chapter we present the main theoretical contribution of our work. We apply stochastic geometry to characterise the performance of a network of UAV small cells operating above UE hotspots in an

urban environment. We derive analytical expressions for the coverage probability of a typical UE in that scenario and we explore the impact of various UAV design parameters on the achieveable performance. For comparison, we also consider a heuristic optimisation algorithm for positioning UAVs around UE hotspots, as well as a regular grid UAV deployment.

Chapter 4 – The UAV Wireless Backhaul Link In this chapter we apply stochastic geometry to the wireless backhaul of a typical UAV belonging to the UAV small cell network. We consider a network of dedicated GSs deployed to provide backhauls to the UAVs, we provide expressions for the probability of a successful backhaul of a typical UAV in the presence of the GS network. In the results section we investigate the impact of a number of UAV and GS design parameters on the backhaul performance. We also consider the difference between a dedicated GS network and a typical terrestrial BS network at providing backhaul connectivity.

Chapter 5 – UAV Energy Consumption and Battery Life In this chapter we consider the energy consumption of UAVs. We outline three battery charging options that may be considered by a network operator and use simulations to demonstrate the performance impact of incorporating those options into a cellular network where UAV small cells provide wireless service. We additionally consider several new battery technologies that are expected to become commercially available in the foreseeable future, and demonstrate how their implementation can increase the UAV small cell lifetime.

Chapter 6 – Conclusions & Open Questions In the last chapter we summarise the key findings of our work, and discuss issues with UAV networks that are still open to be addressed, such as the legal aspects of UAV operation.

1.5 Dissemination

In this section we describe the output of our work, which took the form of publications, technical workshops and public engagement.

1.5.1 Publications

Over the course of this research a number of works have been published. The technical content of this thesis is taken from publications marked with •. The listed numbers of citations are valid as of the time of publication.

Journals

- J. Kibiłda, B. Galkin, and L. A. DaSilva, "Modelling Multi-Operator Base Station Deployment Patterns in Cellular Networks," *IEEE Transactions on Mobile Computing,* December 2016
  Number of citations according to Google Scholar (ex. self-citations): 25
- B. Galkin, J. Kibiłda, and L. A. DaSilva, "A Stochastic Model for UAV Networks Positioned Above Demand Hotspots in Urban Environments ," *IEEE Transactions on Vehicular Technology (TVT),* submitted April 2018, Under Review, available on Arxiv
  Number of citations according to Google Scholar (ex. self-citations): 1
- B. Galkin, J. Kibiłda, and L. A. DaSilva, "UAVs as Mobile Infrastructure: Addressing Battery Lifetime," *IEEE Communications Magazine,* Accepted for Publication 2019.
  Number of citations according to Google Scholar (ex. self-citations): 0

Conferences

- J. P. Miranda, B. Galkin, and L. A. DaSilva, "Experimental assessment of eigenvalue-based detection for cognitive radio," *IEEE Sensor Array and Multichannel Signal Processing Workshop (SAM),* June 2014
  Number of citations according to Google Scholar (ex. self-citations): 0
- B. Galkin, J. Kibiłda, and L. A. DaSilva, "Stochastic Modelling of Downlink Transmit Power in Wireless Cellular Networks," *IEEE International Workshop on Computer Aided Modelling and Design of Communication Links and Networks (CAMAD),* September 2015
  Number of citations according to Google Scholar (ex. self-citations): 0
- B. Galkin, J. Kibiłda, and L. A. DaSilva, "Deployment of UAV-Mounted Access Points According to Spatial User Locations in Two-Tier Cellular Networks," *IFIP Wireless Days,* March 2016
  Number of citations according to Google Scholar (ex. self-citations): 31
- B. Galkin, J. Kibiłda, and L. A. DaSilva, "Coverage Analysis for Low-Altitude UAV Networks in Urban Environments," *IEEE Global Communications Conference (GLOBECOM),* December 2017.
  Number of citations according to Google Scholar (ex. self-citations): 20
- B. Galkin, J. Kibiłda, and L. A. DaSilva, "Backhaul For Low-Altitude UAVs in Urban Environments," *IEEE International Conference on Communications (ICC),* May 2018.
  Number of citations according to Google Scholar (ex. self-citations): 5

Non Peer Reviewed

- B. Galkin, J. Kibiłda, and L. A. DaSilva, "A Stochastic Geometry Model of Backhaul and User Coverage in Urban UAV Networks," Available on Arxiv, October 2017.
  Number of citations according to Google Scholar (ex. self-citations): 11
- B. Galkin, J. Kibiłda, and L. A. DaSilva, "Impact of UAV Antenna Configuration on Wireless Connectivity in Urban Environments ," *IEEE Transactions on Vehicular Technology (TVT) Correspondence Letters,* available on Arxiv, June 2018.
  Number of citations according to Google Scholar (ex. self-citations): 1

1.5.2 Public Engagement

The research carried out on UAV networks was presented in an article of The Liffey Champion (see Fig. 1.4), a local newspaper in the Kildare region. Research progress was also reported on social media and the CONNECT website on several occasions [22, 23].

1.5.3 Technical Workshop

The research carried out as part of this PhD program attracted the attention of Nokia-Bell Labs representatives working in the area of UAV communication. This led to the organisation of the first CONNECT UAV workshop in April 2018, where researchers from


Leixlip man Boris Galkin with one of the drones at Trinity College, Dublin.

Leixlip man's been talking to the world

by Gerry Hand

A PHD researcher from Leixlip has just returned from addressing the world's biggest telecommunications conference which took place in Singapore just prior to Christmas.

Boris Galkin spoke at the Globecom conference on the use of drones in the telecommunication centre, and he told LIFFEY CHAMPION this week that he got a very positive response.

"To be fair it went very well there was a lot of interest in what we in the CONNECT centre on Dublin are doing at the moment," said Boris who lives in Riverforest in Confey.

"I gave a powerpoint presentation and hosted a Q&A session on the work we are undertaking, and afterwards representatives of universities in Singapore itself and also in Belgium approached me for more detailed discussions.

• Continued on page 3

Figure 1.4: Newspaper Article from The Liffey Champion (13/1/2018 issue)

the universities involved in the CONNECT project presented their work on UAV systems to representatives from Nokia-Bell Labs and each other. Our work was presented in a talk titled "UAV Placement Above User Hotspots in Urban Environments".

2 A Review of Existing Literature

In the previous chapter we outlined our vision for UAVs as flying small cells to help with flash demand in urban environments. Over the previous several years, the wireless community has recognised the potential of using UAVs in areas of wireless communications such as wireless sensor networks [24], public safety networks [25], and commercial cellular networks [26, 27]. The purpose of this chapter is to explore existing literature from the wireless community which is relevant to our envisioned UAV use case, to identify the key research trends and position the contribution of our work. Each section focuses on a specific aspect of UAV networks. In each section we cite notable works and summarise their contributions; then we summarise the key research trends of the referenced literature, while highlighting any gaps in the work that we can address. We conclude the chapter with an overall summary of the research directions taken by the wireless community with regards to UAV networks.

2.1 UAV Movement Optimisation

As already established, UAVs are capable of freely moving in three-dimensional space. The location of a UAV small cell will have an impact on the performance of the wireless channel between the UAV and the UEs that are being served by it, therefore the coordinates of a UAV small cell are a variable that needs to be optimised to maximise the performance of the UAV network. The issue of UAV positioning optimisation with respect to the terrestrial UEs is perhaps the most widely analysed UAV issue in the wireless networks community. As we demonstrate below, most work on the issue of optimally positioning UAVs either optimise the horizontal coordinates of the UAV while keeping its height above ground constant, or optimise the height while keeping its horizontal position constant; as such we separate the UAV placement problem into two categories.

2.1.1 Optimising Horizontal UAV Positioning

In this subsection we review the works on horizontal positioning of UAV infrastructure, unless stated otherwise the following works assume the height above ground is fixed. The problem of determining optimum locations for infrastructure pre-dates the UAV small cell concept. A typical example is [28], where the authors use mixed integer linear programing to selectively place small, terrestrial picocells within a heterogeneous network. The solution seeks the minimisation of cost functions representing either data delivery cost or BS load. In [29] the authors consider a scenario where two UAVs at a certain height above ground and a certain distance apart are providing service to UEs inside a rectangular area of interest, while creating interference on one another. The authors provide a mathematical expression for the optimum distance that the UAVs need to have to one another to achieve maximum coverage of the area of interest. In [30] the authors investigate optimum UAV placement in an IoT scenario, for the purpose of reducing the required transmit power of the IoT devices. The authors partition the IoT devices into clusters and determine where the UAVs must be placed to communicate with each cluster. The authors then apply optimum transport theory to determine what path each UAV should take when travelling across the clusters. In [31] the authors consider a network of UAVs with downtilted directional antennas that need to cover a circular area of interest. Using circle-packing theory the authors optimise the position of the UAVs and their coverage areas, while demonstrating the relationship between the number of deployed UAVs and the maximum achieveable coverage percentage of the area of interest. In [32] the authors consider a scenario where a single UAV is providing service to a group of UEs while a set of UEs are communicating amongst themselves in a device-to-device network. The authors treat the UAV positioning problem as a disk-covering problem and determine an optimised travel path for the UAV that achieves full coverage of the area of interest. In [33] the authors consider the problem of placing a UAV in 3D space to maximise the number of UEs that are covered, subject to a QoS constraint. The authors describe the scenario as a mixed integer non-linear problem which they solve given different environmental parameters.

If the UAV is not tethered to a GS then it will rely on a wireless backhaul connection into the core network. Certain papers recognise this and consider the UAV positioning problem from the perspective of optimising the UE access and the backhaul link simultaneously. In [34] the authors consider a scenario where a single BS enters an outage state and a number of UAVs are used to serve the coverage hole by relaying data from the neighbouring BSs. Assuming a hexagonal BS distribution the authors determine the optimum placement of the UAVs between the disabled BS and the neighbouring BSs for

different numbers of UAVs and different UAV transmit powers. In [35] the authors consider a single fixed-wing UAV acting as a relay between two ground terminals, and the overall throughput is maximised by optimising the trajectory and the transmit power of the UAV across discrete timeslots with respect to the two terminals. The authors demonstrate how the trajectory can be optimised using convex optimisation methods when the transmit powers are fixed, and propose an iterative algorithm for the case where both the trajectory and the transmit powers are variable. The same authors optimise the trajectory to maximise energy-efficiency in [36], and they optimise the spectrum efficiency for a fixed-wing UAV with a circular orbiting pattern in [37]. In [38] the authors consider a scenario where a UAV relay iteratively searches an urban environment for locations where it can establish a LOS connection to the UE and BS, meeting the channel rate requirements. The authors present a converging algorithm which significantly outperforms direct BS-UE communication. In [39] the authors use binary integer linear programming to determine the hovering coordinates of a UAV which maximise the QoS for a set of UE clusters, given that the UAV has a wireless backhaul into a nearby BS. The authors consider the cases where the UAV is positioned to serve as many UEs as it can equally, as well as cases where the UAV prioritises some UEs over others. The authors extend this work in [40] to consider the optimisation of multiple UAVs.

In some scenarios the UEs are mobile and move as the UAV provides service. The authors of [41] and [42] investigate a scenario where the UEs move randomly around an area of interest during UAV operation. They propose the use of an iterative optimisation algorithm where the UAV updates its position after a given time interval to maximise the achievable spectral efficiency of the UAV-UE link. In [43] the authors attempt to optimise the energy consumption of a UAV by adjusting its placement with respect to a UE distribution with a time-varying density, using an algorithm to predict fluctuations in UE density.

2.1.2 Optimising UAV Height

The most basic UAV height optimisation scenario is considered in [44], where a single UAV with an omnidirectional antenna is hovering over an urban area, and providing coverage to the terrestrial UEs below. The authors assume no interference sources so that the QoS is limited purely by signal pathloss. The authors propose a sigmoid model to describe the probability of a LOS channel between a UE and the UAV as a function of the vertical angle between them: a greater angle reduces the likelihood of a building being in the way of the signal. The authors demonstrate that there exists a certain optimum height for the UAV which maximises its coverage area: below this height UEs experience low

QoS because of LOS blockage from the buildings; above this height there is excessive distance-dependent pathloss due to the increased distance between the UE and the UAV. The value of the optimum height depends significantly on the type of environment the UEs are operating in, and the maximum acceptable pathloss threshold.

Similar observations on UAV height behaviour have been reported in [45–48]. The authors of [45] consider a UAV with several different antenna radiation patterns, and demonstrate the existence of an optimum height which minimises the Signal-to-Noise Ratio (SNR) outage probability. In [46] and [47] the authors consider a channel with Rician multipath fading; they derive a closed-form expression for the maximum coverage radius of the UAV, and also closed-form expressions for the optimum height in terms of outage probability, received power gain, and data rate gain. In [48] the authors optimise the height of a UAV subject to UE channel delay and backhaul constraints, using the golden section search method.

Note that the work [44–48] all explore the performance of a single UAV acting in an interference-free environment, with the QoS being determined purely by pathloss, fading and channel noise. A more complicated system model is considered in [49]. The author explores a scenario where multiple UAVs are deployed in a disaster scenario to serve terrestrial UEs. The UAVs use the same frequency bands and therefore cause interference for one another. The author attempts to optimise the performance of the network, and as the UAVs can negatively affect each other's UEs the optimisation problem is intractable, therefore the author proposes a heuristic algorithm which allows the individual UAVs to iteratively adjust their locations in three dimensions to improve their own signals. The author reports that the UAVs are not able to converge on an optimum height which maximises the overall performance of the network.

2.1.3 Section Summary and Observed Research Trends

A review of the literature addressing the optimisation of UAV placement suggests that there are a variety of methods and algorithms available for a variety of scenarios and UAV use cases. We note, however, that the existing state of the art tends to focus on interference-free UAV operation, where the network is limited entirely by pathloss and noise. With the exception of [29], [31], [34] and [49] the works cited above assumed that the network uses dedicated spectrum resources for each UAV. By making this assumption the optimisation problem becomes tractable, as moving one UAV will not negatively impact the performance of another UAV's UEs. Without interference the wireless links are limited by the geometry of the environment, and therefore the network performance is generally optimised through minimising the distance between the UAV and the receiver,

as this minimises the pathloss, increases the LOS probability and enables the network to reduce transmit power. This assumption may be valid for certain scenarios such as rural UAV deployment, but for the main use case that we are interested in, a low altitude UAV network in urban environments, it may not be realistic. In the presence of interference, decreasing the distances between transmitters and receivers may also have the result of decreasing the distances between interferers and receivers, potentially causing a net decrease in channel performance. Because of this, the insights published in the above works may not be entirely applicable to our scenario of interest.

Another observation to be made has to do with the way the literature models LOS probability and behaviour. The authors of [44] propose a sigmoid function to model the LOS probability; this function has become very popular in subsequent works as it is a tractable, closed-form expression. The sigmoid model is based on the assumption that the aggregate LOS blockage of the buildings in the environment can be approximated as a function of the vertical angle between the UAV and the UE. This approximation is only accurate for the cases where the UAVs operate at very large heights, as the authors of the original paper themselves point out. For our scenario we expect UAVs to be much closer to the UEs on the ground, with distances that the sigmoid model is unsuited for[4]. It follows that a different LOS model is needed for capturing the channel behaviour of very low altitude UAVs in urban environments.

2.2 Stochastic Geometry Modelling of the Wireless Network

Stochastic geometry is an alternative method for modelling the spatial relationships in a wireless network, capturing the effect of interference on network performance and giving us new insight into the resulting performance trade-offs. In a stochastic geometry model, the locations of the transmitters and the receivers are modelled as random events, whose spatial distributions are known in advance. Knowing the spatial distributions and the channel propagation model, it is possible to derive mathematical expressions for network Key Performance Indicators (KPIs) such as coverage probability as a function of the network parameters such as transmitter density [50]. Stochastic geometry has seen widespread use for analysing the behaviour of terrestrial networks. A landmark work on the subject is [51], in which the authors calculate the coverage probability and the expected data rate that a typical UE can experience given a macrocell BS network where the

[4]we demonstrate this numerically in Fig. 3.6 in Chapter 3.

BSs are uniformly and randomly deployed according to a Poisson Point Process (PPP). The UE is assumed to connect to the nearest BS, as it provides the strongest signal due to the reduced pathloss. The authors provide a general expression for the coverage probability for arbitrary random channel fading behaviour, and then provide closed-form expressions for the special case when the random fading is modelled as Rayleigh fading. The methodology applied by the authors for deriving the coverage probability involves first conditioning on the horizontal distance to the serving BS, then calculating the conditional coverage probability using a Laplace transform of the random aggregate interference experienced by the UE, followed by deconditioning the coverage probability using the known Probability Density Function (pdf) of the serving BS distance distribution. This derivation procedure has subsequently become widely used in stochastic analysis of cellular networks. An alternative methodology is presented in [52], in which the authors derive an expression for the expected data rate using the moment-generating function of the aggregate interference. In [53] the authors consider a similar scenario for a BS network distributed according to a Binomial Point Process (BPP) inside a bounded area, where the number of the BSs is fixed. The authors provide an expression for the coverage probability of a typical UE, for the case when the UE is served by the closest BS and also for the cases when there are interfering BSs closer to the UE. In [54] the authors consider the association probability of a typical UE to a terrestrial small cell, assuming a channel with Nakagami-m multipath fading and interference from other small cells. The work in [55] characterises the spectral efficiency and average Signal-to-Interference-and-Noise Ratio (SINR) of a multi-tier wireless network with kappa-mu channel fading. The individual network tiers represent macrocells and small cells, and are modelled as independent PPPs with different densities, with the reference UE associating to the device which provides it with the strongest signal.

The above works model the distributions of the BSs and small cells as being distributed independently of the locations of the UEs. In contrast, the authors of [56, 57] explore a multi-tier network scenario where the picocells are placed in the center of UE clusters, to represent intelligent network deployment. Given multiple tiers of networks in the operating area the UEs can be served by one of several different network types, in [56] the authors provide expressions for the probability of a UE associating to a specific network tier over the others. The authors then use this association probability to calculate the coverage probability of a typical UE belonging to a UE cluster with a picocell in its center. In [57] the authors extend this analysis to consider small cell deployments where the small cells are clustered around certain areas of interest.

Stochastic geometry has also been used to characterise the performance of networks which employ millimeter-wave technology. In [58] the authors characterise the per-

formance of a millimeter-wave network with directional antennas. The authors assume the network is noise-limited and propose a LOS blockage model based on experimental measurements. In [59] the authors explore a two-tier network where the small cells use millimeter-wave bands to provide service to the UEs. The authors characterise the association probability and the coverage probability for a reference UE that can choose between the macrocell tier and the small cell tier for service. In [60] the authors consider the impact of LOS blocking and high antenna directionality on millimeter-wave networks, and examine several models for both factors.

There is a growing interest in the wireless community in applying stochastic geometry analysis to UAV networks. Note that some of the following works were published subsequent to our own publicatons. In [61] and [62] the authors derive the coverage probability for a stochastic UAV network under guaranteed LOS conditions for a fading-free and Nakagami-m fading channel. The authors describe a fixed number of UAVs operating within a fixed area at a certain height above ground and demonstrate how an increase in height results in a decrease in the coverage probability. Additionally in [62] they demonstrate how larger values of fading parameter m reduce the variance of the random Signal-to-Interference Ratio (SIR) experienced by the UE. Stochastic geometry is applied by the authors of [63] to optimise UAV density in a radio spectrum sharing scenario under guaranteed LOS conditions. In [64] the authors evaluate the performance of a network of UAVs acting alongside a terrestrial BS network in an emergency outage scenario. The authors of [65] and [66] use stochastic geometry to evaluate the performance of a terrestrial BS network that is serving terrestrial UEs and UAVs simultaneously. In [67] the authors characterise the coverage probability of a typical UE when it connects to the nearest UAV in a PPP distributed network. The authors assume Rayleigh fading and use a channel model which combines LOS and non-Line-of-Sight (NLOS) pathloss components. In [68] the authors explore a scenario where randomly distributed UAVs have random heights. The authors model the height of a given UAV using a random waypoint model, provide expressions for the pdf of the distance of a given UAV to the reference UE, and then derive an expression for the coverage probability. In [69] the authors analyse the uplink performance of a UAV operating above a terrestrial BS, with uniformly and randomly distributed UEs in the area. These UEs are separated into those which communicate with the BS and those which communicate with the UAV. The authors characterise the uplink coverage probability for both networks assuming that the same uplink frequency bands are used by both networks, and UEs from one network interfere with the signal from UEs of the other network. The work in [70] evaluates the coverage probability of a PPP UAV network for three different LOS models; the sigmoid model presented in [44] and two models provided by the 3GPP. In [71] the authors consider the performance of a UAV

operating above an area that is not covered by an underlying terrestrial BS network. The authors assume the UAV uses the same spectrum resources as the BS network and capture the impact of the interference from the BSs on the performance of the UAV channel.

2.2.1 Section Summary and Observed Research Trends

Stochastic geometry is a powerful tool for network analysis, and over the past several years it has seen widespread use by the wireless community. Despite this, we observe several gaps in the stochastic geometry analysis which need to be addressed when approaching the topic of low-altitude UAV networks.

We note that when analysing terrestrial networks the majority of publications model the network in only two dimensions. The justification for this is that terrestrial infrastructure is relatively close to the ground (even if it is on a rooftop), therefore all the devices can be approximated as existing on the same vertical plane, with only horizontal distances impacting the performance. However, for UAV networks the impact of the height is important and should be reflected in the system model.

The PPP distribution is the most popular for modelling randomly distributed infrastructure in a network due to the analytical tractability it affords. Under the PPP distribution the locations of infrastructure devices are unaffected by the locations of any other devices or other environmental effects. The assumption of independent positioning may be valid for terrestrial networks where a number of real-world factors determine the placement of infrastructure, and the locations of infrastructure and the UEs that they serve may appear uncorrelated. As has been established in the previous section, UAVs can be intelligently positioned around the locations of UEs, which results in a UAV network distribution which is not independently positioned with respect to the UEs. There is currently a lack of publications from the wireless community which model non-independent UAV positioning around the UEs, and as a result the insight given by the existing state-of-the-art is somewhat limited.

Due to its tractability, Rayleigh fading is the most common multipath fading model used by the literature for modelling channel performance. Terrestrial networks operating inside built-up areas experience significant multipath effects, as such the Rayleigh model may be appropriate as an approximation of the channel performance. UAVs, on the other hand, may experience reduced multipath behaviour, due to their aerial positions which result in fewer channel obstructions. Because of this, a different multipath model (such as Nakagami-m fading) is more appropriate for characterising the performance of UAV networks.

A simplication that is commonplace in the current literature is to model the infrastructure antennas as being omnidirectional with equal antenna gain. This assumption aids tractability, however, it fails to capture the impact of antenna design on the overall network performance. UAVs are very flexible and we expect them to have a variety of different antenna configurations, it is important to reflect this in the analysis by explicitly modelling antenna directionality.

The model we provide in this thesis addresses the observations above, as it models a UAV network in three dimensions and captures the impact from antenna directionality, building blockage, varying multipath effects, and non-random placement of the UAVs with respect to UE positions.

2.3 The Wireless UAV Backhaul

As already discussed, for UAVs to be used to their full potential they must be untethered. An entirely wireless UAV small cell will require a wireless connection to a GS to facilitate communication between the UEs and the core network. In this section we review the existing literature on the topic of wirelessly providing UAVs with backhaul connectivity.

Although terrestrial infrastructure can rely on a wired backhaul (such as optic fibre) there has been some interest from the wireless community in using wireless backhauls. In [72] the authors explore the possibility of using existing macrocell BSs to provide wireless backhaul to terrestrial small cells. The authors consider the sub-6GHz bands, the microwave bands and the millimeter-wave bands for the wireless backhaul, and compare the relative strengths and weaknesses of each. The authors also demonstrate how the distance between the small cell and its backhaul BS affects the capacity of the UE link, for the cases when the small cell operates in full duplex and half duplex modes. The work in [73] explores the different frequency ranges in the millimeter-wave band to determine which are the most appropriate for use in small cell backhaul. The authors explore the impact of atmospheric attenuation due to oxygen and water absorption for the different frequencies, using both theoretical propagation models as well as models based on experimental field trials. The authors conclude that millimeter-wave bands are suitable for wireless backhaul use for short ranges (in the order of 1 km), provided that antenna directionality is used to improve the antenna gain of the signal. In [74] the authors explore the problem of managing the spectrum resources for the backhaul links between a macro BS and a number of small cells belonging to multiple MNOs. The authors investigate the possibility of using certain small cells to relay the wireless backhaul to other small cells, given a pricing incentive. Using simulations the authors demonstrate how such a cooperative network can greatly enhance the backhaul performance of the small cells.

With the growing presence of vehicular networks there has been a number of publications on the topic of providing a wireless backhaul to small cells onboard vehicles. In [75] the authors report on a scenario where a number of remote radioheads are deployed alongside a high speed train track for the purpose of providing millimeter-wave backhaul to passing trains. In [76] the authors investigate the performance of a network of GSs that provide wireless backhauls to small cells mounted inside commercial aicraft. Each GS is assumed to have an antenna array which it uses to steer its beam across the sky to align with aircraft. The authors demonstrate that there is an inverse relationship between the density of the GS network and the number of elements that are required for each GS to avoid antenna misalignment and meet the data rate requirement.

A variety of technologies have been considered as candidates for providing wireless connectivity to UAVs. The authors of [77] investigate millimeter-wave as an enabling technology for UAV networks. The work addresses the issues of beam tracking, LOS blockage and UAV discovery; the authors conclude that the flexibility of the UAV movement patterns and their ability to adjust their heights can help to alleviate the main issues they may encounter with a millimeter-wave backhaul. The authors of [78] consider using Free-Space Optical (FSO) technology for the UAV backhaul. The authors envision a scenario where high-altitude UAVs relay signals from GSs on the ground to terrestrial small cells, taking advantage of their ability to maintain an LOS channel on both sets of devices. The authors characterise the performance of the network using both visible light and infrared FSO links. They also provide rough comparisons of the financial costs involved in deploying the network. In [79] the authors investigate the performance degradation that can be caused by antenna misalignment or UAV position fluctuation, when using FSO links for the backhaul. The authors model the UAV position as a random variable and provide closed form expressions for signal attenuation as a function of UAV stability. In [80] the authors propose a multi-hop UAV network for connecting terrestrial small cells to a backhaul GS, using sub-6GHz links. The authors propose a network formation algorithm which allows the UAVs to form a multi-hop network in a decentralised manner. With the help of simulations the authors show that the resulting network topology allows for a better data rate and a smaller delay than conventional multi-hop topologies such as a star network.

One of the more popular approaches to UAV backhauling in the state-of-the-art is to use the existing terrestrial cellular network. The works in [34, 38–40, 65, 66] discussed in the previous sections all assume that the UAV network will rely on an existing cellular BS network for connectivity. The issue with the current cellular BS networks is that they are designed for providing service to terrestrial UEs, and as a consequence their antennas are downtilted to focus the antenna lobe towards the ground. The authors of [81] investigate

the performance that a UAV can achieve when connected to a BS, given that the UAV will receive sidelobe signals from the downtilted BS antenna. The authors apply ray tracing simulations and experimental measurements to characterise low altitude UAVs operating in a rural environment. They conclude that, due to the UAVs having LOS on the BSs from their aerial vantage point, the channel quality is sufficient to provide wireless connectivity to the UAVs despite the antenna misalignment. In 2017 the 3GPP began a study item on the feasibility of using terrestrial LTE networks to provide connectivity to low-altitude UAVs; the first revision of the report was published in late 2017 [82]. The report corroborates the findings in [81] that the ability of the UAV to establish a LOS channel to its serving BS can negate the signal deterioration due to BS antenna downtilt; however, the UAVs are reported to experience strong interference from neighbouring BSs due to the LOS channel. As a result, the report concludes that interference mitigation needs to be implemented in some form to allow the UAVs to benefit from terrestrial BS connectivity. One of the proposed solutions is to design the UAVs to have directional antennas which they intelligently steer towards their serving BS. The authors in [83] evaluate the impact of massive Multiple Input Multiple Output (MIMO) in terrestrial BSs on their achievable UAV channel quality. The authors demonstrate that with the implementation of massive MIMO the channel reliability is greatly increased, due to a stronger carrier signal, mitigated interference and spatial multiplexing gain.

2.3.1 Section Summary and Observed Research Trends

The wireless community has recognised UAV connectivity as a key issue that needs to be addressed. A number of technologies have been considered for providing the UAVs with wireless backhaul. One of the most widely considered is to simply connect the UAVs to the existing cellular BS network, alongside terrestrial UEs. While there are a number of UAV applications where cellular connectivity may be sufficient to meet the data requirements, for the scenario of very low altitude UAV small cells operating in urban environments the cellular network may not provide an adequate backhaul. As they are expected to provide data connectivity to a number of terrestrial UEs, we expect that each UAV small cell will have a very high data requirement for its backhaul, which the existing cellular BSs may not be able to meet. Furthermore, in a scenario where UAVs are deployed to service a number of UEs we can expect the existing cellular network to be heavily loaded already, and having the UAVs backhaul through nearby BSs in that scenario may not be viable. We expect that as UAV networks become more widespread and play a greater role in serving the UEs, MNOs will opt to deploy dedicated backhaul GSs to support these networks. UAVs have very different performance requirements and

behave very differently to the typical terrestrial UE; it follows that GS networks designed to serve UAVs will require different deployment strategies to BS networks designed to serve terrestrial UEs. Currently, there is a lack of work in the state-of-the-art which investigates these dedicated GS networks and gives insight into how they need to be designed and deployed. This is one of the problems we address in this thesis.

2.4 UAV Battery Life

In a scenario where UAVs do not have their power fed to them through a physical tether they have to rely on battery power to stay in the air and power their electronic circuits. The result of this is that each UAV can remain operational in the air for a limited amount of time, determined by the amount of energy stored by its battery; once the energy supply is low the UAV will have to land. This has profound implications for UAV small cell network design, as it means that the network must be planned around the relatively short operating time of the UAVs. Network planning must involve both the deployment of dedicated infrastructure to recharge the UAVs and also the implementation of energy-aware deployment mechanisms which can ensure that UAVs use their limited battery life as efficiently as possible when in the air [26]. In certain scenarios it may be possible for UAV networks to operate without dedicated charging stations. The authors of [84] explore several techniques for recharging a UAV battery wirelessly, to avoid the use of dedicated charging infrastructure. The authors consider UAVs using induction power transfer to wirelessly charge their batteries from high-voltage power lines. Using experiments, the authors demonstrate that if a UAV can land within a few centimeters of a typical high-voltage power line it can successfully recharge its battery from the magnetic induction of the cables.

There has been a number of publications from the wireless community on the topic of optimising the energy efficiency of a UAV with respect to the service it delivers to its UEs. In [85] the authors consider an IoT framework where a centralised network controller entity selects UAVs from a fleet of available devices, based on the specific requirements of the task and also the energy consumption requirements. The authors set up an optimisation problem based on either minimising the energy consumption or the task completion delay, and demonstrate via simulations the resulting performance. The work in [86] considers aggregating multiple UAVs into a single cluster, with the clusterhead UAV routing data from the other UAVs to the GS. Using a fuzzy logic algorithm the authors demonstrate how the UAVs can be aggregated into the clusters, with a clusterhead selected according to the cluster centroid. The authors then use simulations to demonstrate that

this approach can reduce UAV energy expenditure. The authors of [87] propose a path planning algorithm to determine which UAV to send to a given set of service locations, to minimise the total energy consumed by the UAVs for travel. The authors propose solving the problem using mixed integer linear programming; for comparison the authors also propose a greedy algorithm and an algorithm which minimises UAV path overlap. Using simulations and energy consumption values obtained from an off-the-shelf consumer UAV the authors demonstrate the reduction in UAV network energy consumption that can be obtained using their algorithm. In [88] the authors investigate the possibility of landing UAVs on rooftops during operation to reduce their power consumption and thereby increase their operating time. The authors consider a scenario where a UAV has to provide service to a number of UEs and there are several available landing sites on rooftops in the area, the authors optimise the trajectory the UAV and its velocity to maximise total achieveable data rate over a time period of interest. In [89] the authors consider a network of UAVs being used to monitor vehicle traffic in a city; the authors attempt to determine the most appropriate locations for the UAV charging stations that would allow the UAVs to cover the main road intersections and other areas of traffic congestion. The authors propose two algorithms for determining the charging station locations, a modified clustering algorithm and a particle swarm optimisation algorithm. They then verify the performance of these algorithms using real-world road and traffic maps. In the work [90] the authors consider the issue of UAV recharge scheduling, in a scenario where the number of UAVs exceeds the number of available charging stations. The authors propose both a centralised and a decentralised algorithm for scheduling the UAV recharging in a way that maximises overall UAV flight time without allowing any UAV to run out of battery power. The authors then compare the performance of their algorithms against basic round-robin and probabilistic scheduling, showing an improvement of the UAV network KPI.

2.4.1 Section Summary and Observed Research Trends

The limited flight time of UAVs is one of the bigger obstacles that prevents them from seeing widespread use. The wireless community has recognised this and work has been carried out on designing UAV networks with the energy limitation in mind. We report a current trend in the state-of-the-art: the majority of the work published on the topic focuses on the optimisation of the UAVs themselves, rather than the charging infrastructure. UAVs are highly flexible devices and therefore there is a variety of ways their deployment and operation can be optimised. However, this focus on the UAVs as the solution to the battery life limitation means that there is insufficient discussion on the impact of the charging infrastructure on the overall network performance. There are

a variety of ways that ground infrastructure can be deployed in an area of interest to support the UAV network, how these deployments will affect the performance of the UAV network and ultimately the service experienced by the UEs needs to be carefully analysed. Furthermore, the existing literature tends to focus on modern-day UAV battery technology when analysing UAV network performance; however, the underlying battery technology that enables high-density UAV batteries is constantly improving. There is a lack of discussion on how the UAV network may improve in its ability to service terrestrial UEs as batteries become more capable. In this thesis we explore some of the alternatives for UAV recharging that can lead to continuous coverage.

2.5 Chapter Summary

The growing presence of UAVs in modern society has created new research trends in the wireless community, and over the past several years a number of publications have been made in the area of UAV networking.

The biggest novelty of UAV networks over their terrestrial counterparts is their mobility: as a result, a significant share of the wireless literature focuses on the topic of UAV mobility and how it can be optimised to improve the performance of the wireless network. A variety of optimisation tools and algorithms have been proposed in the literature, for a variety of different UAV scenarios and different KPIs. Unfortunately, the majority of the literature considers scenarios where UAVs operate in interference-free environments, either because they operate in isolation from other devices or because they use orthogonal spectrum resources to devices in the vicinity. This assumption makes the problem of UAV placement optimisation tractable; however, it limits the applicability of the work. In our envisioned UAV small cell scenario we expect the UAVs to be densely deployed in an urban environment where, due to spectrum scarcity, frequency resources may have to be reused between UAVs. We expect the result to be a network which is highly interference-limited; the insights offered by the work on UAV positioning optimisation may not be accurate for our scenario of interest.

Stochastic geometry has emerged as a popular tool for modelling the performance of wireless networks, both terrestrial and UAV. Stochastic analysis can give insight into the performance of interference-limited networks; however, we note certain limitations of existing stochastic geometry work. Analysis which considers terrestrial networks very often approximates the networks as being two-dimensional, with only horizontal distance being relevant. For UAV network analysis this assumption is not suitable, as UAV height above ground plays a key role in their ability to deliver high quality service. The majority of stochastic geometry analysis relies on the assumption that the infrastructure and the UEs are independently positioned with respect to one another; given the intel-

ligent mobility of UAVs this assumption may not hold for UAV networks. It is also very common for the state-of-the-art to assume omnidirectional antenna behaviour for the infrastructure under investigation, while we expect that UAV antenna directionality will play a key role in real-world UAV networks. To carry out a meaningful analysis of low-altitude UAV networks in urban environments we require a stochastic geometry model which can capture the impact of UAV height, their ability to position themselves around UE locations, their antenna directionality and also the impact of channel obstacles in the environment. Currently, there is a lack of work in the wireless community which meets all of these requirements.

Untethered UAVs require wireless backhauls into the core network. Currently the most popular solution to provide UAV connectivity appears to be to use existing cellular networks. The wireless community has published a number of studies investigating the ability of existing terrestrial BSs to provide connectivity to low-altitude UAVs, and the emerging consensus is that UAVs can receive adequate service from terrestrial BSs, despite downtilted antenna misalignment and excessive interference. The use of the cellular network for the UAV backhaul may not be appropriate for the urban UAV small cell scenario, as we expect the UAVs to be deployed in areas where the terrestrial cellular network is heavily loaded by UEs. We expect that networks of dedicated GSs will be deployed to provide UAV backhauls in this scenario; however, there is currently a lack of research into the deployment of such GS networks. As a result, the relationship between the deployment parameters of a dedicated GS network and its UAV network are not well understood. The topic of dedicated wireless infrastructure to support UAV operation must be analysed further.

Untethered UAVs have the disadvantage of having to rely on a battery supply to stay in the air, which results in a limited operating time for a given UAV. The wireless community has approached this problem from the perspective of optimising the deployment and operation of the UAVs to prolong their battery life, or to ensure that they deliver the most efficient service while they are flying. There has been an inadequate amount of exploration of the UAV recharging process, the infrastructure required, or its impact on the performance of UAV small cells. We expect that the design and deployment parameters of the charging stations used for the UAV network will radically affect its ability to serve UEs, this relationship needs to be explored further. The batteries used by the UAVs are expected to evolve as the underlying technology improves, and there is currently a lack of investigation in the wireless community on how UAV networks may improve as the battery technology becomes more advanced.

Our technical contribution in this thesis is to address the highlighted research questions and provide important insight into the performance of low-altitude UAV networks in urban environments.

3 The UAV Access Link

The technical content presented in this chapter is based on the works "Deployment of UAV-Mounted Access Points According to Spatial User Locations in Two-Tier Cellular Networks" presented at IFIP Wireless Days, "Coverage Analysis for Low-Altitude UAV Networks in Urban Environments" presented at IEEE Global Communications Conference (GLOBECOM), "A Stochastic Geometry Model of Backhaul and User Coverage in Urban UAV Networks" published on Arxiv and "A Stochastic Model for UAV Networks Positioned Above Demand Hotspots in Urban Environments" submitted to IEEE Transactions on Vehicular Technology (TVT).

3.1 Introduction

As has been demonstrated in the existing literature, UAV infrastructure can deliver high-quality service to terrestrial UEs, through a combination of intelligent movement and unobstructed wireless channels with direct LOS between transmitter and receiver. The introduction of UAVs also presents new challenges to network deployment, as the unprecedented flexibility of the new infrastructure requires more insight into how the new network variables affect the achievable performance. As the UAVs can move in three dimensions on-demand they can pursue a variety of deployment strategies with respect to the locations of UEs, each other, or a combination thereof. The selection of the appropriate deployment requires an understanding of the performance impact of each deployment strategy in a given situation. In addition to this, the operating UAV height above ground will affect the overall network performance and needs to be selected with care. Based on current UAV operation regulations (discussed in detail in Section 6.2) we expect that UAVs serving urban hotspots will take the form of small, lightweight (below 25kg) devices operating at heights at or below 200m. Given this height range the UAV network may be operating above a built-up urban area or below building heights in so-called urban canyons, which will significantly affect the radio environment of the UAV network.

As already discussed in Chapter 2, the wireless community very often ignores the impact of interference when analysing UAV network performance; this assumption can lead to misleading conclusions about UAV network performance, in particular when analysing a dense deployment scenario where the spectrum scarcity issue is exacerbated. The work in this chapter specifically addresses these issues by modelling a UAV network deployment where the UAVs share the same spectrum resources and therefore cause interference with one another. By focusing on interference-limited networks rather than noise-limited networks we can characterise how the flexibility of the UAVs and their ability to create strong LOS channels can, in some situations, harm the resulting network performance rather than improve it. This, in turn, enables us to comment on which UAV deployment practices work and which do not, for a given set of network parameters and a given operating environment.

The contribution of the work presented in this chapter can be stated as follows:

1. We provide an analytical expression for the coverage probability for a typical UE served by a network of UAVs which are positioned above the centers of UE hotspots. Our model takes into account parameters such as building density, UE hotspot radius and UAV antenna beamwidth, and can represent different wireless fast-fading behaviours through generalised Nakagami-m fading.

2. We investigate the performance of a K-means clustering optimisation algorithm for optimising UAV placement with respect to UE locations; this algorithm is intended to be representative of the sort of placement optimisation that has been carried out extensively in the literature, as it optimally positions UAVs in a way which minimises the distances between them and their UEs. We compare our stochastic model against this heuristic algorithm, and demonstrate how our model can closely approximate the achieveable performance of a UAV network which is optimally positioned to serve UEs.

3. Using our model we demonstrate that there exists an optimum UAV height for a given UE hotspot radius, and that larger UE hotspots require UAVs to increase their heights to maximise performance. We also demonstrate how the optimum UAV height is almost unaffected by varying the density of UE hotspots and UAVs, while being heavily affected by varying the UAV antenna beamwidth. Our numerical results demonstrate how the presence of interference in the UAV network imposes a strict limitation on the range of heights that the UAV network can operate at.

4. We compare the performance of the UAV network deployed above the centers of UE hotspots against UAV networks which are deployed randomly with respect to UEs,

UAV networks which are deployed according to a K-means optimisation algorithm, as well as UAV networks deployed in a rectangular grid. This comparison allows us to demonstrate that for greater UAV heights and larger UAV densities the UAV network benefits more from UAVs positioning themselves with respect to each other rather than with respect to UE hotspots, due to the effect of mitigating interference. This leads us to conclude that there exists a certain UAV threshold density above which the UAV network should not position itself around UE hotposts but should instead spread out the UAVs as much as possible to reduce coverage overlap and interference.

As part of our mathematical analysis we provide expressions for the association probability of a typical UE, its coverage probability given a certain association type, and the overall coverage probability. The intermediate steps required for deriving the analytical expressions for the coverage probability involve expressing the coverage probability in terms of the Laplace transforms of the aggregate interference. This approach is similar to the methodology published in some of the works discussed in Section 2.2; where our work significantly departs from the state-of-the-art is in the characterisation of the association probability and the behaviour of the aggregate interference itself, due to the unique geometry of the intelligently positioned UAV network compared to a fixed terrestrial network.

This chapter is structured as follows. We open with a description of the system model, including a description of the UE spatial distribution model, the wireless channel propagation model, the antenna gain model, and the LOS probability model. We then derive an expression for the coverage probability for the case where the UAVs are positioned above the centers of UE hotspots. We provide a description of our heuristic optimisation algorithm and how it determines optimal UAV positions. We then generate numerical results using both our derived mathematical results, as well as simulations. We conclude the chapter with a high-level discussion of the results and the implications for UAV network design.

3.2 System Model

3.2.1 UAV Positioning

We consider a UAV network which has information on UE hotspot locations, and positions the UAVs accordingly. UE locations can be determined using several methods, for example

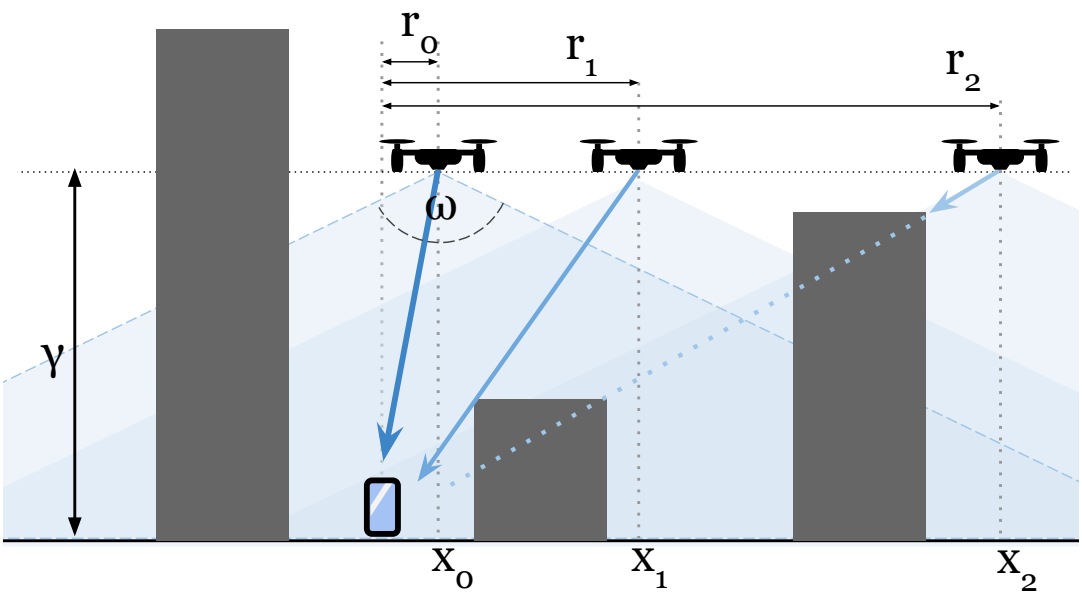

Figure 3.1: Side view showing UAVs in an urban environment at a height γ, with 2D coordinates x_0, x_1, x_2 and antenna beamwidth ω. The UE is serviced by the UAV with the strongest signal, while the remaining UAVs generate LOS and NLOS interference.

via self-reporting of GPS coordinates by the UEs themselves, or by measuring the UE signal at several receivers with known locations (either ground infrastructure, or the UAVs themselves) and calculating the signal origin. If the number of hotspots is known *a priori* (as may be the case where the hotspots are caused by a certain phenomenon which can be measured), then K-means clustering can be used to determine the hotspot centerpoints.

The UAV network positions the UAVs at a fixed height γ above ground, as depicted in Fig. 3.1. These UAVs may be positioned with respect to the UE hotspot locations, or with respect to one another in a regular grid, depending on the UAV positioning strategy selected by the UAV network operator. We denote the set of UAVs as $\Phi_u = \{x_0, x_1, ...\} \subset \mathbb{R}^2$ where x_i corresponds to the projected coordinates of the ith UAV onto $\mathbb{R}^2$.

3.2.2 User Distribution

We consider a scenario where a number of UEs congregate in an area of interest, creating several UE clusters which generate data demand. These clusters are referred to as UE hotspots, which the UAV network attempts to serve. We model the set of hotspots in the area of interest as a Matern Cluster Process (MCP) [56]. The number of UE hotspots in the area of interest is random, with average hotspot density λ_p. The location of each hotspot is random in $\mathbb{R}^2$ and is independent of the location of other hotspots; the set of hotspot centers is denoted as $\Phi_p = \{y_0, y_1, ...\} \subset \mathbb{R}^2$ where y_i corresponds to the ith

hotspot center. From the definition of the MCP, the set of hotspot centers Φ_p is a PPP with intensity λ_p. The UEs belonging to a hotspot i are positioned in a circle of radius $r_{\max}$ centered on the hotspot center y_i. Users are randomly and uniformly positioned inside this circle. In an urban environment we expect that UE hotposts will be restricted in size by buildings and other obstacles in the area: the hotspot radius $r_{\max}$ of the MCP is intended to represent this effect and how it causes UEs to be concentrated in certain geographic areas [91]. We perform our analysis for a reference UE, which is a randomly selected UE of a randomly selected hotspot. As the set of hotspots is stationary, we shift all UE locations and their corresponding hotspot centers such that the reference UE occupies the point at the origin of the plane. We denote $y_0 \in \Phi_p$ as the location of the reference UE's hotspot center.

3.2.3 Interference

The reference UE will be served by one of the UAVs in Φ_u. We assume full-buffer traffic with full frequency reuse, which results in all of the UAVs transmitting simultaneously on the same frequency bands. We also assume that the UAV network does not apply any interference mitigation techniques, and as a result each UAV other than the serving UAV can cause interference at the reference UE.

In the scenario under consideration, the UAV network uses spectrum resources which are orthogonal to the spectrum used by terrestrial cellular networks. As a result of this, the UAV-UE downlink is not affected by the underlying cellular network. This assumption is based on the on-going trend of allocating new spectrum bands exclusively for UAV communication [92], in addition to the allocation of new spectrum in the sub-6GHz bands for use by operators in next-generation cellular networks [93]. The UAV network under consideration takes advantage of these new spectral resources for communicating with the ground UE, such that it does not experience interference from any terrestrial cellular infrastructure in the area.

3.2.4 Channel Propagation

As the UAV network operates in an urban environment the wireless channel between a UAV and the reference UE will be affected by several environmental factors. The distance between the transmitting UAV and the reference UE will cause signal power attenuation. The position of a UAV relative to the reference UE will determine the antenna gain of the

received signal. The multipath behaviour of the signal will result in random fluctuations of the instantaneous signal strength. The buildings in the environment will block LOS between some of the UAVs and the reference UE, which will create two distinct wireless channel types, LOS and NLOS, with their own signal attenuation and multipath fading behaviours [56, 62, 65].

LOS Blockage Probability Model

To model a distribution of buildings in the environment we adopt the model in [65, 94], which defines an urban environment as a collection of buildings arranged in a square grid. There are β buildings per square kilometer, the fraction of area occupied by buildings to the total area is δ, and each building has a height which is a Rayleigh-distributed random variable with scale parameter κ. Let $T_i \in \{\mathtt{l}, \mathtt{n}\}$ denote whether UAV i has a LOS or NLOS channel type to the UE. The probability of a UAV i having LOS channel to the reference UE ($T_i = \mathtt{l}$) is given in [94] as

$$\mathbb{P}_{\mathtt{l}}(r_i) = \prod_{n=0}^{\max(0,d-1)} \left(1 - \exp\left(-\frac{\left(\gamma - \frac{(n+1/2)\gamma}{d}\right)^2}{2\kappa^2}\right)\right), \tag{3.1}$$

where $r_i = ||x_i||$ is the horizontal distance to the UAV i and $d = \left\lfloor r_i\sqrt{\beta\delta}\right\rfloor$. It follows that the NLOS probability $\mathbb{P}_{\mathtt{n}}(r_i) = 1 - \mathbb{P}_{\mathtt{l}}(r_i)$. A variety of LOS probability models have been considered by the wireless community, typically applied to scenarios where UAVs operate at heights in the order of several kilometers. We explore the performance of our chosen model against the popular elevation angle-based model proposed by the authors of [44] in Fig. 3.6 in the numerical results section.

Transmit Power and Antenna Gain

We assume UAVs have identical transmit power μ and a directional antenna with beamwidth ω. The main beam illuminates the area directly beneath the UAV. We assume a uniform and rotationally symmetric beam pattern; using the approximations (2-26) and (2-49) in [95] and assuming perfect antenna radiation efficiency the antenna gain η in the direction of the reference UE from UAV i can be expressed as

$$\eta = \begin{cases} \mu 16\pi/(\omega^2), & \text{if} \quad r_i \leq u(\omega,\gamma), \\ 0, & \text{if} \quad r_i > u(\omega,\gamma), \end{cases} \tag{3.2}$$

where $u(\omega,\gamma) = \tan(\omega/2)\gamma$.

Received Signal Strength

The instantaneous received signal strength from a UAV i at x_i at the reference UE is:

$$S_i = \eta H_{T_i} l(r_i, \gamma, \alpha_{T_i}), \tag{3.3}$$

where H_{T_i} is the Nakagami-m random multipath fading component experienced by the signal from UAV i, $l(r_i, \gamma, \alpha_{T_i}) = (r_i^2 + \gamma^2)^{-\alpha_{T_i}/2}$ is the pathloss function, and α_{T_i} is the pathloss exponent. Note that the channel type T_i will determine the value of the pathloss exponent α_{T_i} as well as the multipath fading H_{T_i}. In this work we model the multipath fading using the Nakagami-m model, as this model allows for convenient mathematical analysis, while at the same time being a generalised fading model which can represent a variety of radio environments [62][96]. For the special case where $m_{T_i} = 1$ the Nakagami-m model becomes equivalent to the Rayleigh model, whereas the Rician-K model with parameter K can be closely approximated by selecting m_{T_i} such that $m_{T_i} = (K+1)^2/(2K+1)$ [96]. This allows us to align our model with empirically-validated models in [97][98].

3.2.5 Serving UAV Selection

The serving UAV is the one from which the reference UE observes the highest received power. The index of the serving UAV is a random variable which we denote as V

$$V = \underset{\{i \in \mathbb{N}: x_i \in \Phi_u\}}{\operatorname{argmax}} \{\bar{S}_i\}, \tag{3.4}$$

where $\bar{S}_i$ denotes the long-term average[5] power received from the ith UAV located at $x_i \in \Phi_u$. It follows that, given $V = v$, the serving UAV location is denoted as x_v, its horizontal distance to the UE is r_v, and so on.

The SINR for the reference UE can be described as:

$$\text{SINR} = S_v/(I + \sigma^2), \tag{3.5}$$

where, given $V = v$, $S_v = \eta H_{T_v} l(r_v, \gamma, \alpha_{T_v})$ is the signal from the serving UAV a distance r_v away with channel type T_v, I denotes the aggregate signal power received from all UAVs in Φ_u other than the serving UAV v, and σ^2 denotes the noise power.

[5]Since cell-level association acts on the order of seconds, we assume that any fast fading effects (like the multipath fading) will be averaged out.

The reference UE is said to be successfully served by the UAV network if it establishes a downlink channel with a SINR above some minimum threshold θ. We refer to the probability of the SINR exceeding this threshold as the coverage probability

$$\mathbb{P}_c(\theta) = \mathbb{P}(\text{SINR} > \theta). \tag{3.6}$$

Using the Shannon capacity bound [99][Eq. 9.62] the Spectral Efficiency (SE) of the UAV network can be expressed in terms of the SINR as

$$\text{SE} = \mathbb{E}[\log_2(1 + \text{SINR})]. \tag{3.7}$$

3.3 Mathematical Analysis

In this chapter we consider several UAV placement strategies, as this allows for our analysis to be applicable to a wide variety of UAV network use cases. For the special case when the UAVs are positioned exactly above each hotspot center we derive analytical expressions for the coverage probability provided by the network of UAVs acting as small cell access points.

In subsection 3.3.1 we explicitly define how the UAVs are positioned with respect to the reference UE on the ground. The probabilistic distribution of the horizontal distances between UAVs and UEs forms the foundation of our entire analysis, as these distances determine the probability of LOS blockage, and ultimately which UAV the UE associates with.

The reference UE associates with the UAV with the strongest signal, following Eq. (3.4). For example, if the UE associates to the UAV above its hotspot center then this is a consequence of the other UAVs being too far away, or being obstructed by buildings. In subsection 3.3.2 we derive the expressions for the probability that the UE associates to a certain candidate UAV, given the location of that candidate UAV and its channel type. These association probability expressions will form a part of the coverage probability expression which we derive at the end of this section.

In subsection 3.3.3 we approach the random aggregate interference power. In our system model we describe the wireless channels as being affected by random Nakagamim fading, independently of one another. Prior work from the wireless community has shown that, given this type of random fading, the coverage probability of a reference UE can be expressed as a function of higher-order derivatives of the Laplace transform of

the aggregate interference power [62]. In subsection 3.3.3 we derive expressions for the Laplace transform of the aggregate interference and demonstrate how the higher-order derivatives can be obtained.

In subsection 3.3.4 we bring our prior derivations together and produce an expression for the coverage probability of the reference UE, in terms of the association probability, the higher-order derivative of the aggregate interference Laplace transform, and the distance distributions to the serving UAV.

3.3.1 UAV Placement and Distance Distribution

We consider a scenario where the UAV network serves the UE hotspots by positioning exactly one UAV above the center of each hotspot. As a result, both the density and coordinates of the UAVs match those of the hotspots exactly, with $\Phi_u \equiv \Phi_p$ and $\lambda_u \equiv \lambda_p$. It follows that the reference UE at the origin will have a UAV above its associated hotspot center; we denote this UAV with the index 0 and its location as $x_0 \in \Phi_u$. We partition the set Φ_u into the sets $\{x_0\}$ and $\Phi_u^! = \Phi_u \setminus \{x_0\}$, containing the reference UE hotspot UAV and all the remaining UAVs, respectively. Note that, following Slivnyak's theorem [91][Theorem 8.10], the set of UAVs $\Phi_u^!$ remains a PPP with intensity λ_u.

The horizontal distance between the reference UE and the UAV at its hotspot center is denoted as random variable R_0. When the UEs in a hotspot are distributed according to an MCP the pdf of R_0 is provided in [56], as

$$f_{R_0}(r) = \begin{cases} 2r/r_{\max}^2, & \text{if} \quad 0 \leq r \leq r_{\max}, \\ 0, & \text{otherwise}, \end{cases} \tag{3.8}$$

where $r_{\max}$ is the radius of a UE hotspot. The UE may be served by one of the UAVs in $\Phi_u^!$ if it provides the strongest signal. The UAVs in the set $\Phi_u^!$ have a mixture of LOS and NLOS channels to the reference UE; the subsequent derivations require us to consider the behaviour of LOS and NLOS UAVs in $\Phi_u^!$ separately. From the definition of the PPP, the set $\Phi_u^!$ can be separated into multiple independent PPP sets using a thinning procedure [91][Theorem 2.36]. With thinning, each UAV in the set $\Phi_u^!$ is removed (or "thinned") from the set with a certain probability. We use this thinning procedure to separate $\Phi_u^!$ into two disjoint sets, one which contains all the LOS UAVs, and the other all the NLOS UAVs. These sets are denoted as $\Phi_{\mathtt{l}} = \{x_i \in \Phi_u^! : T_i = \mathtt{l}\}$ and $\Phi_{\mathtt{n}} = \{x_i \in \Phi_u^! : T_i = \mathtt{n}\}$, respectively, with the thinning probability being given by the LOS function $\mathbb{P}_{\mathtt{l}}(r)$. Both sets are PPP with intensity functions $\lambda_{\mathtt{l}}(x) = \mathbb{P}_{\mathtt{l}}(||x||)\lambda_u$ and $\lambda_{\mathtt{n}}(x) = \mathbb{P}_{\mathtt{n}}(||x||)\lambda_u$, respectively.

The pdf of the distance to the closest UAV in $\Phi_{\mathtt{l}}$ and $\Phi_{\mathtt{n}}$ is defined in [91] as

$$f_{R_j}(r) = 2\pi\lambda_j(r) r \exp\left(-2\pi \int_0^r \lambda_j(r) r \mathrm{d}r \right), \quad j \in \{\mathtt{l}, \mathtt{n}\}, \tag{3.9}$$

where R_j denotes the distance to the closest UAV in Φ_j.

3.3.2 Association Probability

If the UE associates with a UAV in Φ_j it will associate to the closest UAV in the set, as all of the remaining UAVs in the set will, by definition, provide a weaker signal to the UE. The pdf of the serving UAV distance will follow one of the distance distributions given in in Eq. (3.8) and Eq. (3.9), depending on which UAV type the UE associates with. The UE will associate to a UAV of a given type if there are no other UAVs that provide a stronger signal to it. This is referred to as the association probability and is given below.

Conditioned on the serving UAV being a distance r away from the UE with a channel of type t, the association probability is the probability that the serving UAV is either the UE hotspot UAV at x_0 or one of the remaining UAVs at Φ_t.

Proposition 1. The probability that the UE's serving UAV is its hotspot center UAV at x_0, when the serving UAV is a distance r away with channel type t, is expressed as

$$\mathcal{A}_{\mathtt{0}}(t, r) = \mathbb{P}\left(V = 0 \middle| T = t, R_0 = r \right) = \left(\prod_{j \in \{\mathtt{l}, \mathtt{n}\}} \exp\left(-2\pi \int_0^{c_j(t,r)} \lambda_j(z) z \mathrm{d}z \right) \right). \tag{3.10}$$

Proof. The hotspot center UAV at x_0 will have the strongest received signal at the reference UE if the closest UAVs in $\Phi_{\mathtt{l}}$ and $\Phi_{\mathtt{n}}$ are not close enough to provide a stronger signal. The probability $\mathcal{A}_{\mathtt{0}}(t, r)$ is then given as

$$\begin{aligned} \mathcal{A}_{\mathtt{0}}(t, r) &= \mathbb{P}\Big((r^2 + \gamma^2)^{-\alpha_t/2} > \max\left((R_{\mathtt{l}}^2 + \gamma^2)^{-\alpha_{\mathtt{l}}/2}, (R_{\mathtt{n}}^2 + \gamma^2)^{-\alpha_{\mathtt{n}}/2} \right) \Big) \\ &\overset{(a)}{=} \bigcap_{j \in \{\mathtt{l}, \mathtt{n}\}} \mathbb{P}\Big(R_j > c_j(t, r) \Big) \overset{(b)}{=} \left(\prod_{j \in \{\mathtt{l}, \mathtt{n}\}} \exp\left(-2\pi \int_0^{c_j(t,r)} \lambda_j(z) z \mathrm{d}z \right) \right), \end{aligned} \tag{3.11}$$

where (a) comes from the fact that $R_{\mathtt{l}}$ and $R_{\mathtt{n}}$ are distributed independently of each other and (b) comes from the definition of the void probability of a PPP [91]. Here, $c_j(t,r)$ denotes the lower bounds on minimum distances the UAVs can have to the UE while still giving a weaker signal than the serving UAV, which we can express as follows

$$c_j(t,r)=\begin{cases} r, & \text{if} \quad j=t, \\ \min(u(\omega,\gamma), \sqrt{(r^2+\gamma^2)^{\alpha_{\mathtt{n}}/\alpha_{\mathtt{l}}}-\gamma^2}), & \text{if} \quad j=\mathtt{l}, t=\mathtt{n}, \\ \sqrt{\max(0,(r^2+\gamma^2)^{\alpha_{\mathtt{l}}/\alpha_{\mathtt{n}}}-\gamma^2)}, & \text{if} \quad j=\mathtt{n}, t=\mathtt{l}, \end{cases} \tag{3.12}$$

□

Proposition 2. The probability that the serving UAV belongs to the set Φ_t is denoted as

$$\mathcal{A}_i(t,r)=\mathbb{P}\left(V=i\middle|T=t,R_t=r\right)=\exp\left(-2\pi\int_0^{c_j(t,r)}\lambda_j(z)z\mathrm{d}z\right)\mathcal{B}(t,r), \quad i\neq 0, j\neq t \tag{3.13}$$

where $\mathcal{B}(t,r)$ denotes the probability that the hotspot center UAV at x_0 is providing a weaker signal than the serving UAV from Φ_t, and is expressed as

$$\mathcal{B}(t,r)=1-\left(\sum_{k\in\{\mathtt{l},\mathtt{n}\}}\int_0^{c_k(t,r)}\mathbb{P}_k(z)f_{R_0}(z)\mathrm{d}z\right). \tag{3.14}$$

Proof. $\mathcal{A}_i(t,r)$ is the probability that there are no UAVs in the set $\Phi_j\cup\{x_0\}$, with $j\neq t$, which are close enough to the UE to provide a stronger signal than the UAV a distance

r away with channel type t.

$$\begin{aligned}\mathcal{A}_i(t,r) &= \mathbb{P}\Big(R_j > c_j(t,r)\Big)\mathbb{P}\Big(\bar{S}_0 < \bar{S}_i\Big) \\ &\overset{(a)}{=} \mathbb{P}\Big(R_j > c_j(t,r)\Big)\Big(1-\Big(\mathbb{P}(R_0 \le c_{\mathtt{l}}(t,r), T_0 = \mathtt{l}) + \mathbb{P}(R_0 \le c_{\mathtt{n}}(t,r), T_0 = \mathtt{n})\Big)\Big) \\ &= \exp\left(-2\pi\int_0^{c_j(t,r)} \lambda_j(z) z \mathrm{d}z\right)\left(1-\left(\sum_{k\in\{\mathtt{l},\mathtt{n}\}}\int_0^{c_k(t,r)} \mathbb{P}_k(z) f_{R_0}(z)\mathrm{d}z\right)\right), \end{aligned} \tag{3.15}$$

where (a) comes from the probability of the hotspot center UAV providing a weaker signal, which is equivalent to the probability that the hotspot center UAV is neither LOS and closer than $c_{\mathtt{l}}(t,r)$, nor NLOS and closer than $c_{\mathtt{n}}(t,r)$. □

3.3.3 Laplace Transform of Aggregate Interference and Noise

The SINR is affected by the aggregate interference I as well as the noise σ^2, and as I is a random variable the sum of the two components is also a random variable. In this subsection we provide an expression for the k-th derivative of the Laplace transform of the aggregate interference and noise $\mathcal{L}_{(I+\sigma^2)}$; this will be used for derivations in the next subsection.

Proposition 3. The k-th derivative of the Laplace transform $\mathcal{L}_{(I+\sigma^2)}$ is obtained as

$$\frac{\mathrm{d}^k \mathcal{L}_{(I+\sigma^2)}(s)}{\mathrm{d}s^k} = \sum_{i_0+i_{\mathtt{l}}+i_{\mathtt{n}}+i_\sigma=k} \frac{k!}{i_0! i_{\mathtt{l}}! i_{\mathtt{n}}! i_\sigma!} \frac{\mathrm{d}^{i_0}\mathcal{L}_{I_0}(s)}{\mathrm{d}s^{i_0}} \frac{\mathrm{d}^{i_{\mathtt{l}}}\mathcal{L}_{I_{\mathtt{l}}}(s)}{\mathrm{d}s^{i_{\mathtt{l}}}} \frac{\mathrm{d}^{i_{\mathtt{n}}}\mathcal{L}_{I_{\mathtt{n}}}(s)}{\mathrm{d}s^{i_{\mathtt{n}}}} \frac{\mathrm{d}^{i_\sigma}\exp(-s\sigma^2)}{\mathrm{d}s^{i_\sigma}}, \tag{3.16}$$

where $\mathcal{L}_{I_{\mathtt{l}}}$, $\mathcal{L}_{I_{\mathtt{n}}}$ and $\mathcal{L}_{I_0}$ are the Laplace transforms of the aggregate interference from $\Phi_{\mathtt{l}}$, $\Phi_{\mathtt{n}}$ and x_0, respectively. The sum is over all the combinations of non-negative integers i_0,$i_{\mathtt{l}}$, $i_{\mathtt{n}}$ and i_σ that add up to k.

Proof. The aggregate interference power I is the sum of the interference power $I_{\mathtt{l}}$, $I_{\mathtt{n}}$ and I_0 from the UAVs in $\Phi_{\mathtt{l}}$, $\Phi_{\mathtt{n}}$ and x_0, respectively. Recall that, from the definition

of the thinning procedure [91][Theorem 2.36], the sets $\Phi_{\mathtt{l}}$ and $\Phi_{\mathtt{n}}$ are independent PPPs. This means that the number and position of interferers of one type has no impact on the number and position of interferers of the other type. As a result, the sums of the received interference signal powers $I_{\mathtt{l}}$ and $I_{\mathtt{n}}$, are random variables that are independently distributed with respect to one another, as well as I_0. This means that the Laplace transform of the aggregate interference and noise $\mathcal{L}_{(I+\sigma^2)}$ can be represented as the product of Laplace transforms $\mathcal{L}_{I_{\mathtt{l}}}$, $\mathcal{L}_{I_{\mathtt{n}}}$ and $\mathcal{L}_{I_0}$, as well as $\exp(-s\sigma^2)$. The derivative of $\mathcal{L}_{(I+\sigma^2)}$ can be expressed in the form given in Eq. (3.16) following the general Leibniz rule. □

Remark 1: If the UE is served by the hotspot center UAV at x_0 ($V = 0$) then I_0 will be 0 and $\mathcal{L}_{I_0}$ will be 1, as the UAV will not create interference for itself.

Proposition 4. The Laplace transform of the interference I_0, given $V = i, T_V = t, R_V = r$, is given as Eq. (3.17)

$$\mathcal{L}_{I_0}(s) = \frac{1}{(r_{\max}^2)\mathcal{B}(t,r)} \sum_{j\in\{\mathtt{l},\mathtt{n}\}} (\mathcal{C}_j(s) + \mathcal{D}_j), \tag{3.17}$$

where

$$\mathcal{C}_j(s) = \sum_{q=\left\lfloor c_j(t,r)\sqrt{\beta\delta}\right\rfloor}^{\left\lfloor \min(r_{\max},u(\omega,\gamma))\sqrt{\beta\delta}\right\rfloor} \mathbb{P}_j(l) \left((u^2-l^2) + \sum_{k=1}^{m_j} \binom{m_j}{k} (-1)^k \right.$$
$$\cdot \left((u^2+\gamma^2)\,{}_2\mathrm{F}_1\left(k, \frac{2}{\alpha_j}; 1+\frac{2}{\alpha_j}; -\frac{m_j(u^2+\gamma^2)^{\alpha_j/2}}{\eta s}\right) \right.$$
$$\left.\left. - (l^2+\gamma^2)\,{}_2\mathrm{F}_1\left(k, \frac{2}{\alpha_j}; 1+\frac{2}{\alpha_j}; -\frac{m_j(l^2+\gamma^2)^{\alpha_j/2}}{\eta s}\right)\right)\right), \tag{3.18}$$

For the case when $c_j(t,r) < \min(r_{\max}, u(\omega,\gamma))$, with ${}_2\mathrm{F}_1(a,b;c;d)$ denoting the Gauss hypergeometric function, $l = \max(c_j(t,r), q/\sqrt{\beta\delta})$ and $u = \min(r_{\max}, u(\omega,\gamma), (q+1)/\sqrt{\beta\delta})$.

If $c_j(t,r) \geq \min(r_{\max}, u(\omega,\gamma))$ then $\mathcal{C}_j(s) = 0$.

$\mathcal{D}_j$ is given as

$$\mathcal{D}_j = \quad 2 \int\limits_{\max(c_j(t,r),u(\omega,\gamma))}^{r_{\max}} \mathbb{P}_j(z) z \mathrm{d}z, \tag{3.19}$$

if $r_{\max} > \max(c_j(t,r), u(\omega,\gamma))$ and 0 otherwise. Note that $\mathcal{D}_j$ is not a function of s.

Proof. The proof is given in Appendix A. □

Remark 2: The Laplace transform $\mathcal{L}_{(I+\sigma^2)}(s)$ requires higher-order derivatives of the Laplace transform $\mathcal{L}_{I_0}(s)$; the required analytical expressions are given in Appendix B.

Proposition 5. The Laplace transform $\mathcal{L}_{I_j}(s)$ where $j \in \{\mathtt{l}, \mathtt{n}\}$, conditioned on $T_V = t$ and $R_V = r$, is given as

$$\begin{aligned}\mathcal{L}_{I_j}(s) = \exp\Bigg(&- \pi\lambda_u \sum_{q=\left\lfloor c_j(t,r)\sqrt{\beta\delta}\right\rfloor}^{\left\lfloor u(\omega,\gamma)\sqrt{\beta\delta}\right\rfloor} \mathbb{P}_j(l) \sum_{k=1}^{m_j} \binom{m_j}{k} (-1)^{k+1} \\ &\cdot \Bigg((u^2+\gamma^2)\, {}_2\mathrm{F}_1\left(k, \frac{2}{\alpha_j}; 1+\frac{2}{\alpha_j}; -\frac{m_j(u^2+\gamma^2)^{\alpha_j/2}}{\eta s}\right) \\ &- (l^2+\gamma^2)\, {}_2\mathrm{F}_1\left(k, \frac{2}{\alpha_j}; 1+\frac{2}{\alpha_j}; -\frac{m_j(l^2+\gamma^2)^{\alpha_j/2}}{\eta s}\right)\Bigg)\Bigg),\end{aligned} \tag{3.20}$$

where $l = \max(c_j(t,r), q/\sqrt{\beta\delta})$ and $u = \min(u(\omega,\gamma), (q+1)/\sqrt{\beta\delta})$, as before.

Proof. The proof is given in Appendix C. □

Remark 3: The expression for the higher-order derivative of $\mathcal{L}_{I_j}(s)$ with respect to s is given in Appendix D.

3.3.4 General model

In this subsection we present the main analytical result of this chapter.

Theorem 1. The coverage probability of the reference UE served by a UAV network that positions itself above UE hotspots is given as

$$\mathbb{P}_c(\theta,\gamma,\lambda_u,\omega,r_{\max}) = \sum_{t\in\{\mathtt{l},\mathtt{n}\}} \Bigg(\int_0^{u(\omega,\gamma)} \mathcal{A}_0(t,r) \sum_{k=0}^{m_t-1} (-1)^k \frac{s_r^k}{k!} \frac{\mathrm{d}^k \mathcal{L}_{(I+\sigma^2)}(s_r)}{\mathrm{d}s_r^k} \mathbb{P}_t(r) f_{R_0}(r) \mathrm{d}r + \int_0^{u(\omega,\gamma)} \mathcal{A}_i(t,r) \sum_{k=0}^{m_t-1} (-1)^k \frac{s_r^k}{k!} \frac{\mathrm{d}^k \mathcal{L}_{(I+\sigma^2)}(s_r)}{\mathrm{d}s_r^k} f_{R_t}(r) \mathrm{d}r \Bigg). \quad (3.21)$$

Proof. The proof is given in Appendix E. □

For comparison against a network of UAVs positioned according to a PPP at a fixed height, we present the following corollary.

Corollary 1. The coverage probability of the reference UE when served by a UAV network that is positioned according to a PPP independently of hotspot locations is given as

$$\mathbb{P}_c(\theta,\gamma,\lambda_u,\omega) = \sum_{t\in\{\mathtt{l},\mathtt{n}\}} \int_0^{u(\omega,\gamma)} \mathcal{A}_i(t,r) \sum_{k=0}^{m_t-1} (-1)^k \frac{s_r^k}{k!} \frac{\mathrm{d}^k \mathcal{L}_{(I+\sigma^2)}(s_r)}{\mathrm{d}s_r^k} f_{R_t}(r) \mathrm{d}r. \quad (3.22)$$

Proof. If the UAV network is distributed independently of the hotspot centers then the reference UE does not have a UAV above its hotspot center, and can only be served by a UAV from the set $\Phi_u^!$. The expression in Eq. (3.22) is obtained by setting $r_{\max} \to \infty$, which has the effect of setting $f_{R_0}(r) \to 0$ for the range $0 \le r \le u(\omega,\gamma)$, $\mathcal{B}(t,r)$ and $\mathcal{L}_{I_0} \to 1$ and which reduces the expression given in Eq. (3.21) to the one in Eq. (3.22). □

Remark 4: For our system model we have assumed that all of the UE hotspots have the same radius $r_{\max}$. For certain scenarios this assumption can be relaxed. If the reference UE belongs to a hotspot whose radius $R_{\max}$ is a random variable with some arbitrary pdf $f_{R_{\max}}(r_{\max})$, then the coverage probability of that reference UE is given as

$$\mathbb{P}_c(\theta,\gamma,\lambda_u,\omega) = \int_0^{\infty} \mathbb{P}_c(\theta,\gamma,\lambda_u,\omega,r_{\max}) f_{R_{\max}}(r_{\max}) \mathrm{d}r_{\max}. \quad (3.23)$$

The reference UE's coverage probability is only impacted by the radius of its own hotspot, as that affects the pdf of the distance between the reference UE and the hotspot center UAV R_0. The radii of the neighbouring hotspots do not affect the location of the hotspot centers (and therefore the neighbouring UAV locations).

3.4 Heuristic Optimisation of UAV Positions

The stochastic model proposed in this chapter represents a scenario where UAV small cells are intelligently positioned above the exact centers of UE hotspots. In some scenarios the coordinates of the hotspot centers may not be known to the network in advance, it would only be aware of the locations of the UEs themselves. The intelligent UAV small cell positioning would take the form of an optimisation problem (such as those discussed in Section 2.1) where the UAV small cells are positioned with respect to the UE locations in a way that satisfies some objective function. In this section we describe an algorithm which can optimally position a given number of UAV small cells above a set of UEs in a manner that minimises the distances between the set of UEs and their nearest UAVs. In a scenario where the UEs are distributed in hotspots this would result in the UAVs positioning themselves close to the hotspot centers of the UEs.

Let us denote the set of UEs to be served by UAVs as $\Phi_e = \{e_1, e_2, ..., \} \subset \mathbb{R}^2$. Given K available UAVs we wish to assign all UEs in Φ_e to K subsets, one for each UAV. Given an initial set of UAV coordinates $\Phi_u = \{x_1, x_2, ..., x_K\} \subset \mathbb{R}^2$ a Voronoi region is defined as:

$$v_i = \{w \in \mathbb{R}^2 : ||w, x_i|| < ||w, x_j|| \ \forall j \neq i\}. \tag{3.24}$$

We define the UE subset $\Phi_{v_i} \subset \Phi_e$ as the set of UEs which are located inside of the associated Voronoi cell

$$\Phi_{v_i} = \Phi_e \cap v_i, \tag{3.25}$$

and the centroid of Φ_{v_i} is defined as the mean of the coordinates of the UEs belonging to the subset

$$\chi_i = \frac{\sum_{e \in \Phi_{v_i}} e}{|\Phi_{v_i}|}. \tag{3.26}$$

We wish to select the points Φ_u which generate Voronoi cells and UE subsets such that

$$\min \sum_{i=1}^{K} \sum_{e \in \Phi_{v_i}} ||e, \chi_i||. \tag{3.27}$$

In other words, we wish to partition Φ_e into K UE subsets such that the sum of Euclidean distances between each UE in the subset and the subset centroid is minimised. The Hartigan-Wong K-Means clustering algorithm [100] is selected to carry out this optimisation through a heuristic iterative process. Taking K initial points Φ_u the algorithm assigns all of the UEs to the nearest point and generates subsets, then it calculates the centroids for each generated subset. In the second step the algorithm considers for every UE the change to the sum of Euclidean distances that would be observed if the UE was moved from its current subset to the subset with the next closest centroid. Whenever moving a UE from one subset to another decreases the total sum of Euclidean distances the subset assignments are updated and the centroids are re-calculated. Once all of the UEs have been checked the points Φ_u are set to the values of the centroids and another iteration is carried out. This process repeats itself until none of the subsets is updated over several iterations, or until a certain maximum number of iterations have been carried out.

3.5 Numerical Results

In this section we evaluate the performance of the UAV small cell network under multiple UAV placement strategies, using the mathematical expressions derived in the mathematical analysis section as well as simulations in the R software environment. We consider a simulation window of $16\,\text{km}^2$, with a $1\,\text{km}^2$ area of interest in the center. The larger simulation window relative to the area of interest ensures that we eliminate any boundary effects that may be experienced by a UE near the edge of the area of interest, for the range of UAV heights and hotspot radii under consideration. We simulate random distributions of UE hotspots inside the window. The UAVs are positioned according to one of several positioning strategies, and we calculate the SINR for the UEs inside the area of interest. This is repeated across 10,000 Monte Carlo (MC) trials, and from these trials we calculate the coverage probability values. Unless stated otherwise the parameters used for the numerical results are from Table 3.1. The values of the Nakagami-m fading parameters m and the path loss exponents α are chosen to fall inside the range of values reported by the field trials in [98][101]. Fig. 3.2 shows a typical simulation of UEs in the area of interest and the hotspot centers where we can position the UAVs.

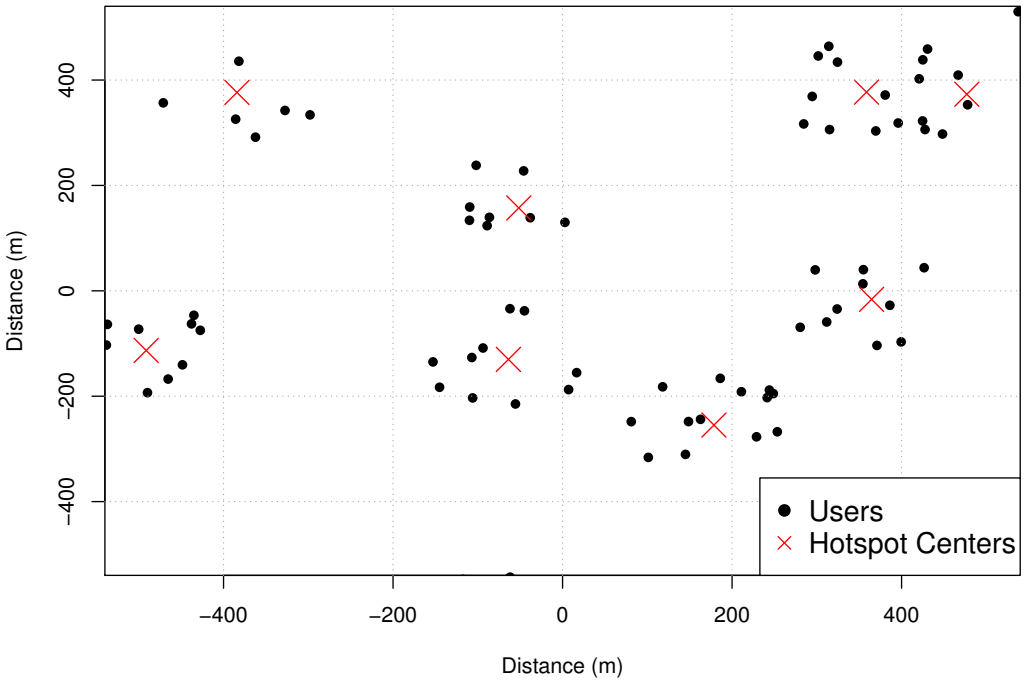

Figure 3.2: A simulation of UE hotspots in the area of interest. Black dots denote UEs; red marks denote MCP hotspot centers.

3.5.1 Independently Positioned UAVs

Before exploring the performance of a UAV network that is positioned above the centers of UE hotspots we are interested in a more basic scenario, where the UAVs in the UAV network are positioned entirely independently of UE locations, or one another. This corresponds to the special case outlined in the corollary of Theorem 1 where the reference

Table 3.1: Access Link Numerical Result Parameters

Parameter	Symbol	Value
Antenna beamwidth	ω	150 deg
LOS pathloss exponent	$\alpha_{\mathtt{l}}$	2.1
NLOS pathloss exponent	$\alpha_{\mathtt{n}}$	4
LOS Nakagami-m fading term	$m_{\mathtt{l}}$	3
NLOS Nakagami-m fading term	$m_{\mathtt{n}}$	1
UAV Transmit power	p	0.1 W
Noise power	σ^2	10^{-9} W
Number of buildings per square km.	β	300 /km^2
Fraction of total area occupied by buildings	δ	0.5
Building height scale parameter	κ	20 m
SINR threshold	θ	0 dB

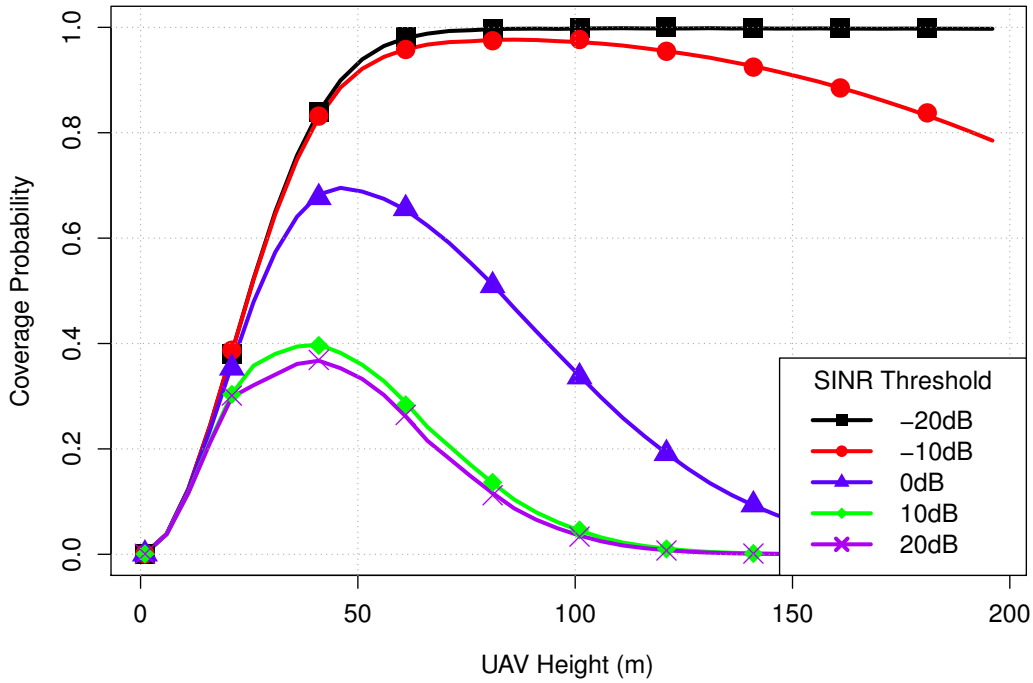

Figure 3.3: Coverage probability given a UAV density of 25 /km^2

UE has no UAV at its hotspot center and is always served by an independently positioned UAV. We generate random deployments of UAVs across multiple MC trials and record the mean coverage probability values. In Figs. 3.3 to 3.6, solid lines denote the analytical values for the coverage probability (from Eq. (3.22)) and the markers denote results from MC trials.

Fig. 3.3 shows the effect of varying the UAV height on the coverage probability, given different SINR threshold values. We can see that initially the coverage probabilities for all the SINR thresholds improve as we increase the height. This is due to the UAVs increasing their coverage areas, which maximises the probability that there is at least one UAV within range of the UE and providing sufficient SINR. Past a certain height, however, coverage probability starts to decrease with increased height. This shows how the signals are more vulnerable to the increasing number of LOS interferers that appear as the UAV heights increase.

In Fig. 3.4 we consider how increasing the UAV height affects the coverage probability, for UAV networks of different densities. The figure shows how for each UAV density there is a corresponding height which maximises the coverage probability, and that this height decreases as the density increases. This is explained by considering the effect of the buildings on the networks. At low densities the serving UAV for the reference UE may be concealed behind several buildings, and increasing the UAV height increases the chances

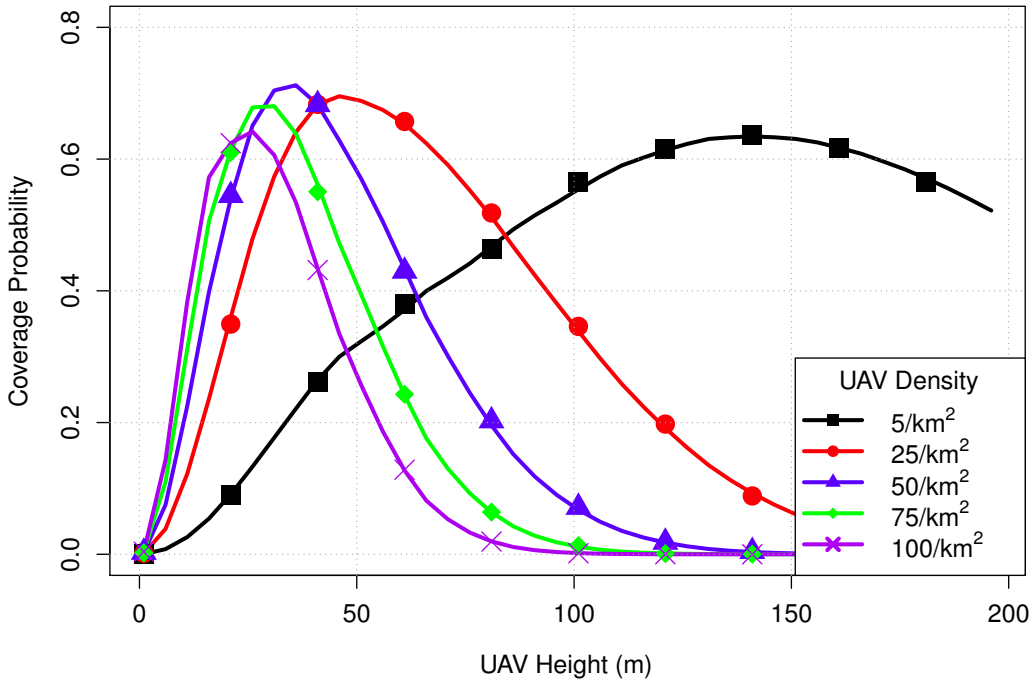

Figure 3.4: Coverage probability for multiple densities given a threshold of 0 dB

of establishing an LOS channel. The low number of interferers within range means that as the channel between a UE and its serving UAV improves, the net impact on the network performance is positive. In a high density network the serving UAV to a UE is likely to be close enough that there are few buildings to interfere with the signal. The buildings in this scenario do not impede the serving UAV signal but instead shield the UE from interfering UAVs a further distance away. Increasing the UAV height then will expose the UE to these interferers while at the same time worsening the serving signal, resulting in a drop in coverage.

In Fig. 3.5 we demonstrate the effect of the UAV antenna beamwidth on the coverage probability. The coverage curves suggest that narrower beamwidths perform best at larger UAV heights. This is due to the effect of the beawmidths on the probability of the UE being within range of a UAV: narrow beamwidth UAVs create a narrow coverage cone and as a result must operate at larger heights to ensure that UEs can be within range of service. We see that each beamwidth value has an associated optimum UAV height for a given SINR threshold, UAV density and building environment.

In Fig. 3.6 we show the probability that a UE that is within range of the network will have an LOS link to the serving UAV under our LOS model and the sigmoid approximation adopted in [44], given two different UAV densities. The sigmoid model gives the LOS probability as a function of the vertical angle between the UAV and the UE, and as such

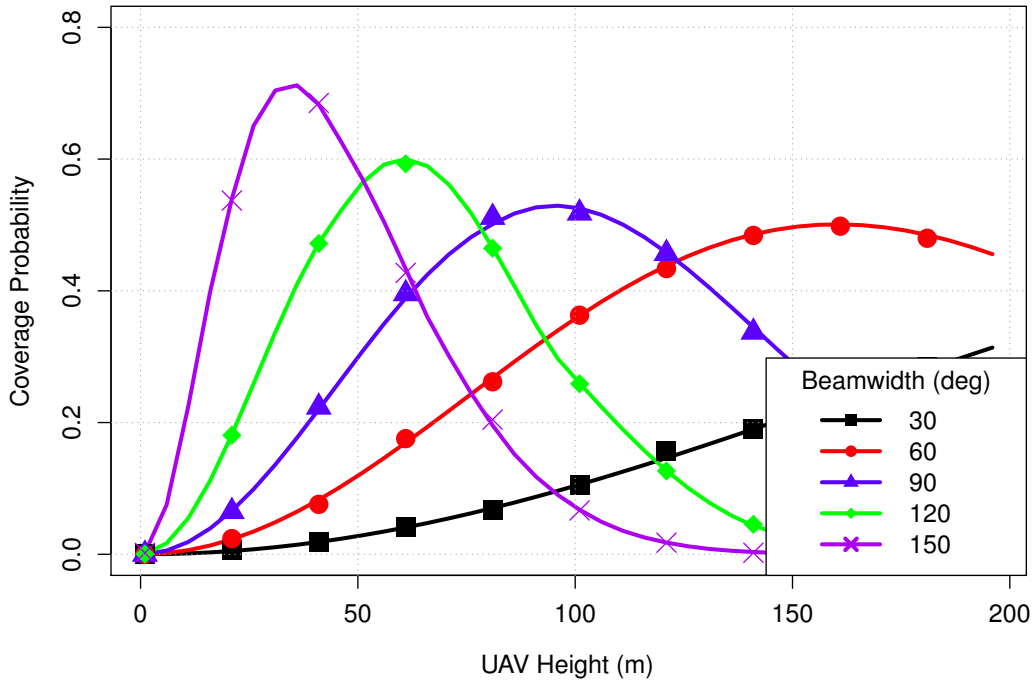

Figure 3.5: Coverage probability given a threshold of 0 dB and UAV density of 50 /km^2

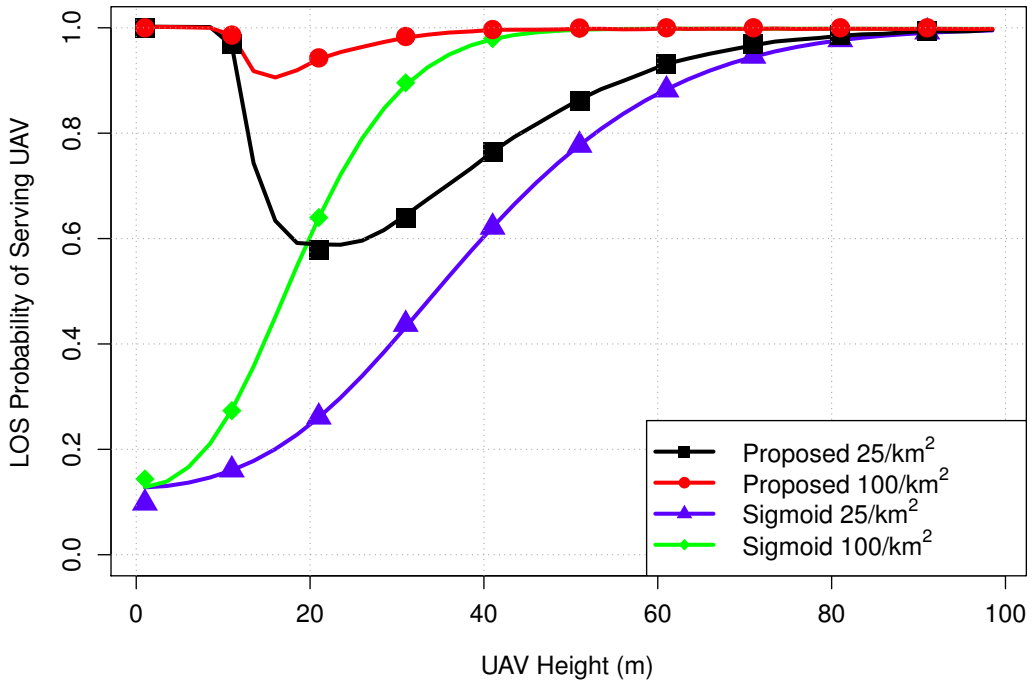

Figure 3.6: Probability of an LOS channel between a UE and its serving UAV

when the UAV is close to the ground the LOS probability to its UEs approaches zero, despite the fact that the UAV coverage cone is very small and therefore the UEs are

very close to the UAV. As the height increases this probability steadily improves due to the increasing vertical angle. Our model captures a more realistic behaviour of the LOS probability; when the UAV is very low to the ground, due to the size of its coverage cone its UEs are close enough that no LOS-blocking buildings are in the way, ensuring an LOS probability approaching unity. As the height increases the increasing coverage cone allows UEs further away to associate to the UAV, resulting in more UEs behind buildings being served by the UAV, which negatively affects the LOS probability. Finally, as the UAV ascends above the majority of buildings this LOS probability steadily improves to reflect the fact that there will be fewer buildings tall enough to block the UAV-UE link.

3.5.2 UAVs Positioned Above the Centers of UE Hotspots

In this subsection we consider UAVs positioned directly above UE hotspot centers; we generate the following results using our mathematical expressions, and validate the accuracy of the derivations via simulations. In Figs. 3.7 to 3.14 below, solid lines denote the values for the coverage probability obtained via Theorem 1, and the markers denote results from MC trials.

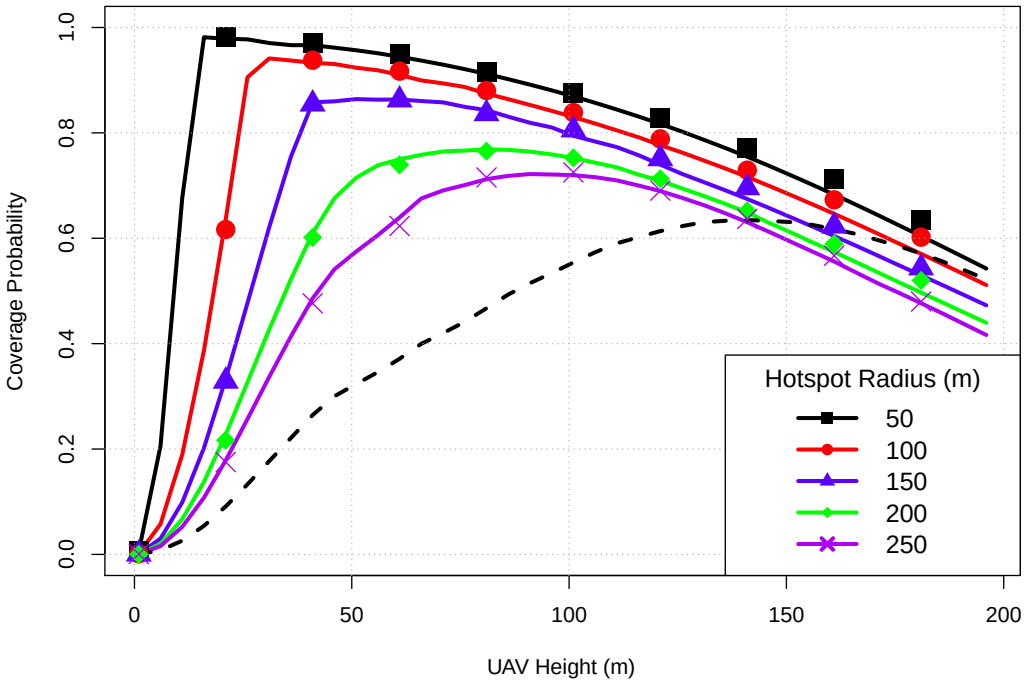

Figure 3.7: Coverage probability given a hotspot density of 5 /km^2 and beamwidth ω of 150 degrees. Solid lines denote analytical results, markers denote simulations, and the dashed line denotes the result for the PPP distribution of UAVs.

In Fig. 3.7 we demonstrate the performance of the UAV network for different values of the UE hotspot radius $r_{\max}$. We can see that when the radius is the lowest, and therefore the UEs are the most concentrated, the performance of the network is best. This is due to the reduced distance between a typical UE and the UAV above the hotspot center, which allows the UE to associate to the hotspot center UAV more often and receive a better signal from it. For each hotspot radius there is a single UAV height which maximises the coverage probability: below this height the serving UAV is more likely to have NLOS to the reference UE, which decreases the received signal strength, and above this height the interfering UAVs are more likely to have LOS on the UE and more interfering UAV will cast their antenna beam over the UE, increasing interference. We note that the UAV height which maximises the coverage probability increases as we increase the hotspot radius; this is due to the fact that the increasing distance between a typical UE and its hotspot center UAV increases the probability of a LOS-blocking building being in the way, and therefore the UAV network must increase its height to compensate. The dashed line denotes the coverage probability for the case where $r_{\max} \to \infty$, which is equivalent to the performance of a UAV network that positions UAVs independently of the locations of the user hotspots, as in the previous subsection. In Fig. 3.8 we present the spectral efficiency of the UAV network for the same parameters. We can see that the spectral efficiency

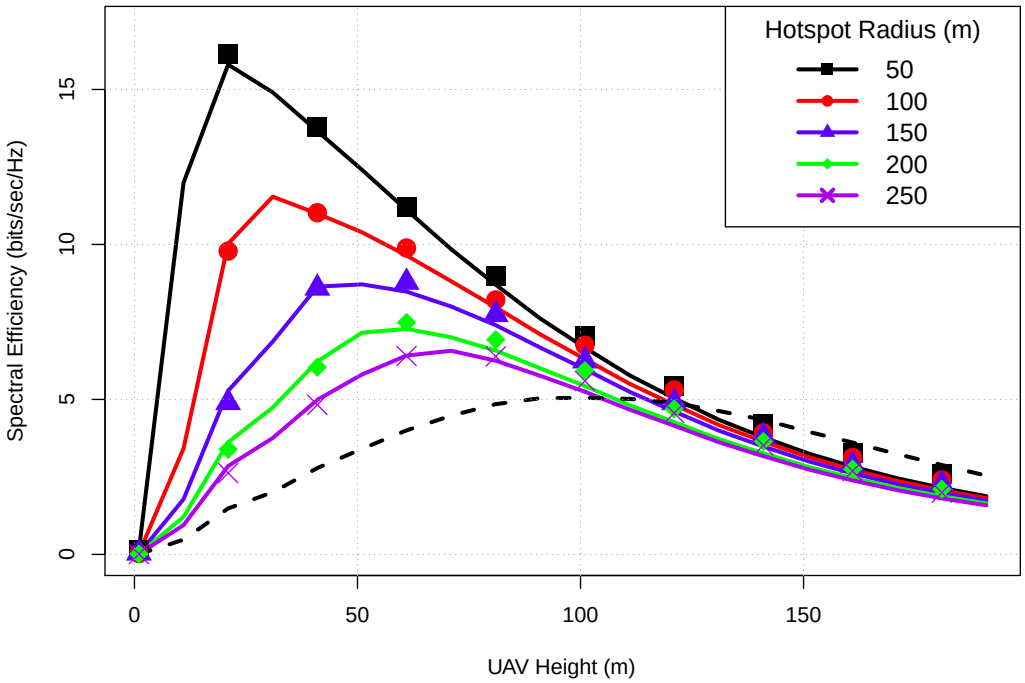

Figure 3.8: Spectral efficiency given a hotspot density of 5 /km^2 and beamwidth ω of 150 degrees. Solid lines denote analytical results, markers denote simulations, and the dashed line denotes the result for the PPP distribution of UAVs.

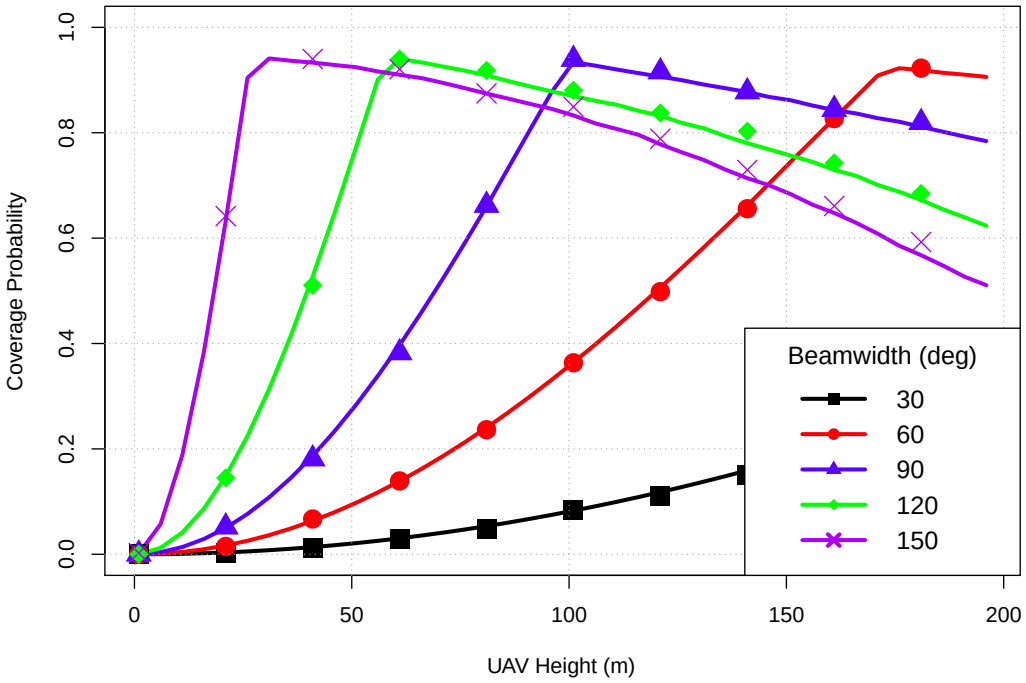

Figure 3.9: Coverage probability given a hotspot density of 5 /km^2 and hotspot radius of 100 m.

curves closely match the shape of those given in Fig. 3.7, including the approximate locations of the optimum UAV height for each correspoding hotspot radius.

It is worth noting that the range of optimum UAV heights for the smaller hotspot radii in Fig. 3.7 and Fig. 3.8 is in the order of 25-50 m above ground. This height may be too low for feasible UAV network operation in an urban environment, due to factors such as wireless backhaul availability (discussed in the next chapter) or safety regulations (discussed in Section 6.2). A possible solution is to design UAV antennas with narrower beamwidths to allow the UAVs to operate at higher altitudes, as shown in Fig. 3.9. We can see that decreasing the antenna beamwidth will have the effect of increasing the height the UAV network would need to operate at to maximise the coverage probability. This result matches the previously shown result in Fig. 3.5 for the case of an independently distributed UAV network.

In Fig. 3.10 we consider the network performance when the density of the UE hotspots (and therefore the UAV network) is increased. We can clearly see that for greater hotspot densities the coverage probability deteriorates, due to the greater number of UAV interferers, which is not offset by the greater number of candidate serving UAVs for the UE. It is also worth noting that the optimum UAV height appears to change very little for the different densities; following the results of the previous plots we conclude

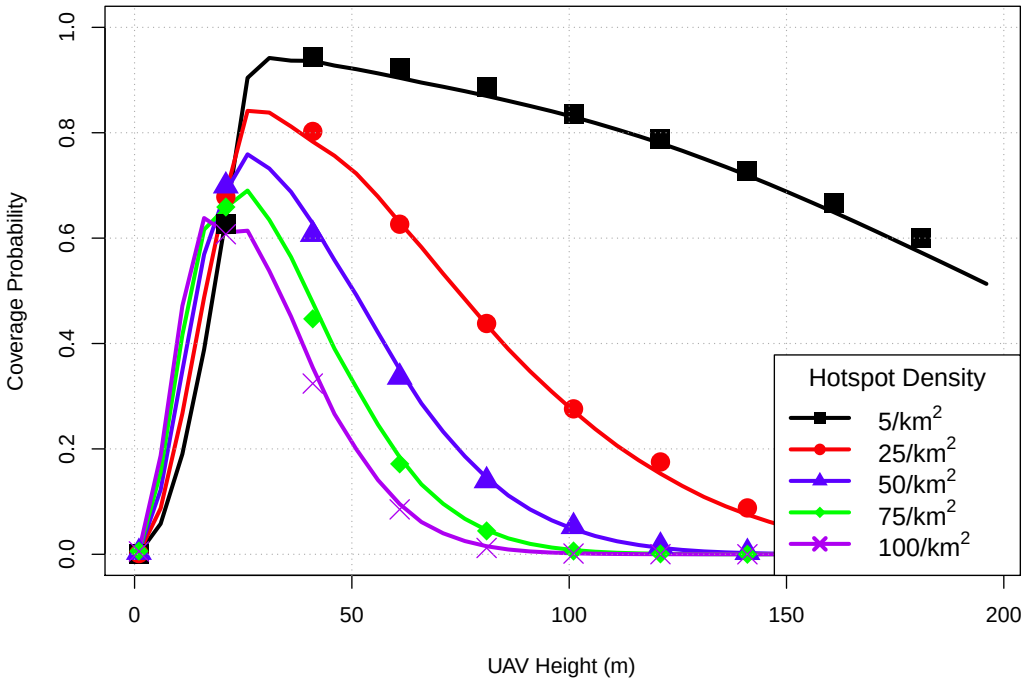

Figure 3.10: Coverage probability given a hotspot radius $r_{\max}$ of 100m. Solid lines denote analytical results, markers denote simulations.

that the optimum height of a UAV network is primarily determined by the radius of the UE hotspots, rather than the number of hotspots in a given area. This result is very different from the independent UAV placement case given in Fig. 3.4.

In Fig. 3.11 we consider the effect of changing the UAV transmit power on the coverage probability of the network. We report that increasing the transmit power will only improve the network performance at low UAV heights, when the UAV network experiences NLOS channels. At greater heights the network becomes interference-limited, as a result any changes to the transmit power will equally affect the received signal strength of both the serving UAV signal as well as the interference signals, thus giving no coverage probability improvement.

In Fig. 3.12 we verify Remark 4. We consider UE hotspots which have random radii, distributed according to a truncated Gaussian distribution (with positive, non-zero radii values). Comparing the numerical results we see that the randomness of the UE hotspot radii does not appear to affect the overall coverage probability, as the results align very closely with the case where the hotspots all have the same radius.

In Fig. 3.13 we consider the network performance as we increase the proportion of area covered by buildings δ. We see that denser environments help the network perform better at greater UAV heights, due to the buildings blocking interference signals from

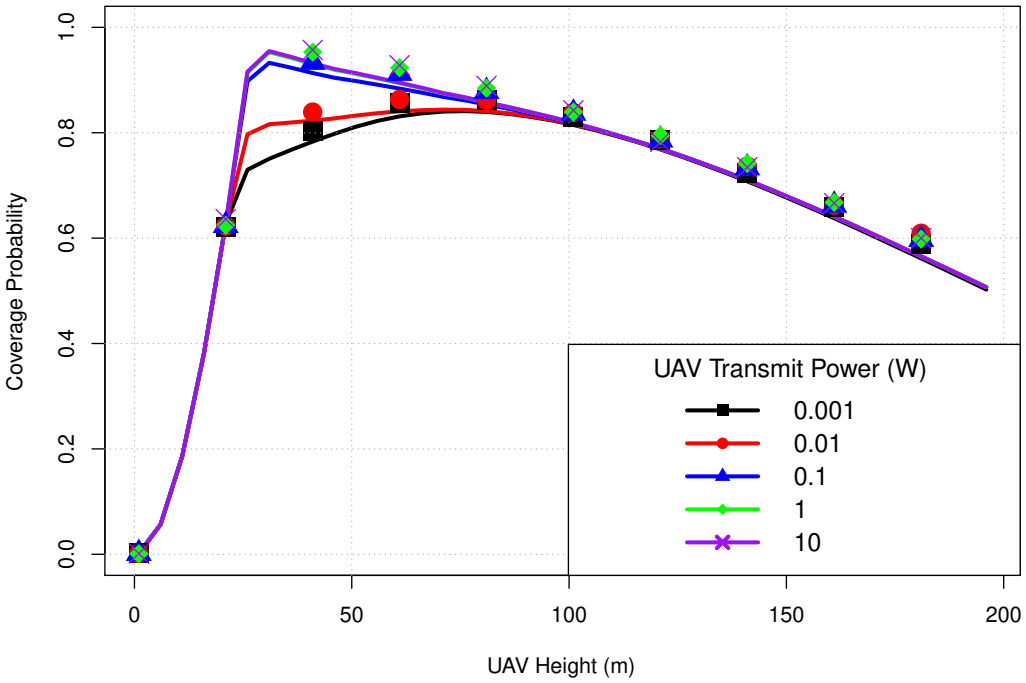

Figure 3.11: Coverage probability as a function of UAV height and transmit power given a hotspot density of 5 /km^2 and hotspot radius of 100 m.

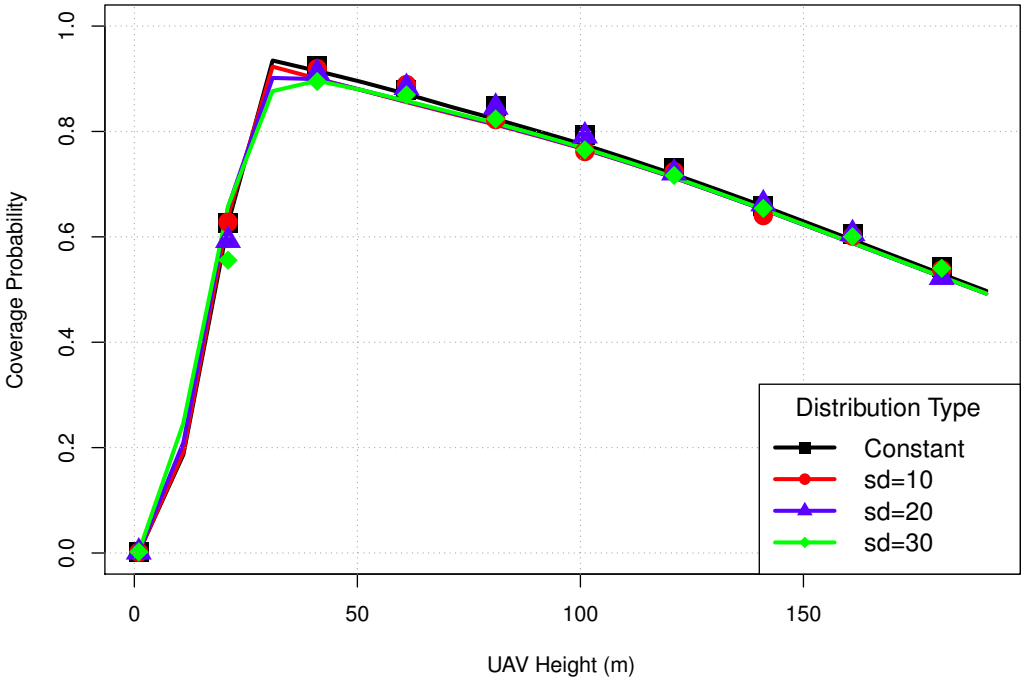

Figure 3.12: Coverage probability given the hotspot radii have either a constant value or are randomly distributed according to a truncated Gaussian distribution, with mean 100 m.

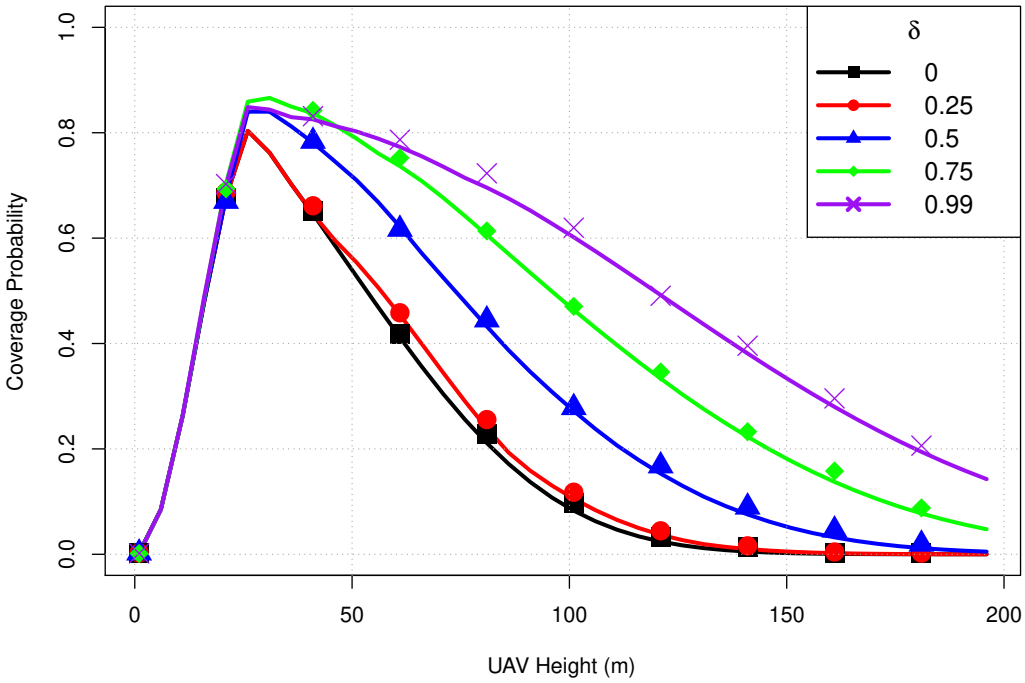

Figure 3.13: Coverage probability given a hotspot density of $25/\text{km}^2$, as a function of the building parameter δ and UAV height above ground.

UAVs further away. At very low heights the performance is the same for all cases, as the limiting factor for the coverage probability is the small area illuminated by the UAV antennas, rather than building blockage.

In Fig. 3.14 we show the impact of the κ building parameter on the network performance. We observe that the maximum achieveable coverage probability does not change with the changing building heights, provided the UAVs adjust their own heights accordingly.

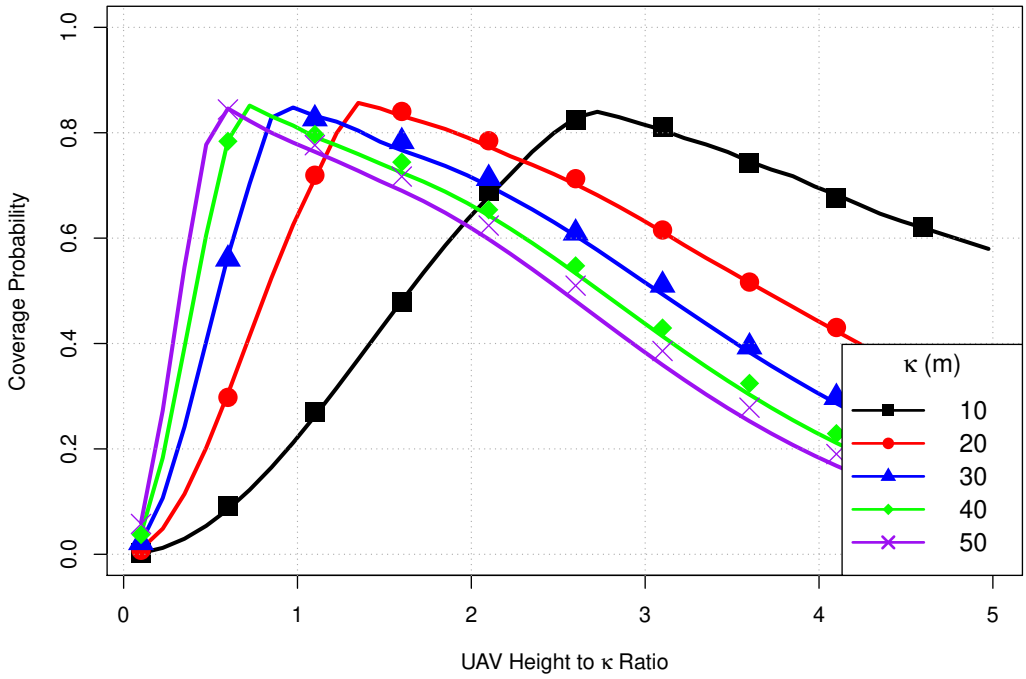

Figure 3.14: Coverage probability given a hotspot density of $25/\text{km}^2$, as a function of the building parameter κ and UAV height above ground. The x-axis shows the UAV height as a multiple of κ.

3.5.3 UAV Placement Comparison

In this subsection we are interested in comparing side-by-side the numerical performance of the UAV network, for different deployment strategies of the UAVs. In addition to placing the UAVs at hotspot centers as before, we consider a network where UAVs are positioned around UE locations via the K-means optimisation algorithm, and a network where UAVs are deployed according to a rectangular grid. Fig. 3.15 and Fig. 3.16 show how the three UAVs placement scenarios compare to one another, given different densities of UE hotspots (and UAVs). Hotspot center results are obtained using the analytical expressions, the K-means optimisation and grid deployment results are obtained via simulation.

The first result we report is that there is a significant degree of similarity in the behaviour of the K-means optimisation algorithm, and our mathematical model where UAVs are positioned above the UE hotspot centers. We conclude from the results that our mathematical model can accurately capture the performance of UAV networks where the UAVs are positioned according to a heuristic optimisation algorithm, with the added benefit of being mathematically tractable, unlike algorithms such as the K-means.

The second interesting result concerns UAV performance when the UAVs are deployed

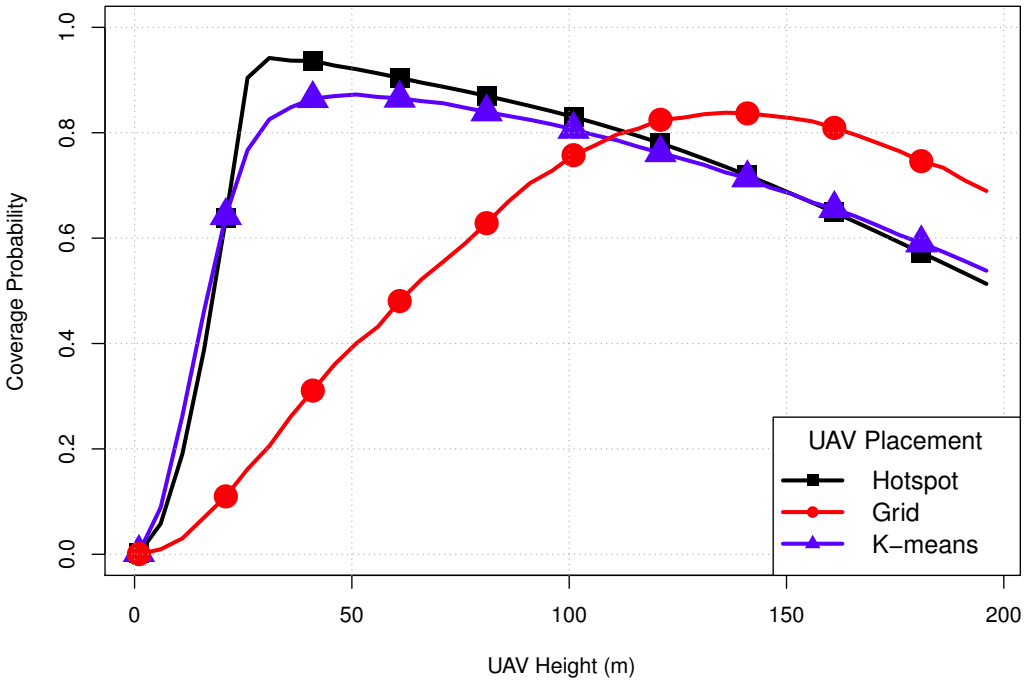

Figure 3.15: Coverage probability for different UAV placement strategies, given a hotspot radius $r_{\max}$ of 100m and a UAV density of $5/\text{km}^2$.

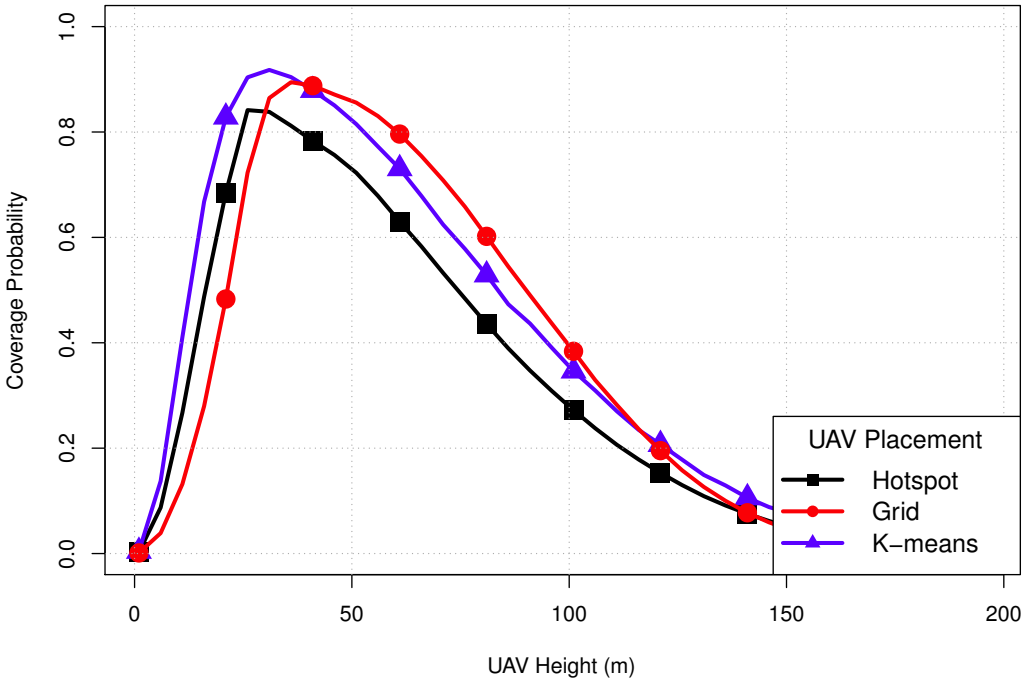

Figure 3.16: Coverage probability for different UAV placement strategies, given a hotspot radius $r_{\max}$ of 100m and a UAV density of $25/\text{km}^2$.

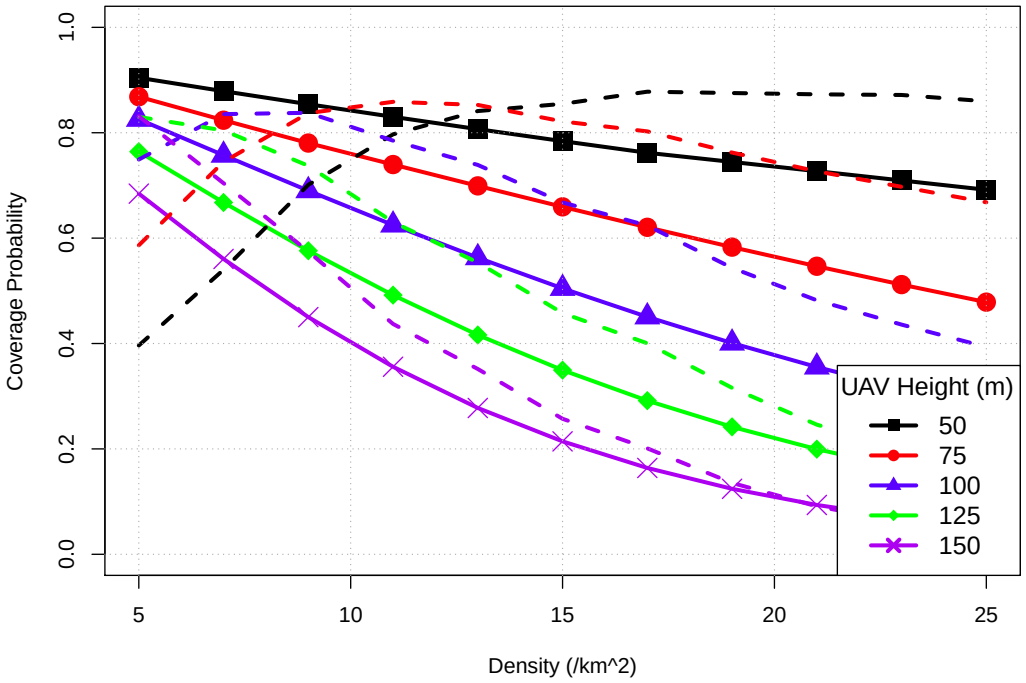

Figure 3.17: Coverage probability given a hotspot radius $r_{\max}$ of 100m. Solid lines denote results for UAVs placed at UE hotspot centers, dashed lines denote UAVs arranged in a rectangular grid.

according to a rectangular grid, independently of UE locations. For the low UAV density scenario in Fig. 3.15 we can see that putting UAVs at hotspot centers (or otherwise optimising the UAV locations with respect to UE locations) gives the best overall performance, due to the shorter distance between UEs and their serving UAVs. The behaviour changes when we increase the UAV density in Fig. 3.16. Given a larger number of UAVs (and therefore interferers) the network benefits from putting UAVs in a grid pattern, even though this pattern does not take into account the actual locations of the UEs. At higher UAV densities the network benefits from a UAV placement strategy which maximises the distances between UAVs and which therefore limits the UAV coverage overlap and interference, even if this placement strategy does not necessarily reduce the distances between UEs and their serving UAVs. The K-means algorithm is able to give the best performance as it both minimises the distance between the UEs and their serving UAVs while also spreading the UAVs out across cells of roughly equal size, which separates out interferers.

In Fig. 3.17 we further explore the effect of the UAV density on the coverage probability of the two UAV placement policies. We can see that there exists a maximum UAV density for a given UAV height, above which the grid deployment will outperform the hotspot center deployment, and that this maximum density decreases as we consider

larger UAV heights. It is clear that at larger UAV densities the channel is interference-limited, and therefore the best network performance is achieved only when the UAVs intelligently position themselves with respect to each other, rather than based on the locations of the UEs. As the UAV density is tied to the density of demand hotspots this result also demonstrates that there exists a maximum hotspot density above which the UAV network should prioritise minimising interference rather than maximising the received signal strength.

3.6 Conclusion & Discussion

In this chapter we focused on analysing the performance of the access link between a UE and its serving UAV small cell in a dense urban deployment. Using stochastic geometry and simulations we were able to gain several insights into the performance of such a network and the impact of several design parameters. We discuss our key findings below.

3.6.1 The Impact of Strong LOS Channels

A key result that we have observed in our analysis, and one that needs to be emphasised given its real-world implications, is the impact of the strong UAV LOS channels on the network performance. The research community has recognised that UAVs can, due to their aerial nature, avoid LOS blockage to their terrestrial devices and therefore establish high-quality wireless links. The issue is that by focusing on noise-limited scenarios it is common for the wireless community to treat this LOS channel behaviour as a significant benefit of UAV networks, whereas as we have shown in reality the situation is far more complicated. The UAV LOS channels are a double-edged sword which, if not accounted for correctly, can result in significant signal deterioration, as the LOS channels will equally improve the signal strength of interference links. We observed this in our numerical results, where the UAV network experienced significant signal deterioration at heights above 100 m.

Our analysis suggests two solutions to this phenomenon, assuming the density of UAVs is fixed. The first is to simply lower the heights of the UAV network, leverage their mobility to have them operate at heights where the UAVs are likely to still have LOS channels to their serving UEs, but will have NLOS links to UEs further away that are served by other UAVs. There are several issues with this solution. The first is that reducing the UAV height may compromise a UAV's wireless backhaul connection, as we

will discuss in the following chapter. The second issue is that a sufficiently low height to shield UEs from interference may involve the UAVs having to operate below rooftop level inside urban canyons, which in turn can significantly complicate the challenge of safe UAV movement. Beyond the technical implications there are also legal and social concerns with operating the UAVs at very low heights. Current UAVs can generate a noticeable amount of noise while flying; bringing them closer to the ground will inevitably increase the amount of noise pollution the UAV network generates. Furthermore, there may be legal restrictions in place which regulate how close UAVs can fly to crowds of people or buildings, lowering the UAV network height may complicate its operation from a legal perspective.

The second solution that can be implemented by UAV operators is to design UAV antennas with a more narrow radiation pattern. As we demonstrated in this chapter, by reducing the antenna beamwidth of the UAV network we can significantly increase the operating heights which maximise the achieveable coverage probability. The drawback of highly-directional antennas is their increased design complexity, which directly translates into an increase in cost and, perhaps more crucially, an increase in their weight. The feasibility of leveraging antenna directionality to improve the network performance will therefore be determined by the available budget for the UAV communication electronics and the flying platform itself.

3.6.2 The Impact of Intelligent UAV Positioning

Our analysis has allowed us to characterise the exact impact that intelligent UAV positioning can have on the performance of an interference-limited network. As may be expected, positioning the UAVs directly above UE hotspots improves the network performance over the baseline case where the UAVs are positioned randomly; depending on the UE hotspot size the spectral efficiency of the channel could be more than doubled through this intelligent placement. What is more surprising is how the UAV network performed under a basic rectangular grid deployment pattern. For very low hotspot and UAV densities the grid distribution would closely match the maximum coverage probability achieved by the hotspot center and K-means placements (albeit requiring a greater UAV height to do so), while for larger densities the grid pattern would outperform the hotspot center placement outright. These results have significant implications for UAV network design; in effect what we observe is that a sufficiently large density of UAVs can make UAV placement optimisation with respect to UE locations unnecessary. At large densities the UEs are very likely to have a LOS channel on at least one UAV regardless of how the UAVs are distributed in the air. The UAV distribution will primarily affect the distribution of interference signals, and spacing the UAVs away from each other in a

basic grid pattern appears to be a good way to mitigate interference. In such a scenario the UAVs may be able to outright ignore the UE behaviour on the ground, which would significantly simplify the issue of UAV deployment and allow the network to function without information about the exact UE coordinates. The wireless community imagines UAV networks as inherently mobile, following the data demand wherever it goes, from our results it appears that high density UAV small cell networks may sometimes take the form of a regular grid that hovers in place and only moves in response to UAVs entering and exiting service.

We make another interesting observation regarding our choice of the K-means heuristic algorithm. When optimising UAV placement the wireless community tends to ignore the impact of interference and instead focuses on noise-limited optimisation algorithms (see Section 2.1), the K-means positioning algorithm behaves similarly. Despite the fact that it optimises purely around Euclidean distances of the UEs and their nearest UAVs the algorithm is able to effectively mitigate the interference of the network; as a convenient by-product of the algorithm the UAVs are spaced apart in Voronoi cells of approximately equal size. This demonstrates that it is possible to optimise the performance of an interference-limited network using certain algorithms which do not explicitly take account of UAV interference effects.

4 The UAV Wireless Backhaul Link

The technical content presented in this chapter is based on the works "Backhaul For Low-Altitude UAVs in Urban Environments" presented at IEEE International Conference on Communications (ICC) and "Impact of UAV Antenna Configuration on Wireless Connectivity in Urban Environments" published on Arxiv.

4.1 Introduction

We have demonstrated in the previous chapter how UAV small cell networks can successfully provide high-quality wireless service to terrestrial UEs. The access link between the UE and the UAV is not the only wireless channel that the UAV network needs to be designed around. In cellular networks where the UAV small cells are not tethered to a GS they will require a high-capacity wireless connection of some sort to the core network. As discussed in Section 2.3 the most commonly considered solution for providing wireless connectivity to low-altitude UAVs is to use the existing terrestrial cellular network. This may be a valid solution for a variety of UAV use cases; however, we expect that dedicated GS infrastructure may be more suitable for providing wireless backhauls to UAV small cells. UAVs are a fundamentally new type of communications equipment which have different capabilities to terrestrial devices and which operate in a very different radio environment, therefore a network of GSs designed specifically to target UAV connectivity will have to rely on very different design principles than networks intended for serving terrestrial UEs. The lack of published research from the wireless community on the design and deployment of dedicated GS networks is the motivation behind the work in this chapter.

The contributions of this chapter are stated as follows:

1. We apply stochastic geometry to model the downlink performance of a dedicated GS network which provides backhaul to UAV small cells. We consider sub-6GHz and millimeter-wave communication, and account for different antenna configurations on both the UAVs and the GSs.

2. Using simulations we compare the backhaul performance of the dedicated GS network against a typical LTE BS network, considered by the state-of-the-art. This comparison allows us to demonstrate the superior performance of the dedicated GS network and also show the impact of the UAV antenna configuration on the achieveable performance.

3. Using our model and simulations we investigate the impact of various GS network design parameters on the backhaul performance, for both sub-6GHz and millimeter-wave communication. This allows us to demonstrate the differences in network design that would be required for the two different technologies.

4. We compare our channel model against a model proposed by the 3GPP for modelling the link between UAVs and LTE BSs and demonstrate a close fit for scenarios where the backhaul is limited by interference.

This chapter is structured as follows. We open with a description of the system model, including a description of the different antenna configurations for the UAVs and the GSs. In the analytical results section we derive expressions for the probability of a typical UAV being able to establish a backhaul from the GS network. In the numerical results section we apply our mathematical derivations and simulations to generate quantitative results. We conclude with a discussion of the main observations that can be made from the numerical results.

4.2 System Model

In this section we set up a system model of a network of GSs providing backhaul to UAVs. We consider two technologies for the backhaul channel: sub-6GHz and millimeter-wave. We model the network of GSs as a PPP $\Phi = \{x_1, x_2, ...\} \subset \mathbb{R}^2$ of intensity λ where elements $x_i \in \mathbb{R}^2$ represent the projections of the GS locations onto the $\mathbb{R}^2$ plane. The GSs have a height γ_G above ground. We consider a single reference UAV, positioned above the origin $x_0 = (0, 0)$ at a height γ. Let $r_i = ||x_i||$ denote the horizontal distance between

the GS i and the reference UAV, and let $\phi_i = \arctan(\Delta\gamma / r_i)$ denote the vertical angle, where $\Delta\gamma = \gamma - \gamma_G$.

For the sub-6GHz backhaul we consider three different types of antennas that the UAV may use to communicate with its GS network:

1. An omnidirectional antenna, with antenna gain $\eta = 1$.
2. A directional antenna tilted down to give a cone-shaped radiation lobe directly beneath the UAV (similar to the radiation pattern of the access link antennas

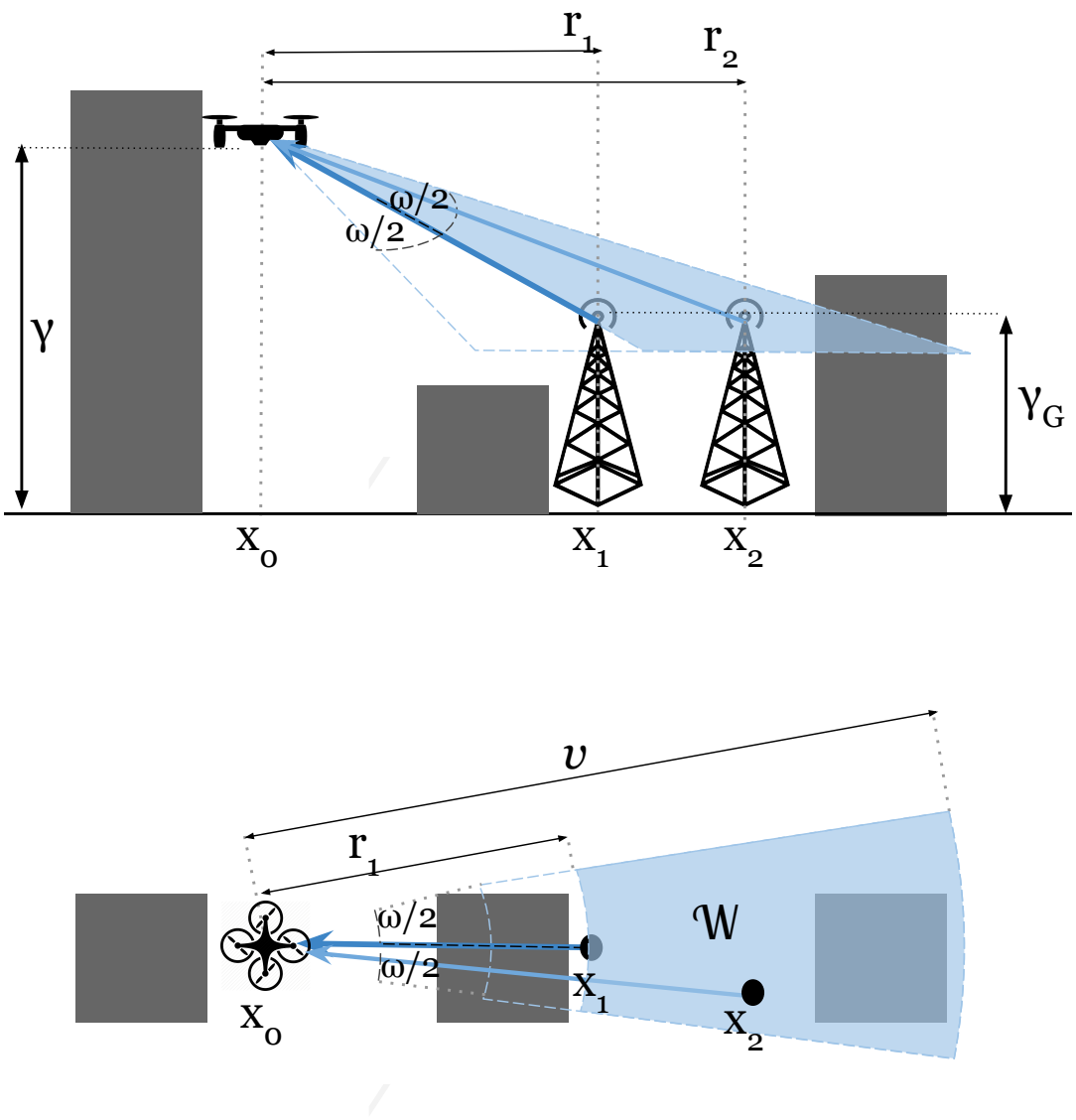

Figure 4.1: Side and top view showing a UAV with a steerable directional antenna in an urban environment at a height γ, positioned above x_0 with antenna beamwidth ω. The UAV selects the nearest GS at x_1 for its backhaul and centers its antenna main lobe on the GS location; the blue area $\mathcal{W}$ illuminated by the main lobe denotes the region where interferers may be found. The GS at x_2 falls inside this area and produces interference.

considered in Fig. 3.1 in Chapter 3). Using the approximations (2-26) and (2-49) in [95] and assuming perfect radiation efficiency, the antenna gain can be expressed as $\eta = 16\pi/(\omega^2)$ inside the main lobe and $\eta = 0$ outside, where ω denotes the antenna beamwidth.

3. A directional antenna which the UAV can intelligently steer and align with its serving GS, as depicted in Fig. 4.1. The antenna has a horizontal and vertical beamwidth ω and a rectangular radiation pattern; the antenna gain is given as $\eta = 16\pi/(\omega^2)$ inside the main lobe and $\eta = 0$ outside.

For the millimeter-wave backhaul we assume that the UAV possesses an antenna array and that it uses beamforming to align its antenna towards the GS, therefore we only consider the steerable directional antenna model.

The UAV selects the nearest GS as its serving GS[6]; we denote this GS as x_1 and its distance to the UAV as r_1. the UAV antenna reception pattern illuminates an area beyond x_1 which we denote as $\mathcal{W} \subset \mathbb{R}^2$. This area takes the shape of a ring sector whose lower radius is r_1 and whose upper radius $v(\gamma, r_1)$ and arc angle ρ are determined by the type of antenna used. For the type 1 antenna $v(\gamma, r_1) = \infty$ and $\rho = 2\pi$, as the omnidirectional antenna can receive a signal from any direction with no upper limit on the transmitter distance. For the type 2 antenna the upper radius $v(\gamma, r_1) = \Delta\gamma \tan(\omega/2)$ as any transmitters outside of this range will be outside of the main lobe of the UAV antenna, and $\rho = 2\pi$. For the type 3 antenna $\rho = \omega$ as depicted in Fig. 3.1 and $v(\gamma, r_1)$ is given as

$$v(\gamma, r_1) = \begin{cases} \frac{|\Delta\gamma|}{\tan(|\phi_1| - \omega/2)}, & \text{if } \ \omega/2 < |\phi_1| < \pi/2 - \omega/2, \\ \frac{|\Delta\gamma|}{\tan(\pi/2 - \omega)}, & \text{if } \ |\phi_1| > \pi/2 - \omega/2, \\ \infty & \text{otherwise}, \end{cases} \tag{4.1}$$

with $|.|$ denoting absolute value. For the case where $\omega \geq \pi/2$, the major radius $v(\gamma, r_1)$ will always be infinite. We denote the set of GSs that fall inside the area $\mathcal{W}$ as $\Phi_{\mathcal{W}} = \{x \in \Phi : x \in \mathcal{W}\}$. The GSs in the set $\Phi_{\mathcal{W}}$ are capable of causing interference to the reference UAV, as their signals may be received by the UAV with non-zero gain. Note that $\Phi_{\mathcal{W}}$ is a PPP with the same intensity λ.

[6]Given a low density of GSs with antennas tilted towards the sky the strongest received signal power at the UAV is expected to come from the nearest GS.

As in the previous chapter, we assume that the wireless channels between the reference UAV and the GSs will be affected by buildings, which form obstacles and break LOS links. To model the LOS probability we use a modified form of the expression Eq. (3.1), which takes into account the heights above ground of both the transmitter and the receiver

$$\mathbb{P}_{\mathtt{l}}(r_i) = \prod_{n=0}^{\max(0,d-1)} \left(1 - \exp\left(-\frac{\left(\max(\gamma,\gamma_G) - \frac{(n+1/2)|\Delta\gamma|}{d}\right)^2}{2\kappa^2}\right)\right), \tag{4.2}$$

where $d = \left\lfloor r_i\sqrt{\beta\delta}\right\rfloor$ as before, with β, δ, and κ being the building parameters. It follows that $\mathbb{P}_{\mathtt{n}} = 1 - \mathbb{P}_{\mathtt{l}}$. We can express the SINR at the reference UAV as

$$\text{SINR} = \frac{pH_{T_1}\eta\mu c l(r_1,\Delta\gamma,\alpha_{T_1})}{I_{\mathtt{l}} + I_{\mathtt{n}} + \sigma^2}, \tag{4.3}$$

where p is GS transmit power, H_{T_1} is the random multipath fading component, $l(r_1,\Delta\gamma,\alpha_{T_1})$ $= (r_1^2 + \Delta\gamma^2)^{-\alpha_{T_1}/2}$ is the pathloss function, α_{T_1} is the pathloss exponent, $T_1 \in \{\mathtt{l},\mathtt{n}\}$ is random indicator variable which denotes whether the UAV has LOS or NLOS to its serving GS, μ is the serving GS antenna gain defined in the next subsections, c is the near-field pathloss, σ^2 is the noise power, and $I_{\mathtt{l}}$ and $I_{\mathtt{n}}$ are the aggregate LOS and NLOS interference, respectively.

The backhaul data rate, in Mbits/sec, can be calculated from the SINR using the Shannon capacity bound

$$\mathcal{R} = b\log_2(1 + \text{SINR}), \tag{4.4}$$

where b denotes the bandwidth of the backhaul channel. We define an SINR threshold θ for the UAV backhaul link: if SINR $< \theta$ this represents the UAV failing to establish a backhaul of the required channel quality and therefore being in an outage state.

4.2.1 Sub-6GHz Backhaul

For the sub-6GHz backhaul case we assume that the GSs are equipped with tri-sector antennas similar to those already in use in terrestrial BSs, as this allows them to serve UAVs in any horizontal direction. For tractability we model the horizontal antenna gain μ_h of these antennas as having a constant value. The antennas are tilted up towards the sky, to model the behaviour of the antennas in the vertical plane we adopt the 3GPP

model [102], such that

$$\mu_v(\phi_i) = 10^{-\min\left(12\left(\frac{\phi_i-\phi_T}{10}\right)^2,20\right)/10}, \tag{4.5}$$

$$\mu_l(\phi_i) = \max\left(\mu_h\mu_v(\phi_i), 10^{-2.5}\right), \tag{4.6}$$

where $\mu_v(\phi_i)$ is the vertical antenna gain, ϕ_T is the vertical uptilt angle of the GS antenna (in degrees) and $\mu_l(\phi_i)$ is the total antenna gain.

4.2.2 Millimeter-Wave Backhaul

For the millimeter-wave backhaul we assume each GS is equipped with an antenna array that uses beamforming to direct a directional beam towards the UAV to which it provides a backhaul link. We adopt a similar approach to modelling the GS antenna array as in [59] and [60]. The GS antenna is modelled as having a single directional beam with a beamwidth of ω_G and a gain of μ_m inside the main lobe, and a gain of 0 outside. The reference UAV will always experience an antenna gain of μ_m from its serving GS. The beam patterns of the remaining GSs will appear to be pointed in random directions with respect to the reference UAV; as a result each interfering GS will have non-zero antenna gain to the reference UAV with a certain probability ζ.

4.3 Mathematical Analysis

In this section we derive an analytical expression for the probability that the reference UAV will receive a signal from the GS network with an SINR above θ, thereby establishing a backhaul. We refer to this as the backhaul probability. To derive an expression for the backhaul probability we need an expression for the conditional backhaul probability given the serving GS of the reference UAV has either LOS or NLOS to the reference UAV, and given it is located at a horizontal distance r_1 from the UAV. We then decondition this conditional backhaul probability with respect to the LOS probability of the serving GS as well as its horizontal distance. The LOS probability for a given horizontal distance r_1 is given in Eq. (4.2). Given a PPP distribution of GSs the serving GS horizontal distance random variable R_1 is known to be Rayleigh-distributed with scale parameter $1/\sqrt{2\pi\lambda}$.

4.3.1 Aggregate LOS & NLOS Interference

Sub-6GHz backhaul The interferers will belong to the set $\Phi_{\mathcal{W}}$. We partition this set into two sets which contain the LOS and NLOS interfering GSs, denoted as $\Phi_{\mathcal{W}\mathtt{l}} \subset \Phi_{\mathcal{W}}$ and $\Phi_{\mathcal{W}\mathtt{n}} \subset \Phi_{\mathcal{W}}$, respectively. These two sets are inhomogeneous PPPs with intensity functions $\lambda_{\mathtt{l}}(x) = \mathbb{P}_{\mathtt{l}}(||x||)\lambda$ and $\lambda_{\mathtt{n}}(x) = \mathbb{P}_{\mathtt{n}}(||x||)\lambda$. Note that we drop the index i as the GS coordinates have the same distribution irrespective of their index values. For a sub-6GHz backhaul the aggregate LOS and NLOS interference is expressed as $I_{\mathtt{l}} = \sum_{x\in\Phi_{\mathcal{W}\mathtt{l}}} pH_{\mathtt{l}}\eta\mu_l(\phi)cl(||x||,\Delta\gamma,\alpha_{\mathtt{l}})$ and $I_{\mathtt{n}} = \sum_{x\in\Phi_{\mathcal{W}\mathtt{n}}} pH_{\mathtt{n}}\eta\mu_l(\phi)cl(||x||,\Delta\gamma,\alpha_{\mathtt{n}})$, recalling that $\phi = \arctan(\Delta\gamma/||x||)$.

Millimeter-wave backhaul As defined in the system model, the millimeter-wave interfering GSs will only create interference at the reference UAV if their directional beams happen to align with the UAV location, which occurs with probability ζ. As a result of this $\Phi_{\mathcal{W}\mathtt{l}}$ and $\Phi_{\mathcal{W}\mathtt{n}}$ have intensity functions $\lambda_{\mathtt{l}}(x) = \mathbb{P}_{\mathtt{l}}(||x||)\zeta\lambda$ and $\lambda_{\mathtt{n}}(x) = \mathbb{P}_{\mathtt{n}}(||x||)\zeta\lambda$. The aggregate LOS and NLOS interference is expressed as $I_{\mathtt{l}} = \sum_{x\in\Phi_{\mathcal{W}\mathtt{l}}} pH_{\mathtt{l}}\eta\mu_m cl(||x||,\Delta\gamma,\alpha_{\mathtt{l}})$ and $I_{\mathtt{n}} = \sum_{x\in\Phi_{\mathcal{W}\mathtt{n}}} pH_{\mathtt{n}}\eta\mu_m cl(||x||,\Delta\gamma,\alpha_{\mathtt{n}})$.

4.3.2 Conditional Backhaul Probability

Proposition 6. The expression for the backhaul probability, given serving GS distance r_1 and a channel to the serving GS of type $j \in \{\mathtt{l},\mathtt{n}\}$, is expressed as

$$\mathbb{P}(\text{SINR} \geq \theta | R_1 = r_1, T_1 = j) = \sum_{k=0}^{m_j-1} (-1)^k \frac{s_j^k}{k!} \sum_{i_{\mathtt{l}}+i_{\mathtt{n}}+i_\sigma=k} \frac{k!}{i_{\mathtt{l}}!i_{\mathtt{n}}!i_\sigma!} \cdot \frac{\mathrm{d}^{i_{\mathtt{l}}}\mathcal{L}_{I_{\mathtt{l}}}((p\eta c)^{-1}s_j)}{\mathrm{d}s_j^{i_{\mathtt{l}}}} \frac{\mathrm{d}^{i_{\mathtt{n}}}\mathcal{L}_{I_{\mathtt{n}}}((p\eta c)^{-1}s_j)}{\mathrm{d}s_j^{i_{\mathtt{n}}}} \frac{\mathrm{d}^{i_\sigma}\exp(-(p\eta c)^{-1}s_j\sigma^2)}{\mathrm{d}s_j^{i_\sigma}}, \quad j \in \{\mathtt{l},\mathtt{n}\}, \tag{4.7}$$

where $s_j = m_j\theta/(\mu l(r_1,\Delta\gamma,\alpha_j))$, m_j is the Nakagami-m fading term for a channel of type j, $\mathcal{L}_{I_{\mathtt{l}}}$ and $\mathcal{L}_{I_{\mathtt{n}}}$ are the Laplace transforms of the aggregate LOS and NLOS interference, respectively, and the second sum is over all the combinations of non-negative integers $i_{\mathtt{l}}, i_{\mathtt{n}}$ and i_σ that add up to k. GS antenna gain μ takes the value of either $\mu_l(\phi_1)$ or μ_m depending on whether we are considering sub-6GHz or millimeter-wave backhaul.

Proof. The expression Eq. (4.7) is derived following the methodology of Eq. (7.20) in Appendix E as

$$\begin{aligned}
&\mathbb{P}(\text{SINR} \geq \theta | R_1 = r_1, T_1 = j) = \\
&\mathbb{P}\left(\frac{pH_j \eta \mu c l(r_1, \Delta\gamma, \alpha_j)}{I_{\mathtt{l}} + I_{\mathtt{n}} + \sigma^2} \geq \theta \right) \\
&= \mathbb{P}\left(H_j \geq \frac{\theta(I_{\mathtt{l}} + I_{\mathtt{n}} + \sigma^2)}{p\eta\mu c l(r_1, \Delta\gamma, \alpha_j)} \right) \\
&\overset{(a)}{=} \mathbb{E}\left[\frac{\Gamma(m_j, (p\eta c)^{-1} s_j (I_{\mathtt{l}} + I_{\mathtt{n}} + \sigma^2))}{\Gamma(m_j)} \right] \\
&\overset{(b)}{=} \mathbb{E}\left[\exp(-(p\eta c)^{-1} s_j (I_{\mathtt{l}} + I_{\mathtt{n}} + \sigma^2)) \sum_{k=0}^{m_j - 1} \frac{((p\eta c)^{-1} s_j (I_{\mathtt{l}} + I_{\mathtt{n}} + \sigma^2))^k}{k!} \right] \\
&\overset{(c)}{=} \sum_{k=0}^{m_j - 1} (-1)^k \frac{s_j^k}{k!} \mathbb{E}\left[\frac{\mathrm{d}^k \exp(-(p\eta c)^{-1} s_j (I_{\mathtt{l}} + I_{\mathtt{n}} + \sigma^2))}{\mathrm{d} s_j^k} \right] \\
&\overset{(d)}{=} \sum_{k=0}^{m_j - 1} (-1)^k \frac{s_j^k}{k!} \frac{\mathrm{d}^k \mathcal{L}_{(I_{\mathtt{l}} + I_{\mathtt{n}} + \sigma^2)}((p\eta c)^{-1} s_j)}{\mathrm{d} s_j^k}.
\end{aligned} \tag{4.8}$$

As in Eq. (7.20), (a) comes from the random fading H_j being gamma distributed with channel-dependent fading parameter m_j, (b) comes from expressing the incomplete gamma function as in [103][8.352.2], (c) arises from the substitution $\exp(-(p\eta c)^{-1} s_j (I_{\mathtt{l}} + I_{\mathtt{n}} + \sigma^2))((p\eta c)^{-1}(I_{\mathtt{l}} + I_{\mathtt{n}} + \sigma^2))^k = (-1)^k \mathrm{d}^k \exp(-(p\eta c)^{-1} s_j (I_{\mathtt{l}} + I_{\mathtt{n}} + \sigma^2))/\mathrm{d} s_j^k$, (d) comes from the Leibniz integral rule. The final expression Eq. (4.7) is obtained by applying the general Leibniz rule to $\mathcal{L}_{(I_{\mathtt{l}} + I_{\mathtt{n}} + \sigma^2)}$ and representing it in terms of the products of $\mathcal{L}_{I_{\mathtt{l}}}$ and $\mathcal{L}_{I_{\mathtt{n}}}$, as in Proposition 3. □

4.3.3 Laplace Transform of Aggregate Interference

Sub-6GHz backhaul

Proposition 7. The Laplace transform of the aggregate LOS interference $\mathcal{L}_{I_1}((p\eta c)^{-1}s_j)$ given a serving GS of channel type j is expressed as

$$\exp\left(-\lambda\rho\int_{r_1}^{v(\gamma,r_1)}\Big(1-g(r,s_j,m_1,\alpha_1)\Big)\mathbb{P}_1(r)r\mathrm{d}r\right), \tag{4.9}$$

where

$$g(r,s_j,m_1,\alpha_1)=\left(\frac{m_1}{s_j\mu_l(\phi)(r^2+\Delta\gamma^2)^{-\alpha_1/2}+m_1}\right)^{m_1}. \tag{4.10}$$

Proof. Eq. (4.9) is derived as

$$\begin{aligned}
&\mathcal{L}_{I_1}((p\eta c)^{-1}s_j)=\mathbb{E}\left[\exp\left(-(p\eta c)^{-1}s_jI_1\right)\right]\\
&=\mathbb{E}_{\Phi_{\mathcal{W}1}}\left[\prod_{x\in\Phi_{\mathcal{W}1}}\mathbb{E}_{H_1}\left[\exp\left(-H_1s_j\mu_l(\phi)l(||x||,\Delta\gamma,\alpha_1)\right)\right]\right]\\
&\overset{(a)}{=}\mathbb{E}_{\Phi_{\mathcal{W}1}}\left[\prod_{x\in\Phi_{\mathcal{W}1}}g(||x||,s_j,m_1,\alpha_1)\right]\\
&\overset{(b)}{=}\exp\left(-\int_{\mathcal{W}}\Big(1-g(||x||,s_j,m_1,\alpha_1)\Big)\lambda_1(x)\mathrm{d}x\right),
\end{aligned} \tag{4.11}$$

where (a) comes from the power-series representation of the Nakagami-m distribution, (b) comes from the probability generating functional of the PPP [91]. The final expression in Eq. (4.9) comes from switching to polar coordinates where $r=||x||$, $\lambda_1(x)=\mathbb{P}_1(||x||)\lambda$, and the integral is over $\mathcal{W}$ which has major and minor radius of $v(\gamma,r_1)$ and r_1, and an angular arc of ρ, as defined in the system model. □

Remark 5: Note that the Laplace transform for the NLOS interferers $\mathcal{L}_{I_n}((p\eta c)^{-1}s_j)$ is obtained by simply substituting $\lambda_1(x)$ with $\lambda_n(x)$ and $g(r,s_j,m_1,\alpha_1)$ with $g(r,s_j,m_n,\alpha_n)$ in Eq. (4.11) and solving as shown.

Millimeter-wave backhaul

Proposition 8. The Laplace transform of the LOS interferers for a millimeter-wave backhaul is expressed in closed-form as

$$\mathcal{L}_{I_1}((p\eta c)^{-1}s_j) = \exp\Bigg(- \frac{\omega\zeta\lambda}{2} \sum_{q=\left\lfloor r_1\sqrt{\beta\delta}\right\rfloor}^{\left\lfloor v(\gamma,r_1)\sqrt{\beta\delta}\right\rfloor} \mathbb{P}_1(l) \Bigg(\sum_{k=1}^{m_1} \binom{m_1}{k} (-1)^{k+1} \cdot \Bigg((u^2+\Delta\gamma^2)\,{}_2\mathrm{F}_1\Big(k, \frac{2}{\alpha_1}; 1+\frac{2}{\alpha_1}; -\frac{m_1(u^2+\Delta\gamma^2)^{\alpha_1/2}}{\mu_m s_j}\Big) - (l^2+\Delta\gamma^2)\,{}_2\mathrm{F}_1\Big(k, \frac{2}{\alpha_1}; 1+\frac{2}{\alpha_1}; -\frac{m_1(l^2+\Delta\gamma^2)^{\alpha_1/2}}{\mu_m s_j}\Big)\Bigg)\Bigg)\Bigg), \tag{4.12}$$

where $l = \max(r_1, q/\sqrt{\beta\delta})$ and $u = \min(v(\gamma, r_1), (q+1)/\sqrt{\beta\delta})$.

Proof. The Laplace transform of the LOS interferers for a millimeter-wave backhaul is derived as in Eq. (4.9), with the intensity λ being multiplied by ζ (as explained in the previous subsection), and with $\mu_l(\phi)$ being replaced with μ_m. Note that, unlike $\mu_l(\phi)$, μ_m is a constant value with respect to r; as a result of this it is possible to represent the integral in Eq. (4.9) in closed-form for the case of millimeter-wave backhaul. We begin by recognising that $\mathbb{P}_1(r)$ is a step function. We use this fact to separate the integral in Eq. (4.9) into a sum of weighted integrals, resulting in the following expression

$$\omega\zeta\lambda \sum_{q=\left\lfloor r_1\sqrt{\beta\delta}\right\rfloor}^{\left\lfloor v(\gamma,r_1)\sqrt{\beta\delta}\right\rfloor} \mathbb{P}_1(l) \int_l^u \Big(1 - g(r, s_j, m_1, \alpha_1)\Big) r\mathrm{d}r. \tag{4.13}$$

Using a similar derivation procedure to the one given in Eq. (7.7) in Appendix A the expression Eq. (4.13) can be expressed in the closed form to give Eq. (4.12). □

Remark 6: The higher-order derivative of the Laplace transform of the millimeter-wave backhaul can be obtained using a very similar derivation process to the one given in Appendix D.

4.3.4 Backhaul Probability and Expected Rate

To obtain the overall backhaul probability for the reference UAV in the network we decondition the conditional backhaul probability as defined in the previous subsection with respect to the indicator variable T_1 (we use the LOS probability function in Eq. (4.2)). We then decondition with respect to the horizontal distance random variable R_1.

$$\mathbb{P}(\text{SINR} \geq \theta) = \int_0^\infty \Big(\mathbb{P}(\text{SINR} \geq \theta | R_1 = r_1, T_1 = \mathtt{l}) \mathbb{P}_{\mathtt{l}}(r_1) + \mathbb{P}(\text{SINR} \geq \theta | R_1 = r_1, T_1 = \mathtt{n}) \mathbb{P}_{\mathtt{n}}(r_1) \Big) f_{R_1}(r_1) \mathrm{d}r_1. \quad (4.14)$$

The expected rate for the backhaul can be calculated using the backhaul probability as

$$\mathbb{E}[\mathcal{R}] = b \int_0^\infty \mathbb{P}(\text{SINR} \geq 2^s - 1) \mathrm{d}s. \quad (4.15)$$

4.4 Numerical Results

In this section we explore the trade-offs that occur between the parameters of the GS network and the resulting backhaul probability of the reference UAV. We generate our results using the analytical expressions given in the previous section and validate them via MC trials. As in Chapter 3, we run our simulations in the R software environment. We simulate a window of $100\,\text{km}^2$, the reference UAV is positioned in the center, and the GSs are distributed inside the window via a PPP. Unless stated otherwise the parameters used for the numerical results are taken from Table 4.1.

4.4.1 Dedicated GS and Terrestrial BS Performance Comparison

We begin our numerical results section by comparing the performance of the dedicated GS network against that of a typical terrestrial LTE BS network, given different UAV antenna types. The terrestrial BSs are modelled as having downtilted tri-sector antennas [102].

In Fig. 4.2 we compare the coverage probability achieved by the dedicated GS network against a typical terrestrial BS network, when UAVs are equipped with omnidirectional

Table 4.1: Wireless Backhaul Numerical Result Parameters

Parameter	Symbol	Sub-6GHz	mmWave
Carrier frequency	-	2 GHz	73 GHz
Bandwidth	b	20 MHz	1000 MHz
UAV steerable antenna beamwidth	ω	30 deg	10 deg
LOS pathloss exponent	$\alpha_{\mathtt{l}}$	2.1	2
NLOS pathloss exponent	$\alpha_{\mathtt{n}}$	4	3.5 [104]
LOS Nakagami-m fading	$m_{\mathtt{l}}$	1	3
NLOS Nakagami-m fading	$m_{\mathtt{n}}$	1	1
GS transmit power	p	40 W	10 W [74]
Near-field pathloss	c	-38.4 dB [59]	-69.7 dB
GS sub-6GHz horizontal antenna gain	μ_h	-5 dB	N/A
GS millimeter wave antenna gain	μ_m	N/A	32 dB
millimeter wave GS interference term	ζ	N/A	0
SINR threshold	θ	10 dB	10 dB
Noise power	σ^2	$8 \cdot 10^{-13}$ W [59]	$4 \cdot 10^{-11}$ W
GS antenna uptilt	ϕ_T	$\arctan(\Delta\gamma/\mathbb{E}[R_1])$	N/A
GS millimeter-wave antenna beamwidth	ω_G	N/A	10 deg
GS height above ground	γ_G	30 m	30 m
Buildings per square km	β	300 /km^2	300 /km^2
Fraction of area occupied by buildings	δ	0.5	0.5
Building height scale parameter	κ	20 m	20 m

antennas. We can see that the performance for both networks is relatively poor. In both cases, omnidirectional UAV antennas receive a large amount of interference, and the greater the height at which the UAV operates, the greater the likelihood of LOS interferers. We observe that the dedicated GS network provides a superior signal quality compared to the terrestrial network as the UAV heights increase. The downtilted antennas of the terrestrial BSs mean that at large heights the UAV receives side-lobe signals from its serving BS; combined with the greater interference strength, this causes significant reduction of signal quality. The GS network is able to provide a signal at full strength with its antennas which are tilted towards the sky, and as a result the achievable coverage probability remains relatively stable for the different UAV heights. Note that the GS network only requires a fraction of the density of the terrestrial BS network to achieve better performance.

In Fig. 4.3 we consider a UAV equipped with a downtilted directional antenna. The antenna directionality means that the UAV will only receive signals from devices within a certain horizontal distance of its location, with the UAV height determining this distance. When connecting to the BS network, a greater distance means that the UAV can connect to BSs further away which provide a stronger signal due to better BS antenna alignment [65]; however, it also means that the UAV will receive interference from more devices.

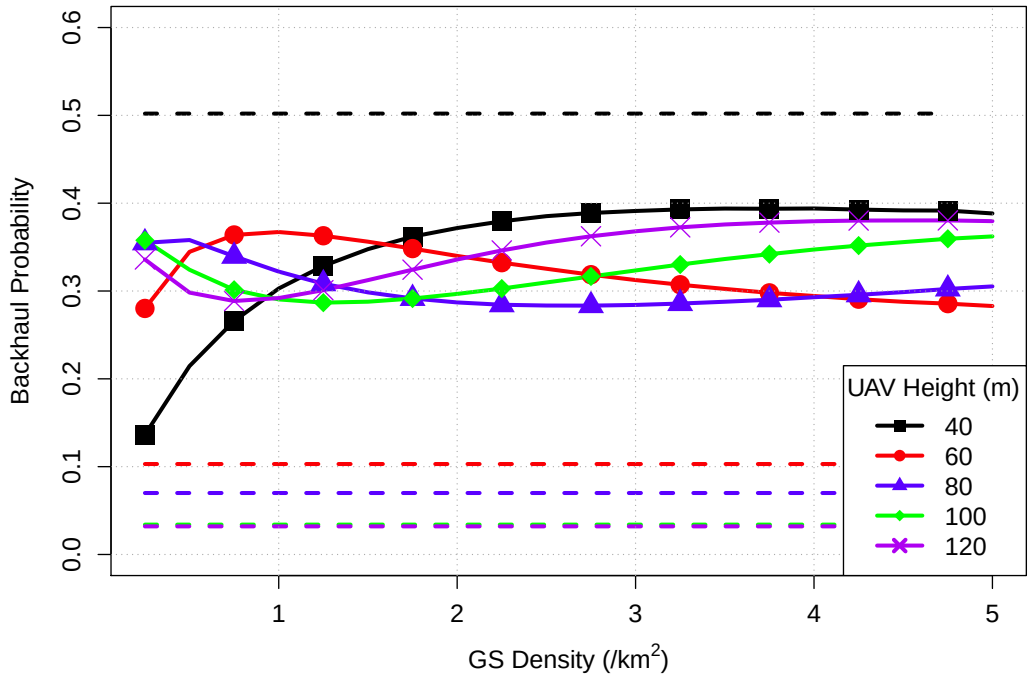

Figure 4.2: Coverage probability as a function of the GS density and UAV height for the omnidirectional UAV antenna case, given SINR threshold $\theta = 0$. Solid lines denote the GS network, dashed lines denote the terrestrial BS network.

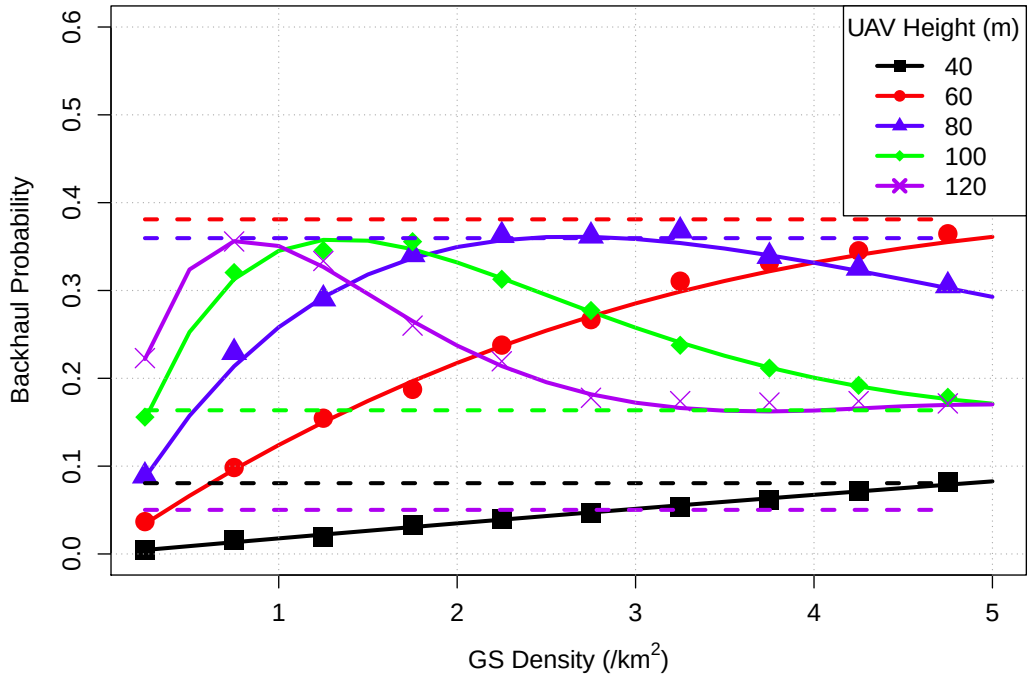

Figure 4.3: Coverage probability as a function of GS density and UAV height for the downtilted directional UAV antenna case, given a downtilted antenna beamwidth of 165 degrees. Solid lines denote the GS network, dashed lines denote the terrestrial BS network.

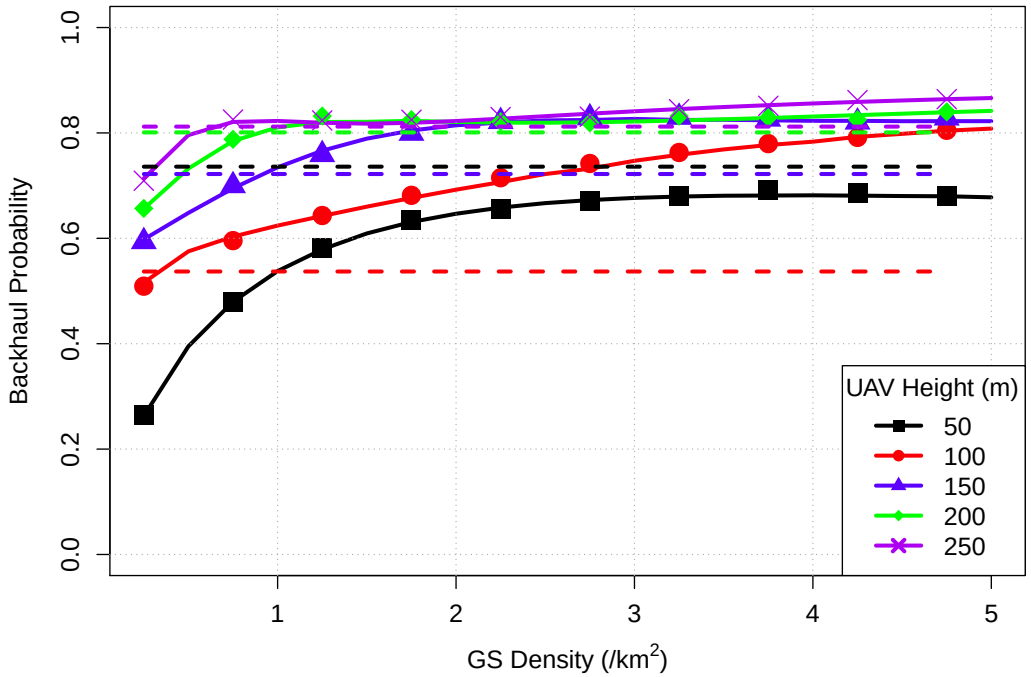

Figure 4.4: Coverage probability as a function of GS density and UAV height for the steerable directional UAV antenna case. Solid lines denote the GS network, dashed lines denote the terrestrial BS network.

The dedicated GS network with uptilted antennas can outperform the terrestrial BS service, but only when the UAV operates above a certain height. The decision to deploy a dedicated GS network for UAV service is therefore based on the specific height range the target UAV will operate at.

In Fig. 4.4 we show the network performance when the UAV is equipped with a steerable antenna, which it points at its serving GS or BS. Similar to the results in Figs. 4.2 and 4.3, the GS network outperforms the BS network when the UAVs operate at certain heights. Note that the coverage probability for the terrestrial BS case is improved over the previous two antenna cases, with the steerable UAV antenna being able to reduce the amount of received interference. The results show that equipping the UAV with a high quality antenna may provide a wireless signal of sufficient quality even through an unmodified terrestrial BS network.

4.4.2 Impact of GS Network Design Parameters on the Sub-6GHz Backhaul Probability

Having demonstrated that the GS network can provide superior performance to an ordinary terrestrial BS network we are interested in exploring the effect of the GS network density and height above ground on the achieveable backhaul probability. For the following results we assume the UAV has a steerable directional antenna. In Fig. 4.5 to Fig. 4.8 solid lines denote numerical results obtained via the analytical expressions, while marks denote simulations.

In Fig. 4.5 we demonstrate how increasing the density of the GSs improves the backhaul probability of the UAV. We consider the upper limit for the GS density to be 5 /km^2, which corresponds to the density of a terrestrial BS network in an urban environment [102]. For all cases the backhaul probability increases monotonically, with more GSs giving diminishing returns on the improved performance. Although the sub-6GHz backhaul is interference-limited, increasing the density of GSs has an overall positive effect on the backhaul probability, for the range of GS densities under consideration. These results suggest that a good UAV backhaul probability can be achieved when the density of GSs is only a fraction of the density of the existing BS network; if the GSs are to be co-located with the BS sites then this result demonstrates that a network operator only has to upgrade a fraction of the existing BS network to be able to provide a backhaul

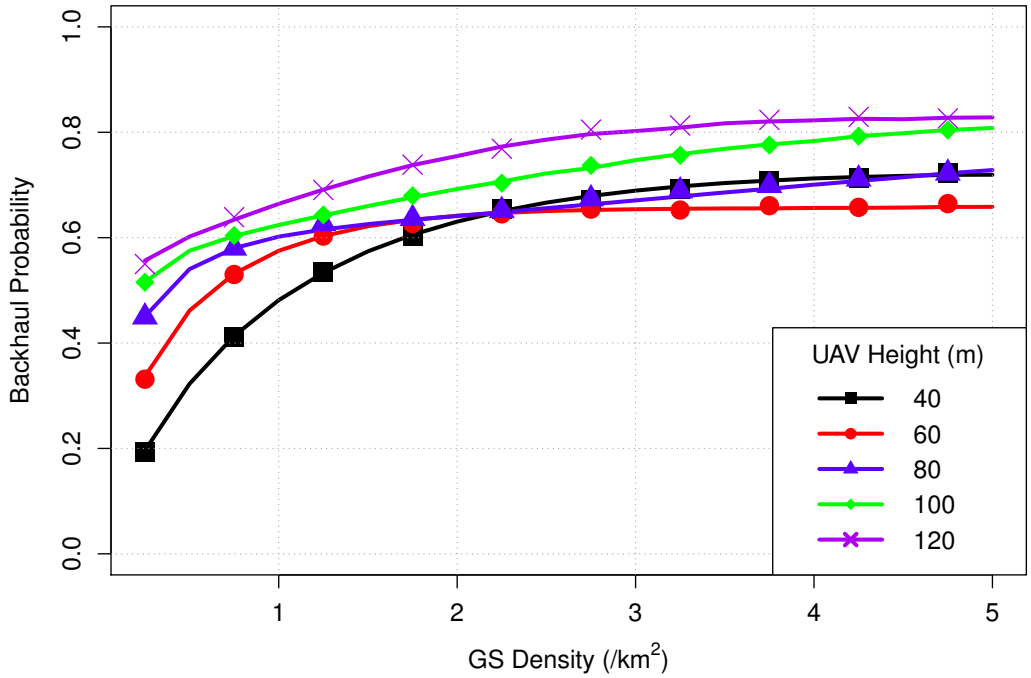

Figure 4.5: Backhaul probability for a sub-6GHz backhaul as a function of the GS density.

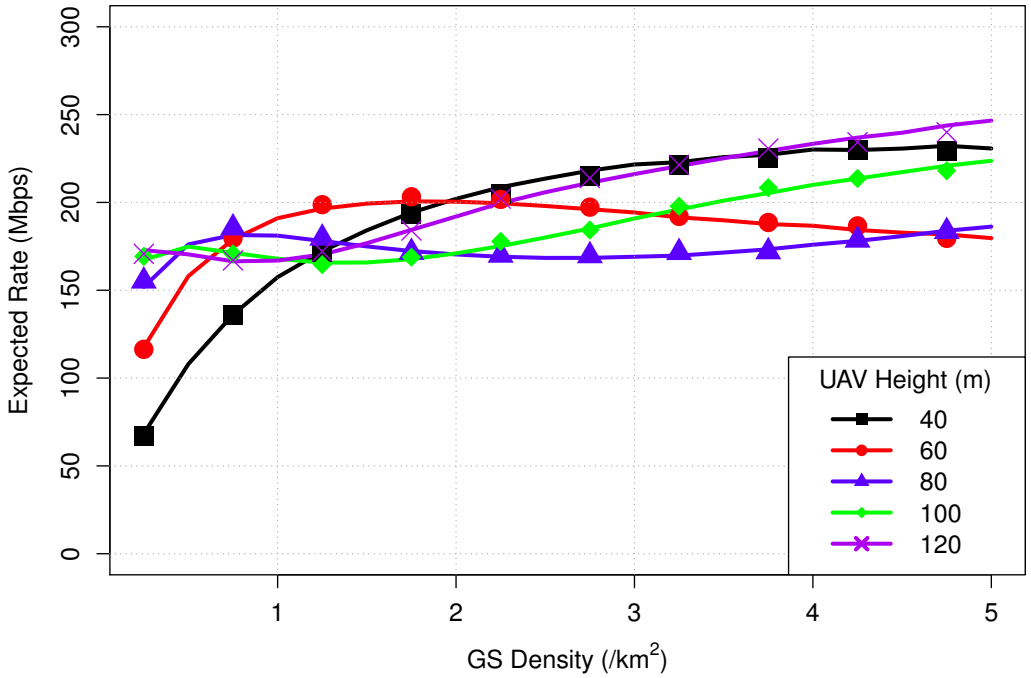

Figure 4.6: Expected data rate of a sub-6GHz backhaul as a function of GS density.

for a network of UAVs.

In Fig. 4.6 we plot the expected data rate supported by the sub-6GHz UAV backhaul as a function of the density of GSs. We can see that the expected rate initially increases as we increase the density of the GSs. However, due to the effect of interference the expected rate appears to behave differently depending on the UAV height. For the lowest UAV height the LOS probability on the interfering GSs is low due to building blockage, and therefore the rate monotonically increases with increased GS density. At the mid-range heights (60 and 80 m) the UAVs have a higher LOS probability on the interfering GSs; as a result increasing the density of the GSs improves the signal from the serving GS, but at the same time increases the aggregate interference. For the large heights (100 and 120 m) the UAV has a steep vertical angle to its serving GS, which results in a smaller area $\mathcal{W}$ illuminated by the UAV antenna and which limits interference. The height the UAVs will operate at will be largely determined by the UE link (as shown in Chapter 3); however, an operator may wish to avoid operating the UAVs within the range of heights which cause deteriorated backhaul performance, if such an option exists.

In Fig. 4.7 we consider the effect of the GS height on the backhaul probability of a sub-6GHz backhaul, for different UAV heights. We immediately observe that for larger GS heights the backhaul probability appears to deteriorate for all but the lowest UAV height. This effect is due to the increasing interference that is experienced by a typical

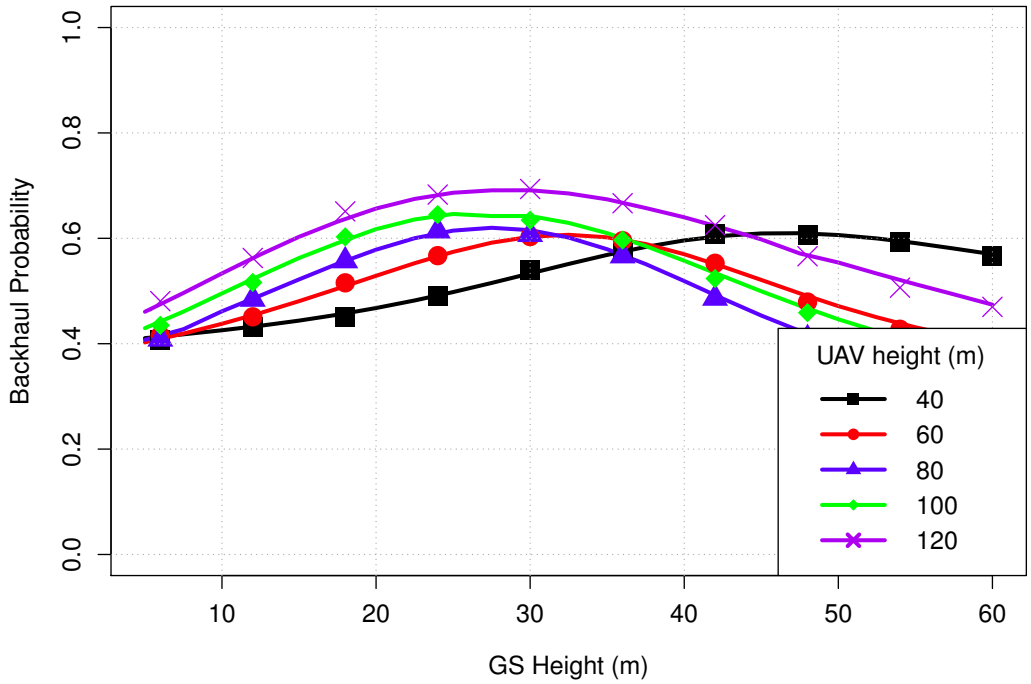

Figure 4.7: Backhaul probability for a sub-6GHz backhaul, given a GS density of 1.25 /km^2.

UAV as the GS heights increase; the improved wireless channel to the serving GS does not compensate for the improved wireless channels to the interfering GSs. The GS height cutoff point above which the interference deteriorates appears to be around 30 m, which corresponds to the height of LTE BSs in urban environments as proposed by the 3GPP model [102]. These results suggest that when deploying dedicated GSs for backhauling the UAVs using the sub-6GHz bands the operators should avoid placing the GSs any higher than the standard height used for the current terrestrial BS network, which also suggests that existing BS sites are suitable for hosting the backhaul GSs. It is also worth noting that the backhaul probability only marginally decreases for GS heights lower than 30 m; this suggests that it is possible to provide UAV backhaul using GSs that are positioned at heights very close to ground level.

4.4.3 Impact of UAV Placement on Sub-6GHz Backhaul Probability

We now consider the effect that the UAV placement has on the backhaul probability. In Chapter 3 we considered several UAV positioning schemes, with the UAVs being positioned with respect to the UE hotspots or other UAVs. As the UE hotspots are assumed to represent flash demand we assume that the placement of the GS network is independent of the hotspot locations, which means that the UAV network is also positioned independ-

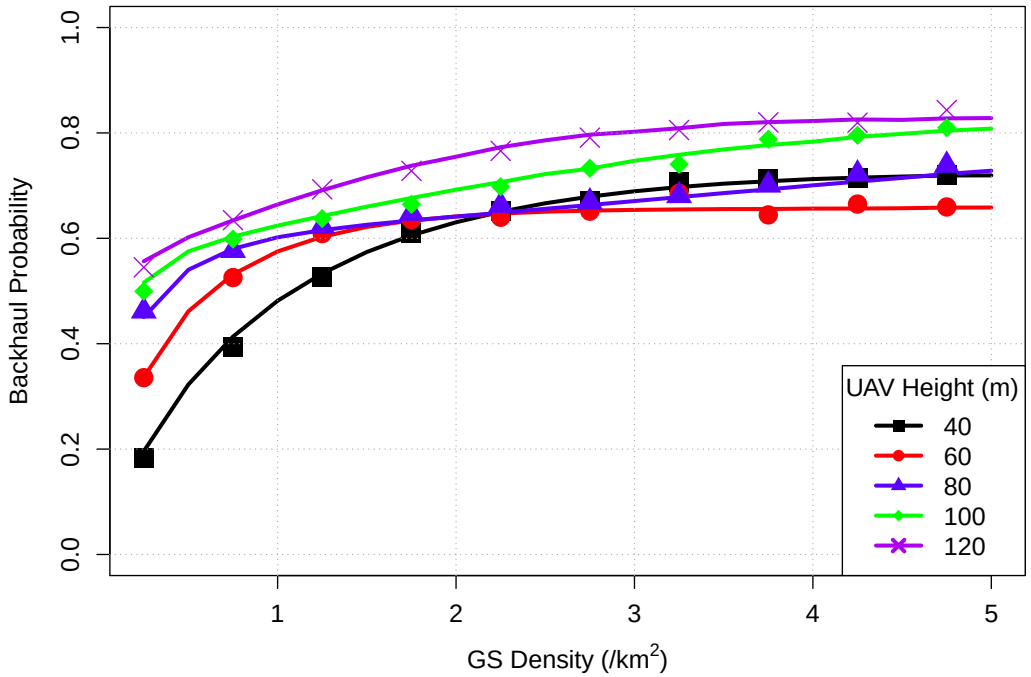

Figure 4.8: Backhaul probability as a function of the GS density. Lines denote our analytical results and marks denote simulation results, when UAVs are distributed according to a PCP.

ently of the GS network. As a result of this (lack of) spatial relationship between the UAVs and the GS network the backhaul probability will remain the same irrespective of the type of placement of the UAVs. To demonstrate this, the plot in Fig. 4.8 compares our analytical results against a simulation where a network of UAVs are distributed according to a Poisson Cluster Process (PCP); that is, they are clustered around certain locations. The two sets of results are perfectly aligned, demonstrating that our analytical model is applicable to a wide range of potential UAV spatial distributions, both random as well as optimised.

4.4.4 Impact of GS Network Design Parameters on the Millimeter-Wave Backhaul Probability

We now consider the performance of the backhaul when using millimeter-wave technology. In Figs. 4.9 and 4.10 the lines denote analytical results, while marks denote simulations. In Fig. 4.9 we consider the performance of the millimeter-wave GS backhaul when we vary the density of the infrastructure. Note that we set the millimeter-wave interference probability parameter ζ to zero, to reflect the fact the millimeter-wave antennas have very narrow beamwidths and therefore have an extremely low probability of alignment occuring by chance. As a result of this the millimeter-wave signal is

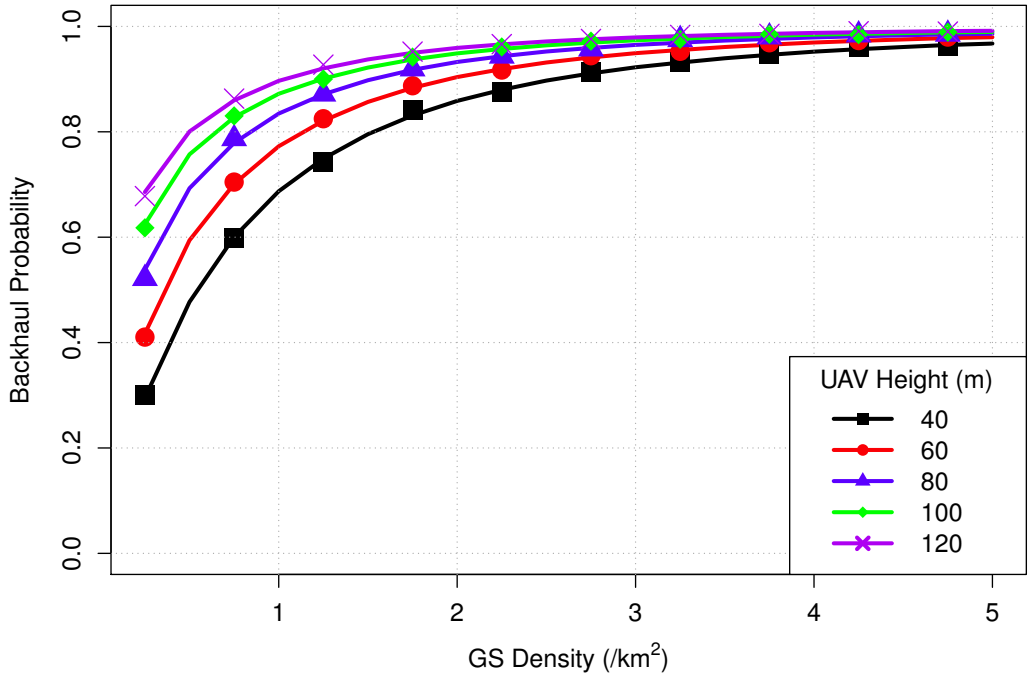

Figure 4.9: Backhaul probability for a millimeter-wave backhaul as a function of the GS density.

noise limited, with a resulting higher backhaul probability for the UAV compared to the interference-limited sub-6GHz signals.

In Fig. 4.10 we show the effect of the GS height on the backhaul probability when the backhaul uses a millimeter-wave signal. We see that the backhaul probability monotonically increases with increased GS height. This is due to the increase in the LOS probability between the UAV and the serving GS. Recall that for a millimeter-wave signal high-directionality antennas are assumed on the part of both the UAV as well as the backhaul, and as a result of this the UAV is assumed to receive no interference from other GSs, even when those GSs have LOS to the UAV. It follows then that the network operator should consider deploying the GSs as high as possible above the ground to maximise backhaul performance, which makes the existing BS sites sub-optimal for hosting the GS equipment, in contrast to the sub-6GHz backhaul case. As in the previous plots, we observe that greater UAV heights correspond to larger backhaul probability, showing the importance of operating UAVs at heights which can strike a balance between ensuring a good signal for the UEs while simultaneously allowing the UAVs to meet their backhaul requirements.

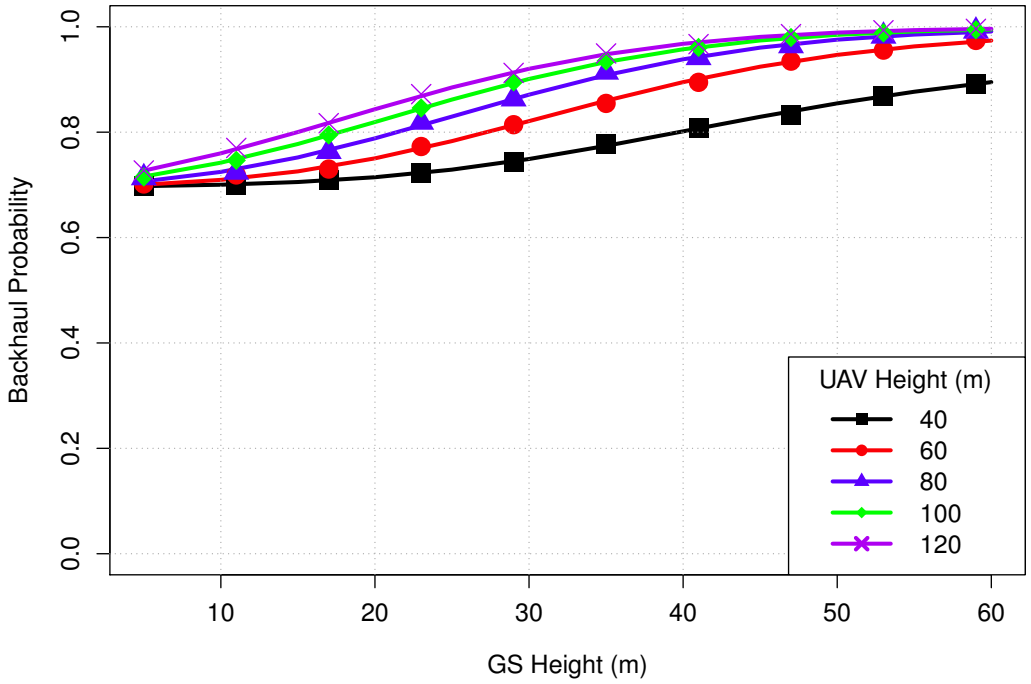

Figure 4.10: Backhaul probability for a millimeter-wave backhaul, given a GS density of $1.25\,/\mathrm{km}^2$.

4.4.5 Comparison With 3GPP Channel Model

As mentioned in Chapter 2 the 3GPP has recently released a set of specifications for analysing communication between a UAV and a terrestrial LTE BS, with an approved channel model for simulations [82]. We now compare the performance of our model to the model proposed by the 3GPP. The 3GPP model considers the scenario of UAV being served by a terrestrial BS network; however, the wireless propagation behaviour proposed in the model applies to our dedicated GS network scenario, as the GS hardware is assumed to be similar to terrestrial BS hardware when considering a sub-6GHz technology such as LTE. In Figs. 4.11 and 4.12 solid lines denote the results obtained via the analytical model, and markers denote simulation results using the pathloss and shadowing model for urban macro cells given in Tables B-2 and B-3 in [82]. In both cases we consider steerable UAV antennas.

In Fig. 4.11 we consider the backhaul probability as we vary the density of GSs, for different UAV heights. Compared to the 3GPP model our analytical expression provides a pessimistic view of the backhaul at low UAV heights and GS densities, when the channel is noise-limited and the UAV is likely to have an NLOS channel to its serving GS. At greater GS densities our model closely matches the 3GPP model, suggesting a good fit

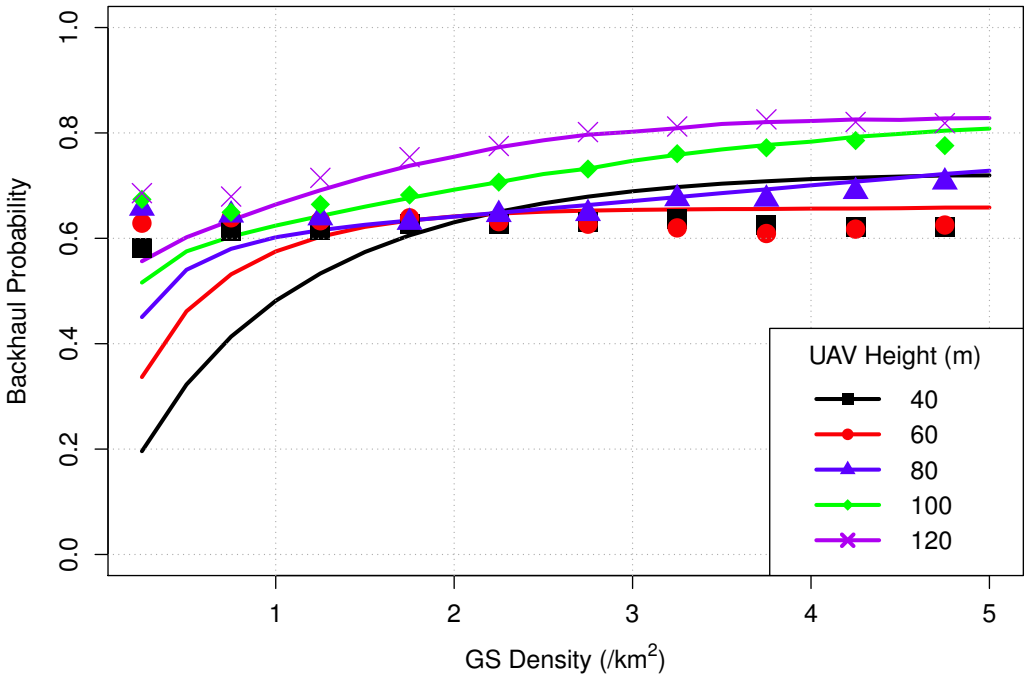

Figure 4.11: Backhaul probability as a function of the GS density.

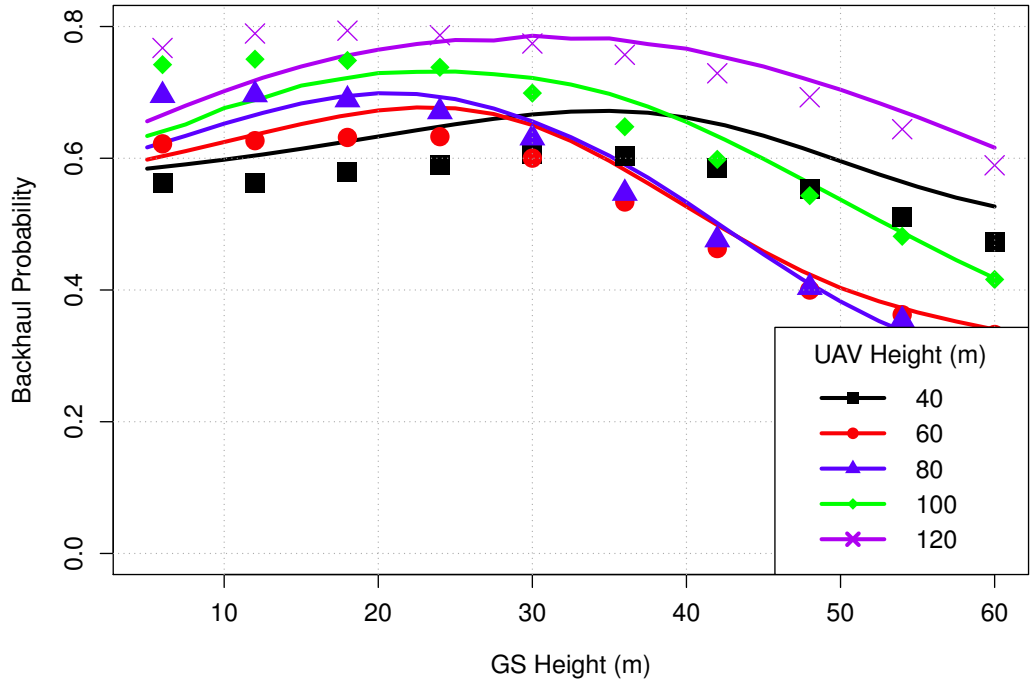

Figure 4.12: Backhaul probability given a GS density of 2.5 /km^2.

when the backhaul is likely to be LOS and interference-limited.

In Fig. 4.12 we consider the effect of the GS height on the backhaul probability, for different UAV heights. As with the previous figure, there is a good fit with the 3GPP model simulation results.

4.5 Conclusion & Discussion

In this chapter we applied stochastic geometry to model the ability of a network of UAV small cells to establish wireless backhauls into the core network, using dedicated GS infrastructure. As UAV infrastructure is an entirely new concept with its own unique strengths and weaknesses there are a number of questions about the network design that need to be answered, our analysis permits us to address some of these.

4.5.1 Use Existing BSs or Deploy Dedicated GSs?

The key questions which we intended to answer with the work in this chapter are: how would a dedicated GS network perform at providing a backhaul to UAV small cells, and whether deploying the dedicated infrastructure is warranted over using existing cellular BSs. Our results have shown that the answers to these questions depend heavily on the type of communications equipment carried by the UAVs themselves. Less complicated antenna configurations on the UAV small cells require dedicated GSs to achieve good performance, in a scenario where the UAVs are equipped with high-quality antennas which they can intelligently steer towards their serving devices the performance is very closely matched by both types of networks, assuming both the GSs and the BSs have access to the same spectrum resources. We see here a fundamental network design trade-off; if an MNO decides to invest in more complicated and more expensive equipment for the UAV side of the network this can permit the MNO to cut costs on the terrestrial infrastructure side. The weight restrictions of the UAV may play the decisive role in determining which option an MNO chooses; depending on the flying platform used and its operating requirements it simply may not be feasible to implement overly-complicated communications equipment, forcing the MNO to shift the complicated communications equipment to the ground.

This trade-off becomes even more complicated in scenarios where the terrestrial infrastructure and the UAVs are operated by different entities. In such a situation one entity investing more capital into their side of the network can dramatically improve performance (or save resources) for the other entity, which can lead to non-trivial market relationships between the two.

4.5.2 Sub-6GHz or Millimeter-wave for the Backhaul?

We have analysed the performance of the backhaul for both sub-6GHz and the millimeter-wave technologies; we note that both have their own advantages and disadvantages, which need to be considered carefully by an MNO before investing in the UAV network.

The big advantage of the sub-6GHz bands is that the technology is well established, with widely available hardware. Because of this, it should prove to be easier to successfully adopt for the new use-case of UAV networks. The hardware availability may also translate into lower capital costs for the network. Another reduction of capital costs may come from reusing existing BS sites, as we have demonstrated from our results. The two big disadvantages are the lack of bandwidth and the potential for interference. The sub-6Ghz bands are very congested, the available bandwidth for the backhaul that a typical UAV will be able to reliably obtain is potentially orders of magnitude lower than the sort of bandwidth offered by millimeter-wave, this may prove to be a significant bottleneck on the UAV network performance. Because the bands are so congested we may expect the UAVs to experience interference on their backhaul link, which will also limit the achieveable data rates in the backhaul. This issue may be alleviated by technologies such as massive MIMO [83], which are predicted to become widespread in future generations of cellular networks.

The obvious advantage of millimeter-wave for the backhaul is the available bandwidth, in the order of hundreds of MHz at certain frequencies. This can enable data rates of several Gbps across a single wireless link. The antenna directionality and beam steering also means that interference effects can be greatly reduced if not outright negated. Antenna beam steering also introduces one of the drawbacks of millimeter-wave communications: the potential for antenna misalignment. To ensure high-quality wireless links both the GS and the UAV have to align their antenna lobes towards one another; in our model we assumed that the antenna alignment is carried out successfully, but in a real-world scenario this may prove to be challenging, particularly when UAVs are mobile. Another issue with millimeter-wave communications is the complexity of the required components, such as the antenna array. This directly translates to greater infrastructure costs, and possibly heavier equipment to be carried by the UAVs. As our results demonstrated, the optimum heights for the millimeter-wave GSs are far above building rooftops and existing BS sites; deploying the infrastructure in a way that maximises performance may prove to be more costly than for the sub-6GHz case, due to the requirement for larger towers or entirely new sites.

5 UAV Energy Consumption and Battery Life

This chapter is based on the work "UAVs as Mobile Infrastructure: Addressing Battery Lifetime" published in IEEE Communications Magazine.

5.1 Introduction

In the previous chapters we have demonstrated how the flexibility of the UAV small cells allows them to provide high-quality signals to terrestrial UEs while wirelessly backhauling into the core network. This flexibility comes at a cost; as the UAV infrastructure is untethered it means that the devices must use a battery for power, which limits the operating time of a given UAV. An MNO who wishes to use a network of UAVs for serving UEs with cellular service must be aware of the limited flight time of the UAVs, and must plan around this limitation.

Due to the relatively young age of the UAV infrastructure concept the wireless community has not yet adequately explored the limited battery limitation of UAVs and the potential solutions to the issue. A number of papers have been published on the topic of optimising the battery usage by a UAV through optimisation of UAV movement or transmit power, as we have demonstrated in Section 2.4. More efficient use of the battery means that the UAV will be able to deliver a greater amount of data to the UE for a fixed battery life; however, optimising the battery use by the individual UAVs is not a sufficient solution to make UAV infrastructure an attractive option for MNOs. Cellular networks which use UAV infrastructure will have to be designed from the ground up to accommodate the limited flight times of the UAVs, how they accommodate this limitation and the resulting trade-offs need to be well understood.

Our contributions in this chapter are as follows:

1. Using simulations, we quantitatively evaluate three design solutions that can allow UAV networks to operate in an area of interest beyond the flight time of the individual UAVs. We demonstrate the impact the design parameters of the charging infrastructure on the overall performance of the UAV network.

2. We review several key battery technologies that are expected to become commercially available within the next several years. Using publications on the topic we provide approximate estimates of the performance improvement that the UAV network may experience in the foreseeable future.

This chapter is structured as follows. We begin with a discussion of the energy consumption of UAV platforms using battery technology available today, and how it impacts the performance of UAVs operating in the urban small cell scenario. We then discuss three techniques that could be applied to the UAV small cell network under consideration to allow UAVs to recharge and operate for extended periods of time. We review several new battery technologies that are expected to enter commercial use in the near future, and demonstrate how they can positively impact the UAV network. We then conclude by summarising our findings.

5.2 UAV Battery Life Today

We consider the scenario from Chapters 3 and 4, where UAV small cells with downtilted antennas are deployed in an urban environment to supplement terrestrial infrastructure in providing UE hotspots with wireless service. The UAVs are stationed at dedicated charging stations distributed on rooftops around the city where they are kept ready for rapid deployment. When a UAV is issued with the instructions to cover a demand hotspot it takes off, travels to the hotspot and hovers above it until it has just enough power left to safely return to its charging station and recharge. The amount of energy the UAV has to spend on travel between its charging station and the hotspot depends on the UAV speed and also the distance between the two locations. We assume that the locations of the charging stations and the hotspots are random with respect to one another, as the hotspots represent unpredictable spikes in UE demand. In Chapter 3 we demonstrated that there exists an optimum height for the UAVs to operate at, depending on the size of the hotspots and the directionality of the UAV antennas, and we assume that the UAVs position themselves directly above the hotspot centers at the optimum height. The simulation parameters are given in Table 5.1. The power consumption during horizontal

movement in watts, given velocity v in meters per second, is provided in [105] as

$$p_{con} = 0.0037v^4 + 0.0225v^3 - 0.6962v^2 + 0.3298v + 221.27. \tag{5.1}$$

Fig. 5.1 shows the length of time the UAVs can hover over the hotspots before they have to return to their charging stations, as a function of hotspot radius and UAV antenna beamwidth. Larger hotspot radii and narrower antenna beamwidths correspond to greater optimum UAV heights, which means that the UAV must expend more battery power getting into position and must preserve more battery power for the return trip. We can see that the UAVs will have 15-25 minutes of useful flight time on a single battery before they have to recharge, given that an outdoor event which creates UE hotspots may last several hours its clear that the operator may wish to take certain steps to ensure that UAV infrastructure can stay in the air for a sufficiently long period of time. Note that, while they may not be able to stay in the air for very long, the UAVs are capable of moving quite quickly through the environment; Fig. 5.2 shows the average length of time it takes for a UAV to travel from its charging station to its assigned operating point. Given this rapid response time and short operating time the UAVs available today may be most suited for use in emergency scenarios where a device needs to transmit or receive critically important data quickly, but not necessarily for an extended period of time.

Table 5.1: Battery Consumption Simulation Parameters

Parameter	Value
Charging Station Density	$1\,/\mathrm{km}^2$
Hotspot Density	$5\,/\mathrm{km}^2$
Optimum UAV Heights	see Chapter 3
Mean Charging Station Height	30 m
UAV Ascent Speed	2 m/s
UAV Descent Speed	1.5 m/s
UAV Horizontal Power Consumption	see Eq. (5.1)
UAV Ascent Power Consumption	249.01 W
UAV Descent Power Consumption	212.46 W
UAV Hover Power Consumption	221.27 W
UAV Battery Energy Density	250 Wh/Kg
UAV Battery Weight	0.4 Kg

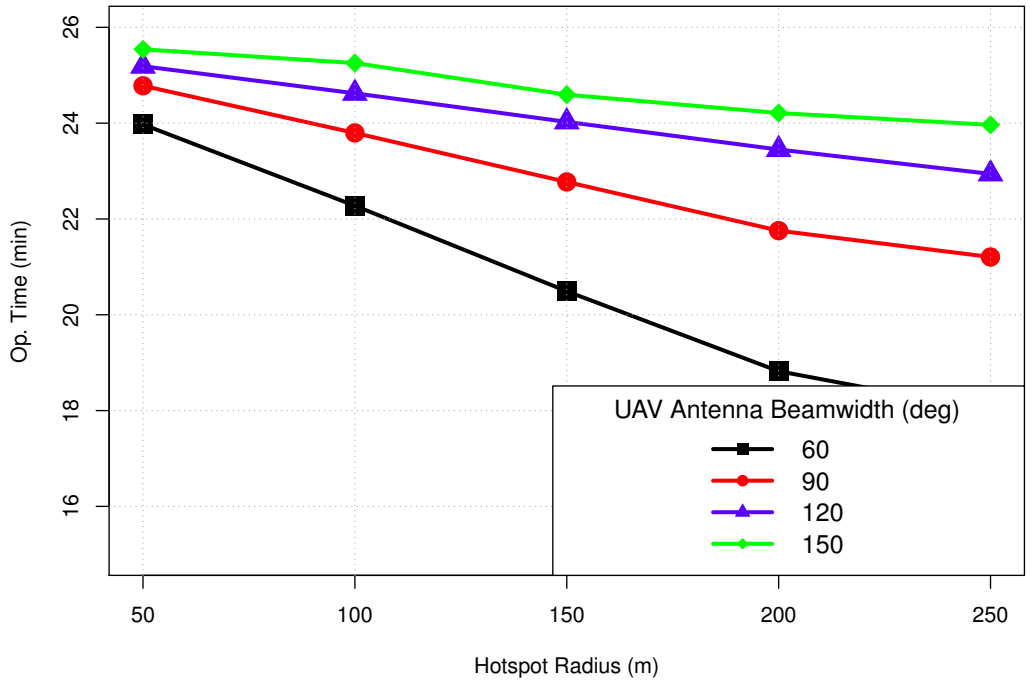

Figure 5.1: Operating lifetime of a UAV when it moves from its charging station to a position at the optimum height above a given hotspot, assuming horizontal speed of 8 m/s. The height is determined by the radius of the hotspot and also the beamwidth of the UAV antenna.

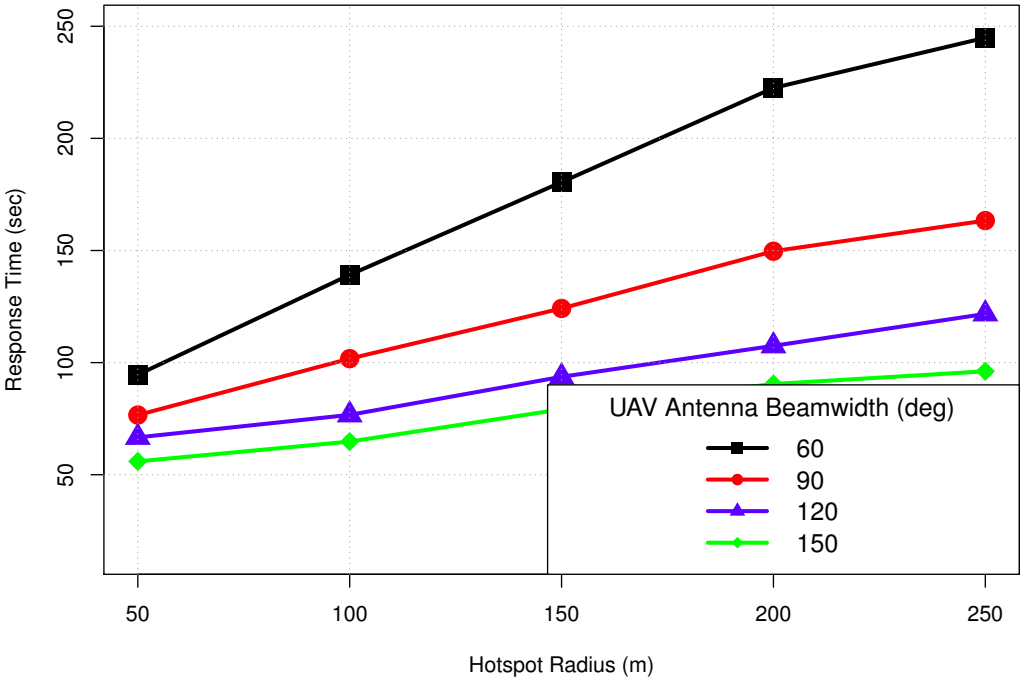

Figure 5.2: Response time of a UAV when it moves from its charging station to a position at the optimum height above a given hotspot, assuming horizontal speed of 8 m/s.

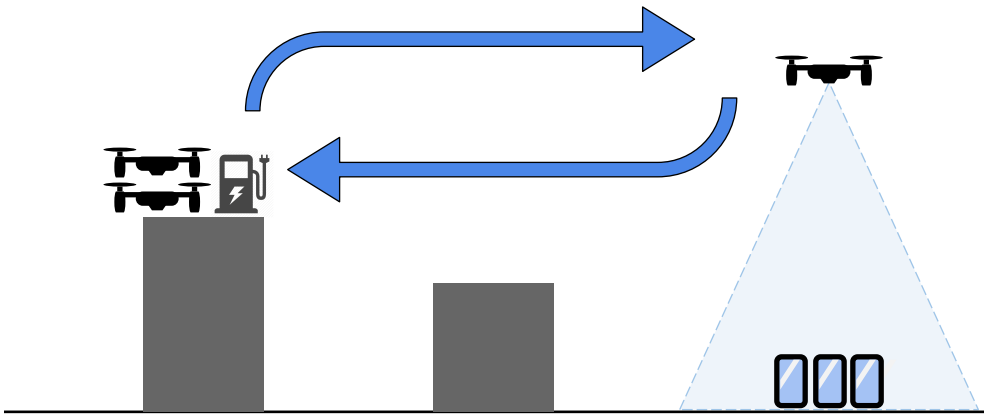

(a) Cycling through multiple UAVs to cover a hotspot

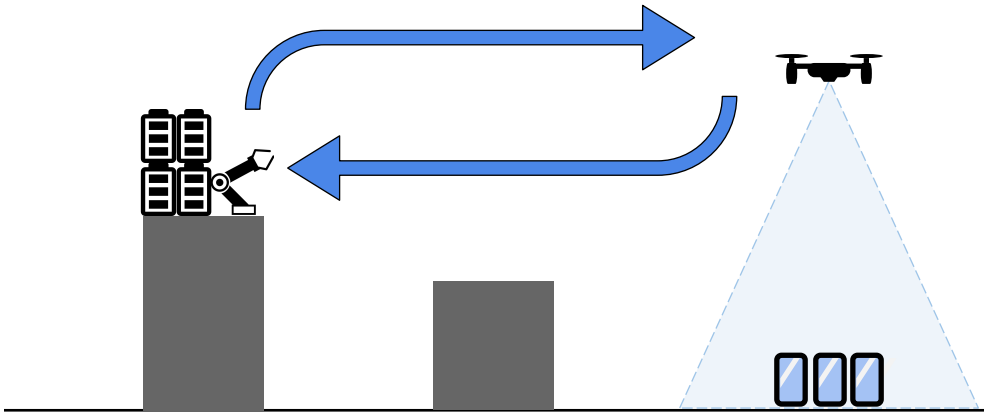

(b) Hotswapping batteries of a single UAV covering a hotspot

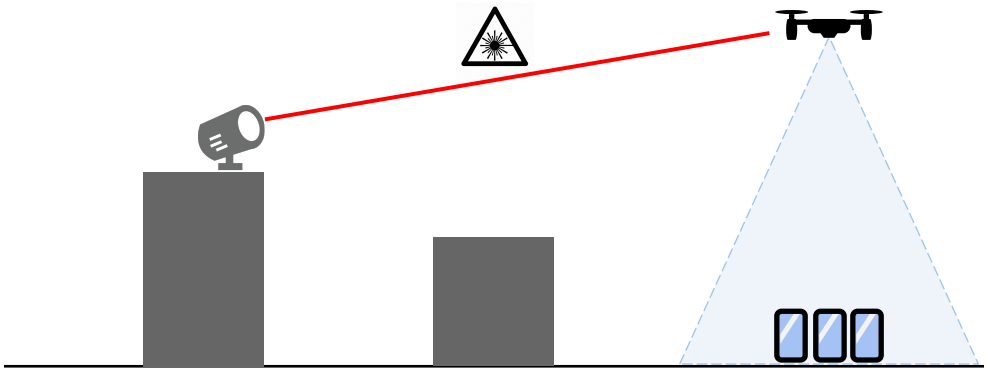

(c) Using lasers to wirelessly power a UAV

Figure 5.3: Proposed UAV battery management solutions.

5.3 UAV Swapping

One of the most straightforward ways of building a UAV network around the limited battery life of the UAV is to sequentially switch out low-power UAVs with ones that are fully charged, as depicted in Fig. 5.3(a). In this scenario, for each UAV that is operating above a user hotspot there are several other UAVs being charged at a charging station, waiting to be deployed. When the first UAV must return to its charging station to recharge it will be replaced by a second UAV, which in turn will be replaced by a third, and so on, until the first UAV is fully charged at the charging station and is ready to be deployed again. By having a sufficiently large number of backup UAVs and by timing their deployments such that one UAV hands over its hotspot seamlessly to another UAV the network can provide continuous, uninterrupted service to an area.

The number of backup UAVs that must be kept in a state of readiness for a given hotspot will be determined by UAV "downtime", that is, the length of time the UAV will need to travel back to its charging station, recharge, and return to the hotspot. The longer the recharge time, the more UAVs are needed to substitute it before it can deploy again. In Fig. 5.4 we demonstrate the number of backup UAVs that are needed, on average, for a given operating UAV as a function of the UAV recharging power and

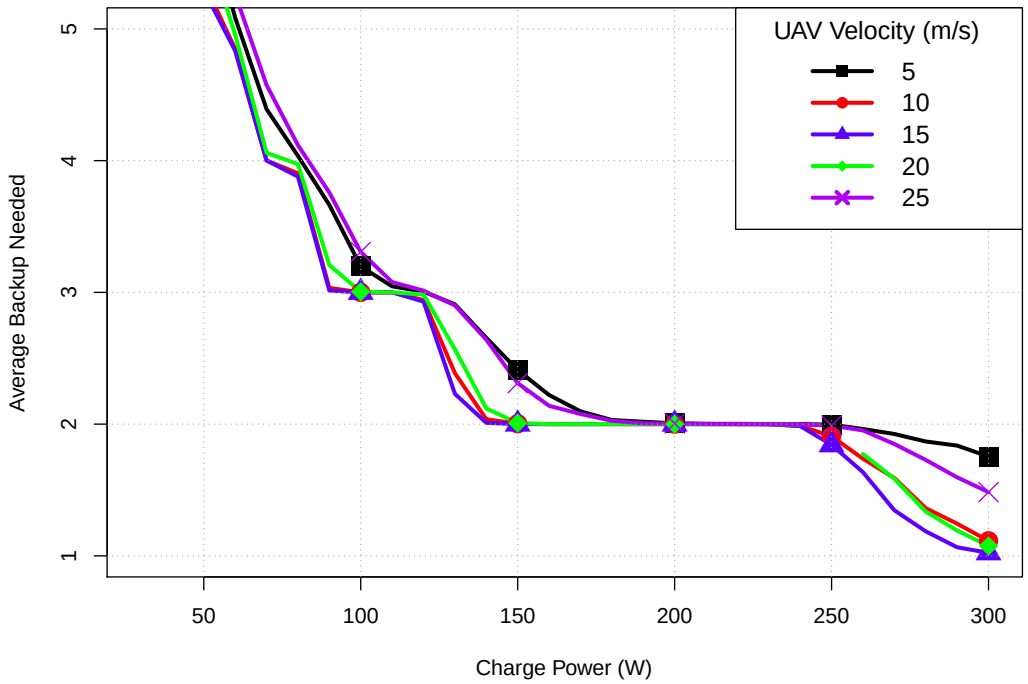

Figure 5.4: Average number of UAV backups that are needed for each UAV, as a function of UAV horizontal speed and the charger power.

the speed that the UAVs move at. If we consider commercially-available UAVs today to have a charging power of 180 W we may require as little as two backup UAVs for each operating UAV in the network to ensure continuous coverage. The figure clearly shows that developing new battery charging technologies to enable faster energy transfer and reduce charging time is needed to reduce the number of backup UAVs and make the UAV network more affordable. Note that the UAV horizontal velocity does not appear to have a significant impact on the number of backups: a higher velocity allows UAVs to spend less time on travel; however, it also consumes more battery power [105].

5.4 Battery Hotswapping

The majority of high-end UAVs nowadays are designed with external battery packs that can be detached from the UAV, thus enabling fast swapping of batteries by the UAV operator. Certain high-end models even carry two external batteries, both for safety reasons and to enable battery hotswapping. Battery hotswapping is when a UAV battery is replaced without the UAV being powered off, which allows it to return to its regular operation the moment the new battery is in place. The drawback of battery hotswapping is that it currently requires a human operator to carry out the mechanical operation of detaching the depleted battery and inserting a new one into the UAV. This introduces human labour into what may otherwise be an automated network. To address this, researchers have explored the concept of automated battery swapping stations, where robotic actuators are used to switch out batteries. The authors of [106] demonstrate a working prototype of such a station, showing how a UAV can automatically land into the charging station and have its battery swapped out within 60 seconds.

To demonstrate the benefits of this setup we consider the scenario depicted in Fig. 5.3(b). A UAV provides service above a user hotspot until its battery is depleted and it must return to its charging station. There, its battery is hotswapped with a backup battery and it returns to its hotspot, while its previous battery is charged up. Instead of having several backup UAVs we have several backup batteries, which reduces the cost of the infrastructure; however, because we only have one UAV per hotspot the hotspot will not be serviced for the length of time it takes the UAV to move to its charging station, hotswap its battery, and return back. Fig. 5.5 shows the duration of this downtime, as a function of horizontal UAV velocity and density of charging stations per unit area, assuming the hotswap procedure takes 60 seconds as in [106]. We can see that the total downtime will last less than 3 minutes for the majority of the UAV velocities. The 3 minutes of downtime (as per Fig. 5.5) may be accepable if the hotspot corresponds to regular user data

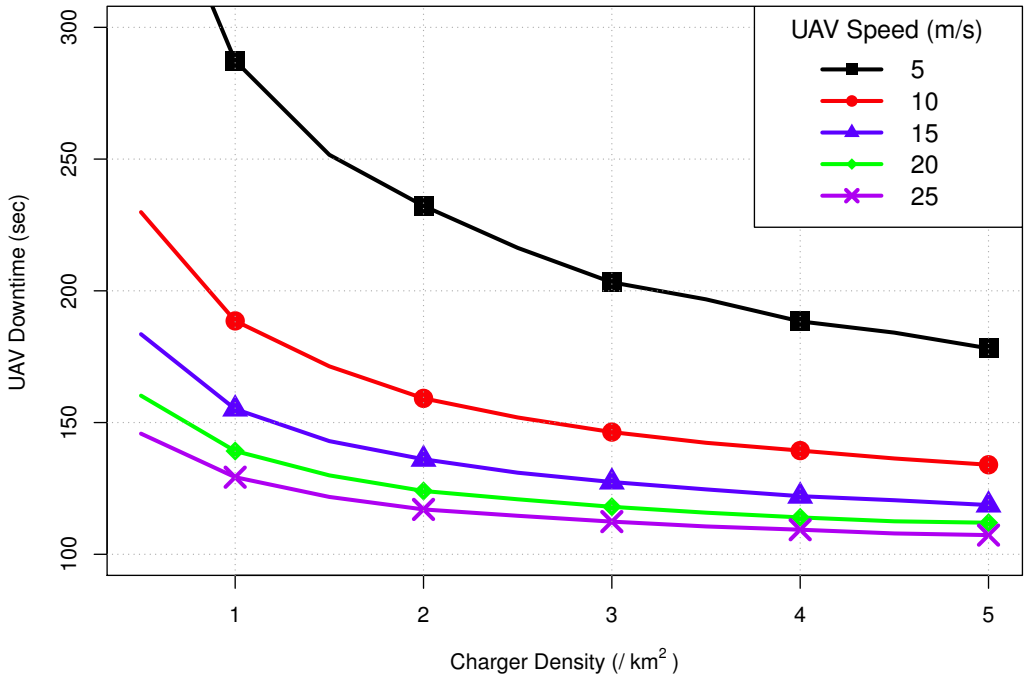

Figure 5.5: Total UAV downtime under battery hotswapping, as a function of charging station density and UAV horizontal speed.

traffic; for emergencies or other scenarios where the data is time-critical the operator may wish to have a backup UAV available, as in the previous section.

5.5 Wireless Power Transfer

Battery hotswapping appears to be a viable solution to the limited UAV battery life. However, it still requires UAVs to regularly move between their serving location and a charging station, which reduces the operating efficiency of the network. An alternative approach is to wirelessly transfer power to the UAVs. A variety of techniques for wirelessly transferring power to a UAV have been researched. These can be roughly separated into two categories: electromagnetic field (EMF) charging and non-EMF charging. EMF charging refers to using electro-magnetic fields to transfer energy, using magnetic induction or similar. These techniques work across a very short range (in the order of centimeters) and are incapable of transferring sufficient energy quickly enough to compensate for the energy consumption of the airborne UAV. Non-EMF refers to using photo-voltaic (PV) cells to charge UAVs, using power sources such as solar radiation.

Solar power has been considered for a variety of applications, including for use in UAVs. Typically, solar-powered UAVs operate at very large altitudes in the order of tens

of kilometers, as solar power generation is the most effective at larger altitudes; however, there has been some interest in applying solar power to small, low-altitude UAVs like the sort discussed in this paper. In [107] the authors present a prototype quadcopter UAV which carries a PV cell array. The authors report that the UAV is capable of staying airborne for 1-2 hours (depending on weather and payload weight), as harvesting solar power allows the UAV to offset some of the power consumed by the motors. Power consumption exceeds the power generation, so the UAV still relies on a battery supply which eventually runs out, forcing the UAV to land. As the UAV can replenish its battery supply using solar power it no longer has to land at dedicated charging stations, which gives the network more flexibility in how it operates. Note that the prototype UAV presented in [107] has a length and width of two meters; the large size may limit its ability to safely land outside of dedicated sites.

Using the UAV design parameters given in [107] we investigate the impact of the PV cell area on the UAV performance. Fig. 5.6 demonstrates that increasing the cell area increases the generated power, but the additional weight of the cells also increases the power consumption of the motors. We observe that the PV cells are incapable of generating sufficient power to drive the motors even when the PV cells are perfectly aligned with the sun, which means that the UAV batteries will always experience a net drain. Note that Fig. 5.6 presents an optimistic set of results, as we consider ideal weather conditions, while also assuming that the weight of the UAV airframe and motors does not increase with the increasing PV cell size.

As an alternative to solar power, we consider the case where the PV cells have energy beamed to them using lasers. The company Lasermotive has demonstrated a working prototype of a UAV which can remain in the air indefinitely using a kilowatt laser which transmits a beam of energy at a specially designed PV panel on the UAV [108, 109]. The difficulty with using lasers for energy transmission is that the lasers require an unobstructed LOS to the UAV to be able to reach it with their beam. In an urban environment with buildings of varying heights it may be difficult to guarantee a LOS link between a given UAV and its laser transmitter.

We explore the viability of radiative power transfer in the scenario depicted in Fig. 5.3 (c). We assume a number of laser transmitters are mounted on rooftops in a city, a UAV deployed above a hotspot will attempt to establish a LOS link to the nearest transmitter and have the transmitter beam power to it. The expression for the energy propagation of the laser beam is given in [109] as

$$p_{rx} = p_{tx} \frac{C \exp(-\alpha \sqrt{r^2 + \Delta\gamma^2})}{(D + \sqrt{r^2 + \Delta\gamma^2}\Delta\theta)^2}, \tag{5.2}$$

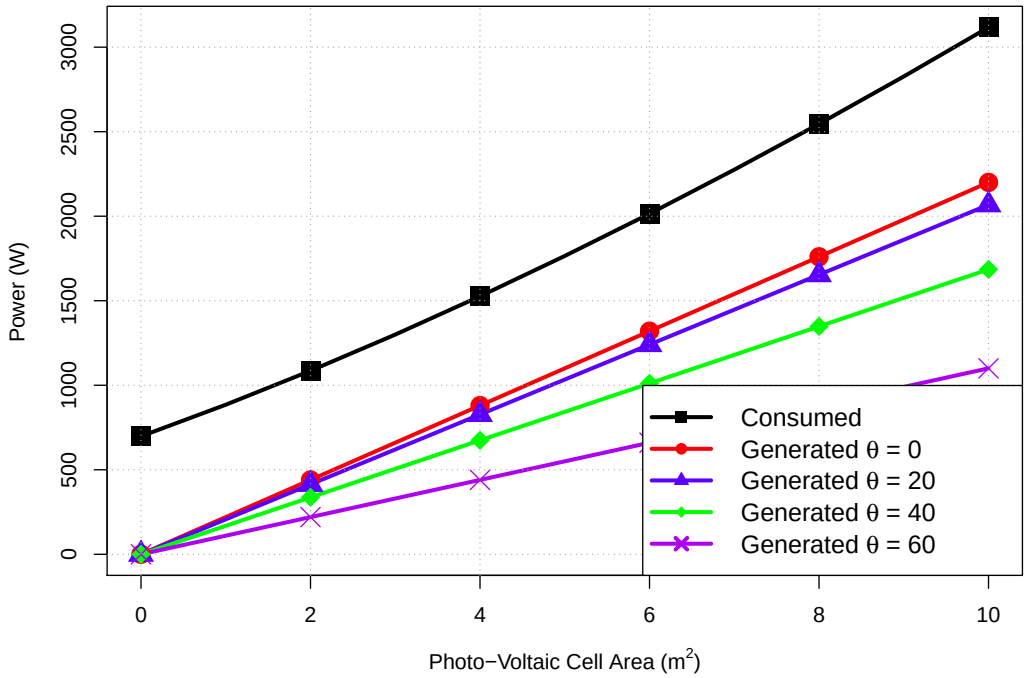

Figure 5.6: Energy consumed and produced by a solar-powered UAV, as a function of the PV panel area and the solar incidence angle θ.

where p_{tx} is laser transmit power, C is the combined efficiency of the transmitter and receiver, α is the distance-dependent attenuation coefficient, D is the size of the laser and $\Delta\theta$ is angular spread. The beam is assumed to be deactivated if there is a LOS obstruction for safety reasons. In Fig. 5.7 and Fig. 5.8 we give the probability that the UAV will receive sufficient power from the laser beam to negate its power consumption, for varying densities and heights of the laser trasmitters.

As the figure shows, the probability will depend significantly on how high the UAV is above ground, with greater heights making it more likely that the UAV can be wirelessly charged. The issue is that relying on wireless charging for the UAVs therefore limits the heights that the UAVs can operate at. Furthermore, the current legal height limit for UAVs in Europe and the USA is approximately 120 m (as discussed in Section 6.2) which, according to our results, will not allow for guaranteed wireless charging unless the laser transmitter density is very high or the transmitters are positioned high above ground. Another issue with the laser transmitter is that it can only power a single UAV at a time, as it has to mechanically steer its laser beam towards the UAV. This limits the amount of laser-powered UAVs that can be deployed in an area, as each UAV has to have its own dedicated laser transmitter when operational. Using laser transmitters to wirelessly power UAVs may be a good solution for UAVs that operate at greater heights than those currently envisioned by aviation authorities, however, for low-altitude UAVs operating in built-up areas it may not be the most practical solution.

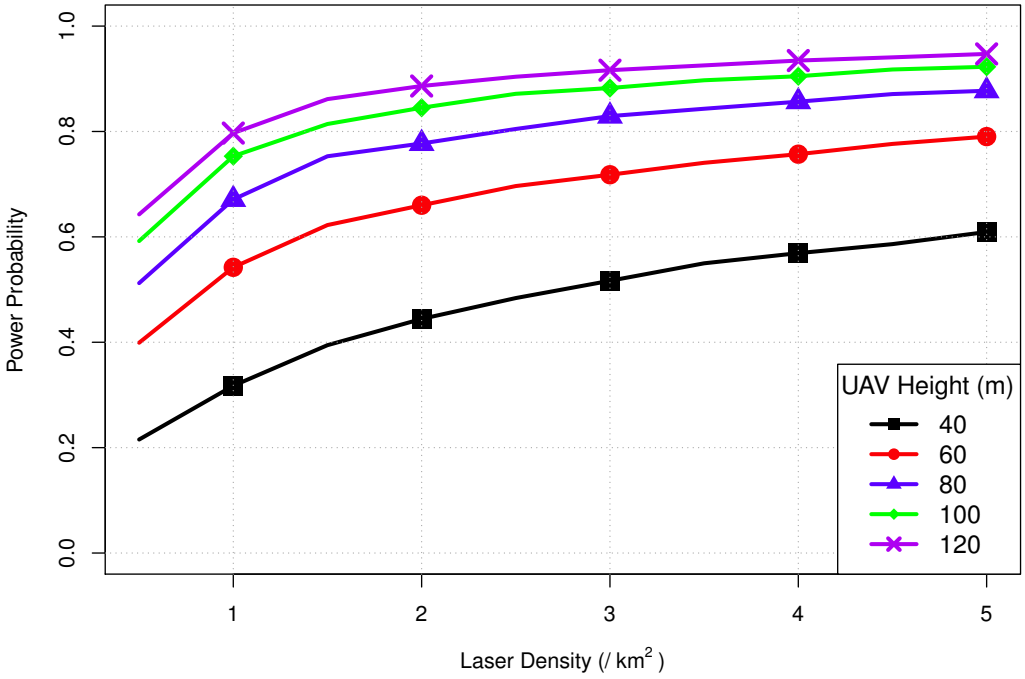

Figure 5.7: Probability that a UAV hovering above a hotspot can be successfully charged by the nearest laser transmitter to it, as a function of laser density.

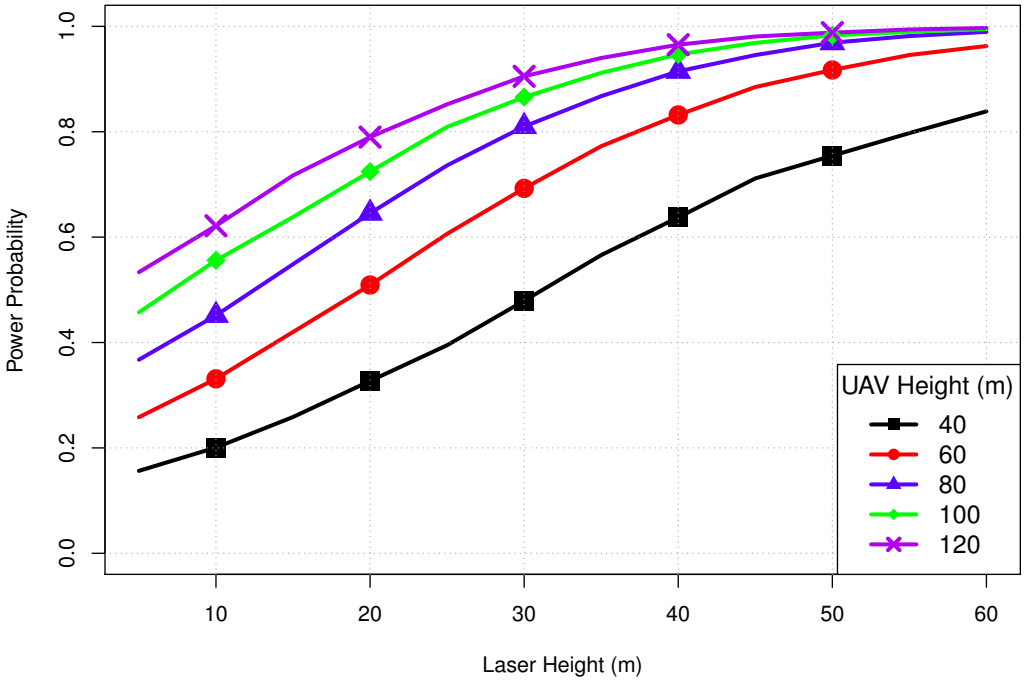

Figure 5.8: Probability that a UAV hovering above a hotspot can be successfully charged by the nearest laser transmitter to it, as a function of laser height above ground.

5.6 Battery Energy Density Improvements

Battery technology continues to advance at a steady pace, spurred on by the demand for greater energy density from the consumer electronics and electrical vehicle sectors. This improvement affects the cost of battery manufacture, the safety of the materials used, and the energy density of the batteries. Given that UAVs are significantly affected by their limited flight time we are particularly interested in the battery energy density, and how its improvement will improve the performance of the UAV network.

The authors of [110] suggest that historical improvement of battery energy density can be approximated as a steady 3% performance increase per year, which the authors point out is far too slow to satisfy the demands of the new, emerging technologies. Current commercially available UAVs use lithium-ion batteries with an energy density in the order of 250 Wh/kg, and the research discussed in [111] suggests that lithium-ion batteries may have their energy density improved by 20-30% within the next 5 years, reaching a performance ceiling by around 2025. So-called solid state batteries which use solid electrolytes are expected to contribute to this performance growth. Sodium-ion batteries are predicted to be one of the new battery variants to act as an alternative to lithium-ion [112], as the required materials are much more abundant than those used for lithium-ion batteries, which means the battery manufacturing cost would be far less vulnerable to market fluctuations. Unfortunately, sodium-ion batteries have a lower energy density than lithium-ion batteries so it is unlikely they will be a key driving technology for UAV networks. Three battery technologies on the horizon that do promise an improvement in energy density are the hydrogen fuel cell, the lithium-sulfur battery and the lithium-air battery, with a theoretical energy density of approximately 490 Wh/kg [113], 500 Wh/kg [114] and 1,300 Wh/kg [115], respectively. Unfortunately, these technologies have drawbacks which delay their adoption and commercialisation. There are concerns with the safety of both hydrogen fuel cells and lithium-sulfur batteries, while lithium-air batteries are known to be very vulnerable to exposure to the outside environment. Because of these drawbacks it is difficult to provide a reliable estimate on the dates when the new batteries may be adopted into UAV networks and the real-world performance these batteries will have. In Fig. 5.9 we aggregate the published findings to show the predicted operating time of UAVs in the coming years. A conservative estimate following the 3% annual performance increase suggests that UAVs may be able to fly in the order of 40 minutes by 2030 if hydrogen fuel, lithium-sulfur or lithium-air batteries are not commercialised by then. If they are, UAVs may be able to operate in the air for 1-2 hours at a time without needing a recharge in the not-too-distant future.

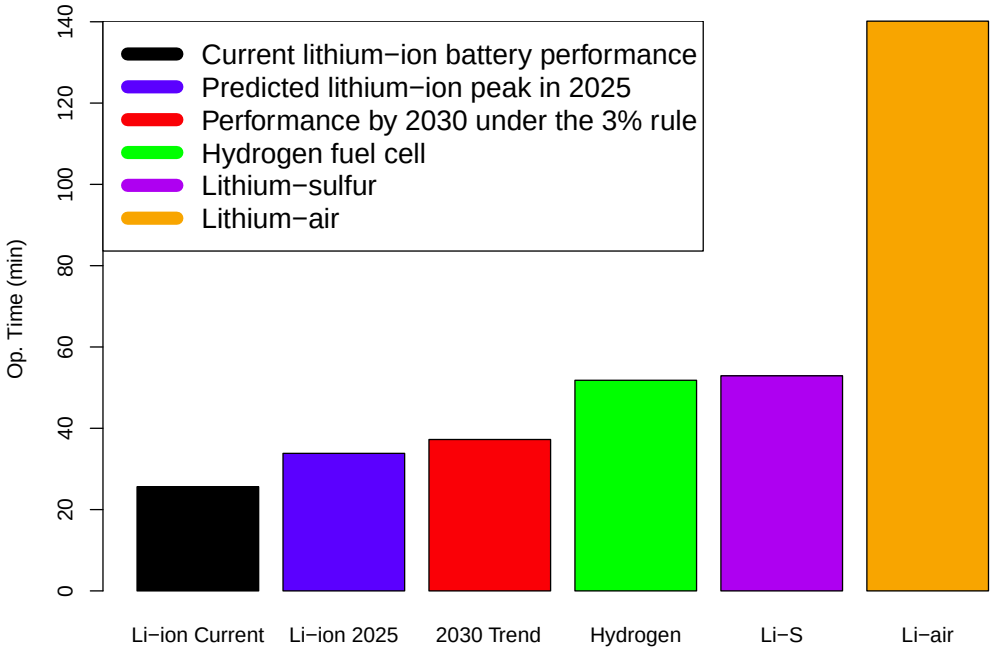

Figure 5.9: Simulated UAV operating time for different battery types.

5.7 Conclusion & Discussion

In this chapter we have considered several network design approaches that an MNO can implement to deal with the issue of limited battery life on UAVs. This allows us to answer several key questions about the battery lifetime of UAV small cells in urban environments.

5.7.1 How Long Can a UAV Small Cell Operate Above a Hotspot?

UAVs are an inherently temporary solution to the issue of excess traffic demand; when considering the option of investing in UAV small cells to supplement terrestrial infrastructure one of the first questions an MNO may ask is: "How long can they operate for?". From our simulations, multi-rotor UAV small cells can remain in the air for 15-25 minutes, not including the time it takes for them to travel to and from their charging stations. This means that UAVs today are limited in the type of hotspots they can continuously serve without stopping; any hotspots that last longer than 15-25 minutes (for example, hotspots caused by special events like football matches) could either receive partial UAV service, or they would force the UAV network to adopt more complicated deployment behaviours. Fortunately, battery technology is seeing continuous improvement from year to year, technologies such as hydrogen cells and lithium-air batteries promise to extend

this operating lifetime to anywhere from one to two hours. Once these batteries become commercially available for use in UAVs we expect UAV small cells to become significantly more capable at serving longer-lasting hotspots, which in turn can make the issue of UAV battery management less complicated.

5.7.2 How Should the UAVs Recharge?

Regardless of their operating lifetime, the UAVs will eventually run out of power and will be forced to land in some sort of charging station. We investigated three designs that an MNO can incorportate into the cellular network to allow the UAV to be recharged in a manner that still ensures the hotspots receive UAV service. Each of the three methods has its own advantages and disadvantages, whether it is cost, service downtime, or safety. Ultimately, the most appropriate solution will depend on the type of UAVs in operation, the environment they operate in and the type of data service that they are expected to deliver. Unlike the mobile UAVs the charging stations will have to be mounted on rooftops or other terrestrial sites, which also introduces the issue of site acquisition into the design process. Regardless of the method selected, our simulations have demonstrated that the UAV small cells can leverage their intelligent mobility and their rapid speed to successfully compensate for their short battery lifetimes, even if the densities of the charging stations are quite low in the area of interest.

6 Conclusions and Open Challenges

In the first section of this chapter we provide a high-level discussion of the outcomes of our research work. In the next section we discuss the legal status of low-altitude UAVs and how it is expected to change in the coming years. In the third section we discuss several open issues that may form the basis of future research on wireless communications using and supporting UAVs.

6.1 Research Outcomes

The core goal of this thesis was to explore the coverage and capacity of networks that rely on UAVs as additional network infrastructure, with a focus on the trade-offs that the features unique to UAVs have on the achieveable network performance. To conduct this analysis, we applied tools from stochastic geometry to characterise the UAV small cell network, and describe mathematically the relationship between the UAV network parameters and the performance of the interference-limited access link and backhaul channels. Our analysis unveiled several interesting aspects of UAV small cell networks.

For the access link, one of our key results was to show that there exists an optimum height that the UAV network should operate at, to mitigate the negative impact of both signal attenuation due to obstacles, as well as interference. The research community has repeatedly praised UAV infrastructure for its ability to establish unobstructed LOS channels to the terrestrial UEs; we have demonstrated how these LOS channels can, under certain circumstances, outright harm network performance. As a result, the height of the UAV network becomes a key optimisation variable, whose optimum value is a function of other UAV network parameters such as antenna beamwidth, as well as environmental parameters such as UE hotspot radius.

We have also demonstrated that the UAV network can mitigate interference by spacing itself out as much as possible, into a regular grid pattern. Given a sufficiently high density of UAV small cells we have also demonstrated that this positioning strategy is more likely

to meet the QoS requirements of the UEs than the strategy of placing UAVs above UE hotspots.

For the wireless backhaul link our contribution was to investigate the performance of dedicated GS infrastructure for providing wireless connectivity to the UAV small cells. We demonstrated that the achieveable backhaul performance will be heavily dependent on the type of antennas the UAVs are equipped with, and that deploying a dedicated GS network is warranted when the UAVs are equipped with less sophisticated antennas.

Using stochastic geometry we were also able to evaluate and compare the performance of sub-6GHz and millimeter-wave technologies for the backhaul link. We have demonstrated that both technologies have their advantages and disadvantages. The main advantages of the sub-6GHz technology have to do with potential ease of deployment. We have demonstrated that the optimum heights for deploying GSs correspond to the heights of typical cellular BSs in urban areas, as such there is potential for deploying the GSs at existing sites, rather than sourcing new ones. The millimeter-wave technology provides superior data rates; however, we demonstrated that the optimum heights for millimeter-wave GSs are far above any buildings in the environment we considered (to guarantee continuous LOS connectivity), which makes the issue of deploying the GSs more complicated than for the sub-6GHz case.

In our battery life chapter we investigated the limited UAV flight time, and how it can be designed around with the deployment of dedicated battery charging infrastructure. We reviewed the methodologies that are available to UAV networks to enable continuous UAV small cell service, and demonstrated via simulations how the performance of the network is affected by the energy charging infrastructure. Our results showed that UAVs today are most suitable for use in emergency scenarios due to their rapid speed; however, with an operating time in the order of 15-25 min they are limited in the type of continuous service they can provide. Dedicated charging infrastructure can allow continuous wireless service which extends beyond the flight time of individual UAVs, either by allowing UAVs to substitute one another, rapidly swapping depleted batteries on the UAVs, or by wirelessly charging the UAVs as they operate in the air. Furthermore, we applied the results of current research on next-generation battery technologies to our simulations, and demonstrated how the next generation of batteries could potentially allow UAV small cells to stay in the air for 1-2 hours at a time, significantly improving their ability to provide wireless service.

6.2 Legislation on UAV Use

One of the bigger challenges for the deployment of UAV small cells in urban areas is not technical, but legal. For our vision of UAV small cells to be realised the legal framework for UAV use must permit commercial operations of small UAVs at low altitudes inside urban areas. In this section we review the legal status of UAV use at the time of writing, we then discuss the legal trends and how they align with the quantitative results of our work.

6.2.1 Legislation Today

A several-ton metal machine travelling at hundreds of kilometers per hour thousands of meters above ground is a natural cause for safety concerns, and as a result conventional aviation is strictly regulated by state aviation authorities. Strict maintenance requirements are imposed on aircraft to ensure that they are kept air-worthy, while the pilots operating the aircraft must receive comprehensive training in all aspects of aviation before being issued a pilot licenses. The licenses themselves apply to different categories of aviation, so that a private pilot who flies a single-engine Cessna airplane is not allowed to operate a commercial jumbo jet. Before taking off into the air the flight plan must be passed on to the concerned aviation authorities, and during flight the pilots must follow instructions from the local Air Traffic Control (ATC).

The growing presence of UAVs has significantly complicated the issue of aircraft legislation. While larger UAVs operating in manned airspace are expected to adhere to the same regulations as conventional aircraft there is currently a great amount of ambiguity on the proper way to legislate small, very low altitude UAVs which operate inside unmanned airspace (the gap between manned airspace and the ground, see Fig. 6.1), like the ones investigated in this thesis [116]. Until a few years ago, small UAVs would fall under the same legal classification as Remote Control (RC) toys like model airplanes with very little regulation on their use. The number of privately-owned UAVs has skyrocketed since then, with the inevitable UAV misuses gaining public attention [117]. As a result, aviation authorities have begun introducing regulations to ensure the safe use of UAVs, for example [118] in the United States and [119] in the Republic of Ireland. The exact rules and registration requirements vary from country to country, but typical requirements can be summed up as:

1. The UAV must operate in unregulated airspace, with a maximum flight ceiling of around 120-150 m, depending on the country [7]

2. The UAV operator must always maintain a LOS on the UAV

3. The UAV must always stay within 300 m of the operator

4. The UAV should not be flown during night-time

5. The UAV should not be flown over other people, cars, or over private property[8]

6. The UAV operator should not operate more than one UAV at any given moment

7. The UAV should not fly within a certain distance (typically 1-5 km) of any airport, and should stay outside of designated no-fly zones, such as those above government buildings, hospitals and prisons.

The reader may note that the regulations that are currently in place outlaw many of the UAV use cases beyond simple hobbyist flight, including the cellular network use case. The 300 m distance restriction, for example, makes the use of UAVs for package delivery, as proposed by Amazon [120], effectively illegal, while the requirement that an operator only control one UAV at a time is a functional ban on autonomous UAV swarms.

[7]Exceptions can be made to this flight ceiling to allow for safe operation around obstacles such as skyscrapers.

[8]As of the time of writing, there is no universal consensus on whether private property extends into unregulated airspace and if operating a UAV over private property constitutes as trespassing. The legal rulings vary from jurisdiction to jurisdiction.

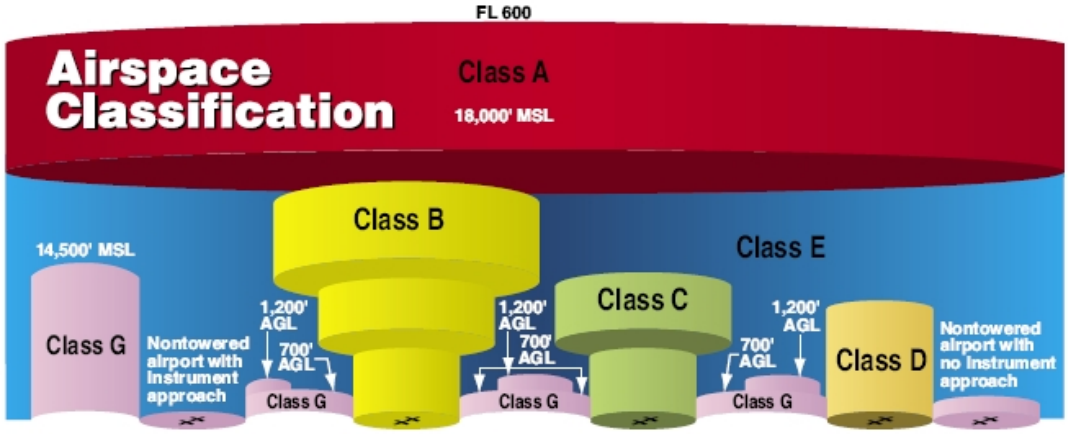

Figure 6.1: Airspace classification in the US. Class A-E airspace is manned and heavily regulated. Class G airspace is unmanned and, until very recently, posed little interest to regulatory bodies. Source : [121]

6.2.2 How Legislation is Changing

As we have shown in the previous subsection, the law today is not favourable towards the deployment of UAV small cells. Fortunately, many governments now recognise the economic value of UAVs being used for commercial purposes and the authorities are willing to accommodate businesses on a case-by-case basis. The Federal Aviation Administration (FAA), for example, offers a waiver program to allow companies to operate outside of the normal regulations. Under this waiver program AT&T was allowed to use a UAV to provide emergency LTE coverage in Puerto Rico after Hurricane Maria (see Section 1.1). In Ireland, licensed UAV pilots can apply for special permission to operate UAVs in restricted airspace or above congested airspace, provided they can demonstrate competence and carry out a risk assessment survey. As the UAV market is developing so quickly the regulations are being constantly revisited. The European Aviation Safety Agency (EASA) is currently developing a regulatory framework for the entire European Union that can accomodate multiple classes of UAVs and which is compatible with the local regulations of the individual member states [122]. The regulations separate the UAVs into multiple weight categories and differentiate between UAVs used for hobbyist and commercial purposes, with the intention of making it easier for commercial operators to apply for permission to use UAVs in a manner that is currently restricted.

One of the existing restrictions that will seemingly remain in place is the maximum flight ceiling [122]. While the other restrictions are more focused on ensuring UAVs are not a hazard to buildings or people on the ground, the flight ceiling restriction is in place to ensure that UAVs do not enter into manned airspace without permission from the ATC, thereby creating a hazard for manned aircraft. The regulatory framework [122] will continue to enforce a strict divide between the unmanned airspace where UAVs can operate, and the manned airspace reserved for aircraft which are part of the ATC controlled ecosystem. It follows then that UAV use cases which require heights above the flight ceiling will still face difficulties in obtaining operating permission.

Fortunately, our numerical results from the previous chapters suggest that the flight ceiling restriction will not hinder UAV small cell operation. The results in Chapter 3 suggest that the optimum height for serving terrestrial UEs is below the flight ceiling, except for cases where the UAV small cells use highly directional antennas. By selecting an appropriate antenna configuration for the UE access link the UAV operator can ensure that the network of UAVs will never need to cross into manned airspace to serve the UEs. The results in Chapter 4 suggest that UAVs can obtain a high quality backhaul signal while operating below the flight ceiling, provided that the GS network is deployed appropriately. The energy consumption analysis in Chapter 5 clearly shows that greater

UAV operating heights result in more energy being consumed in UAV movement, which reduces UAV operating time. Put together, the numerical results in this thesis all suggest that UAV small cells can operate exclusively inside unmanned airspace and thereby avoid creating a hazard for manned aircraft.

6.3 Open Issues and Potential Future Work

In this thesis we have made several contributions in the research area of UAV small cell networks. As one of our contributions we provided a robust UAV small cell model which captures the unique aspects of UAV small cell operation in cities. This model can serve as a platform for further analysis of UAV network performance. As UAV small cells are an entirely new research topic which uses infrastructure with unprecedented abilities, there are still a number of issues that need to be explored. Below we provide some examples of issues that are still open for investigation, and which may form the basis of our future research work into UAV use in cellular networks.

6.3.1 Fixed-wing UAVs

In this thesis we focused on the performance of multi-rotor UAV platforms carrying small cell infrastructure, due to the superior maneuverability of multi-rotor UAV designs over fixed wing or aerostatic designs. Fixed-wing UAVs, however, have one significant advantage which has also drawn the attention of the wireless community: these platforms are more energy-efficient in their propulsion than the multi-rotor variant. A fixed-wing aircraft flies by propelling itself forward and causing air to pass underneath its wings, which pushes the aircraft up due to the wing shape and the resulting airflow. The forward thrust needed to make a fixed-wing aircraft airborne is significantly smaller than the force needed in multi-rotor craft, and this directly translates to less energy consumption and a longer flight time [123]. This design may appear as an attractive alternative to rotor-wing craft; however, it introduces certain additional difficulties into small cell network operation.

The fixed-wing design is less maneuverable than the multi-rotor design because it requires the aircraft to be moving constantly at a minimum speed, otherwise it does not generate the lift needed to fly. This introduces additional complexity to the UAV placement problem, and introduces new variables which affect the service quality delivered to the UEs on the ground. Consider a scenario where each UAV in a UAV small cell network moves around in a circular pattern above a UE hotspot, with the radius of the circular

Figure 6.2: A fixed-wing UAV launched from a catapult. Image used with permission from : [124]

pattern determined either by the buildings in the area or the energy consumption of the UAV [37]. In this scenario the signal quality between a typical UE and its serving UAV will be affected not just by the parameters investigated in Chapter 3, but also by the orbiting patterns of the serving and interfering UAVs. We expect that these additional parameters will make the deployment process for fixed-wing UAVs more complicated than for the hovering rotor-wing UAVs envisioned in this thesis.

The fixed-wing UAV design also suffers from requiring a more complicated take-off and landing process. Whereas rotor-wing UAVs can take-off and land virtually anywhere the fixed-wing variant requires a large, open space to accelerate or decelerate. In some cases to take off the UAVs even require a dedicated catapult to provide the initial speed boost for take-off, as depicted in Fig. 6.2. As a result, the types of charging stations investigated in Chapter 5 may not be applicable to a fixed-wing UAV design.

6.3.2 Mobility Management and UE Handovers

Fixed picocell networks may experience issues with constant UE handovers and the so-called ping-pong effect, due to very small cell sizes, which UEs may enter and leave within a manner of seconds [125–127]. These issues may be exacerbated in UAV small cell networks: we expect that networks where the infrastructure periodically moves would

experience greater handover rates, with a corresponding increase in handover failure. This mobility management issue may not be as severe if the UAVs hover in place after moving to their optimum locations (as we consider for our use case), but given fixed-wing UAVs with their constant movement the increase in handover rates may be significant. Similar to the network coverage probability that was analysed in this thesis, we expect the handover rate (and the corresponding handover failure rate) to be a function of a number of network and environmental parameters; this relationship needs to be explored and understood for UAV network design.

6.3.3 Inter-Operator Resource Sharing

In this thesis we have implicitly assumed that all the components of the cellular network (the UE customers, the UAV small cells, as well as the terrestrial infrastructure) belong to a single MNO; however, there is a growing trend among wireless operators to share their infrastructure and spectrum resources, in an attempt to increase revenue or reduce expenses [128, 129]. For example, we can foresee a scenario where an MNO chooses to deploy UAV small cells without deploying their own dedicated GS network for backhauling, instead deciding rely on existing infrastructure that belongs to another MNO. In this scenario the performance of the UAV small cell network is tied to the performance of the terrestrial infrastructure network and the service delivered to its primary customers, and we can imagine a variety of possible trade-offs occurring in this situation which need to be carefully explored. Another resource-sharing scenario could consist of two or more UAV operators agreeing to service each other's UEs, whenever an operator cannot service its own UEs due to a lack of available UAV small cells (either because they're too far away, they're busy recharging, or there is no suitable backhaul connectivity in the area). In this scenario a number of factors will determine the QoS experienced by the UEs, and the UEs belonging to one MNO will experience different changes to their QoS than the UEs belonging to a different MNO.

The resource-sharing trend in cellular networks is expected to culminate in the vision of Networks Without Borders [130], which suggests that in the future the individual components that comprise a cellular network will be virtualised in a common resource pool, and that Over-The-Top (OTT) service providers will form intermittent networks from the pool to deliver specific services to their customers. The UAV small cell network introduces several new infrastructure resources to cellular networks, and these in turn add a new dimension to the resource sharing topic. In the presence of UAV small cells an OTT will be able to form an intermittent network from either fixed infrastructure, UAV infrastructure, or some combination thereof. Each has its own strengths and weaknesses

from the perspective of delivered QoS as well as the resources consumed from the pool.

It should be clear to the reader that UAV infrastructure introduces a variety of new questions and challenges into the area of resource sharing. While some attempts have been made to analyse resource sharing in UAV networks [63] there is a significant amount of work that still needs to be carried out to understand the new trade-offs, and how they can be leveraged to maximise the utility of UAV infrastructure.

7 Appendices

Appendix A

In this appendix we derive the expression $\mathcal{L}_{I_0}(s)$, given $V = i, R_V = r, T_V = t$. For ease of notation we omit these conditional expressions from the derivations below. The Laplace transform $\mathcal{L}_{I_0}(s)$ is derived as

$$\begin{aligned}
\mathcal{L}_{I_0}(s) &= \mathbb{E}\Big[\exp\Big(-sI_0\Big)\Big] \\
&= \mathbb{E}_{R_0,T_0}\Big[\mathbb{E}_{H_{T_0}}\Big[\exp\Big(-H_{T_0}\eta l(R_0,\gamma,\alpha_{T_0})s\Big)\Big]\Big] \\
&= \mathbb{E}_{R_0,T_0}\Big[g(R_0,s,m_{T_0},\alpha_{T_0})\Big] \\
&= \sum_{j\in\{1,n\}} \int_0^{r_{\max}} g(z,s,m_j,\alpha_j)\mathbb{P}(R_0 = z, T_0 = j|\bar{S}_0 < \bar{S}_i)\mathrm{d}z,
\end{aligned} \tag{7.1}$$

where

$$g(z,s,m_j,\alpha_j) = \left(\frac{m_j}{\eta s(z^2+\gamma^2)^{-\alpha_j/2} + m_j}\right)^{m_j}, \tag{7.2}$$

which comes from H_{T_0} being gamma distributed, with $\mathbb{P}(R_0 = z, T_0 = j|\bar{S}_0 < \bar{S}_i)$ denoting the joint probability of the hotspot center UAV's distance and channel type, given that the hotspot UAV is positioned such that its signal is weaker than the UE's serving UAV signal. This is derived as

$$\begin{aligned}\mathbb{P}(R_0 = z, T_0 = j|\bar{S}_0 < \bar{S}_i) &= \frac{\mathbb{P}(R_0 = z, T_0 = j, \bar{S}_0 < \bar{S}_i)}{\mathbb{P}(\bar{S}_0 < \bar{S}_i)} \\ &\overset{(a)}{=} \frac{\mathbb{P}(\bar{S}_0 < \bar{S}_i|R_0 = z, T_0 = j)\mathbb{P}(T_0 = j|R_0 = z)\mathbb{P}(R_0 = z)}{\mathcal{B}(t,r)} \\ &\overset{(b)}{=} \frac{\mathbf{1}(c_j(t,r) \leq z \leq r_{\max})\mathbb{P}_j(z)f_{R_0}(z)}{\mathcal{B}(t,r)},\end{aligned} \tag{7.3}$$

where (a) follows from replacing $\mathbb{P}(S_0 < S_i)$ with $\mathcal{B}(t,r)$ which is the probability of the hotspot center UAV providing a weaker signal than the serving UAV given in Eq. (3.14), (b) follows from $\mathbb{P}(R_0 = z) = f_{R_0}(z)$, $\mathbb{P}(T_0 = j|R_0 = z) = \mathbb{P}_j(z)$ and $\mathbb{P}(S_0 < S_i|R_0 = z, T_0 = j) = \mathbf{1}(c_j(t,r) \leq z \leq r_{\max})$ where $\mathbf{1}(.)$ is the indicator function. Inserting this expression into Eq. (7.1) we can write the integral as

$$\frac{2}{(r_{\max}^2)\mathcal{B}(t,r)} \sum_{j\in\{\mathtt{l},\mathtt{n}\}} \int_{c_j(t,r)}^{r_{\max}} g(z,s,m_j,\alpha_j)\mathbb{P}_j(z)z\mathrm{d}z. \tag{7.4}$$

Recall that $\eta = 0$ for values of $z > u(\omega,\gamma)$, which will reduce $g(z,s,m_j,\alpha_j)$ to 1. If $r_{\max} > u(\omega,\gamma)$ then the above integral is separated into two sub-integrals as

$$\frac{2}{(r_{\max}^2)\mathcal{B}(t,r)} \sum_{j\in\{\mathtt{l},\mathtt{n}\}} \left(\int_{c_j(t,r)}^{u(\omega,\gamma)} g(z,s,m_j,\alpha_j)\mathbb{P}_j(z)z\mathrm{d}z + \int_{u(\omega,\gamma)}^{r_{\max}} \mathbb{P}_j(z)z\mathrm{d}z \right). \tag{7.5}$$

The integrals in Eq. (7.4) and Eq. (7.5) assume that $c_j(t,r) < \min(r_{\max}, u(\omega,\gamma))$. For the case where $u(\omega,\gamma) \leq c_j(t,r) \leq r_{\max}$ the first sub-integral in Eq. (7.5) reduces to 0 and the second sub-integral takes $c_j(t,r)$ as its lower integration bound, if $c_j(t,r) \geq \max(u(\omega,\gamma), r_{\max})$ then both integrals reduce to 0. From the definition Eq. (3.1) the LOS probability is a step function, therefore the integral $\int_{c_j(t,r)}^{u(\omega,\gamma)} g(z,s,m_j,\alpha_j)\mathbb{P}_j(z)z\mathrm{d}z$ can be written as a sum of weighted integrals

$$\sum_{q=\left\lfloor c_j(t,r)\sqrt{\beta\delta}\right\rfloor}^{\left\lfloor u(\omega,\gamma)\sqrt{\beta\delta}\right\rfloor} \mathbb{P}_j(l) \int_l^u g(z,s,m_j,\alpha_j) z \mathrm{d}z, \tag{7.6}$$

where $l = \max(c_j(t,r), q/\sqrt{\beta\delta})$ and $u = \min(u(\omega,\gamma), (q+1)/\sqrt{\beta\delta})$. The integral $\int_l^u g(z,s,m_j,\alpha_j) z \mathrm{d}z$ can be expressed in analytical form,

$$\begin{aligned}
&\int_l^u \left(\frac{m_j}{\eta s (z^2+\gamma^2)^{-\alpha_j/2} + m_j}\right)^{m_j} z \mathrm{d}z \\
&\overset{(a)}{=} \int_{(l^2+\gamma^2)^{1/2}}^{(u^2+\gamma^2)^{1/2}} \left(\frac{m_j}{\eta s y^{-\alpha_j} + m_j}\right)^{m_j} y \mathrm{d}y \\
&\overset{(b)}{=} \frac{1}{\alpha_j} \int_{(l^2+\gamma^2)^{\alpha_j/2}}^{(u^2+\gamma^2)^{\alpha_j/2}} \left(1 - \frac{1}{1 + w m_j (\eta s)^{-1}}\right)^{m_j} w^{2/\alpha_j - 1} \mathrm{d}w \\
&\overset{(c)}{=} \frac{1}{\alpha_j} \left(\int_{(l^2+\gamma^2)^{\alpha_j/2}}^{(u^2+\gamma^2)^{\alpha_j/2}} w^{2/\alpha_j - 1} \mathrm{d}w + \sum_{k=1}^{m_j} \binom{m_j}{k} (-1)^k \int_{(l^2+\gamma^2)^{\alpha_j/2}}^{(u^2+\gamma^2)^{\alpha_j/2}} \frac{w^{2/\alpha_j - 1}}{(1 + w m_j (\eta s)^{-1})^k} \mathrm{d}w \right) \\
&\overset{(d)}{=} \frac{1}{2} \Bigg((u^2 - l^2) + \sum_{k=1}^{m_j} \binom{m_j}{k} (-1)^k \\
&\cdot \left((u^2+\gamma^2) {}_2\mathrm{F}_1\left(k, \frac{2}{\alpha_j}; 1 + \frac{2}{\alpha_j}; -\frac{m_j (u^2+\gamma^2)^{\alpha_j/2}}{\eta s}\right) \right. \\
&\left. - (l^2+\gamma^2) {}_2\mathrm{F}_1\left(k, \frac{2}{\alpha_j}; 1 + \frac{2}{\alpha_j}; -\frac{m_j (l^2+\gamma^2)^{\alpha_j/2}}{\eta s}\right) \right) \Bigg),
\end{aligned} \tag{7.7}$$

where (a) stems from the substitution $y = (z^2+\gamma^2)^{1/2}$, (b) from the substitution $w = y^{a_j}$, (c) from applying binomial expansion and (d) from using [103][Eq. 3.194.1], The solution above is inserted into Eq. (7.6) which is denoted as $\mathcal{C}_j(s)$ and inserted into Eq. (3.17).

Appendix B

In this appendix we present an analytical expression for a higher order derivative of $\mathcal{L}_{I_0}(s)$ for the case when I_0 is not 0. The ith derivative is given as

$$\frac{\mathrm{d}^i\mathcal{L}_{I_0}(s)}{\mathrm{d}s^i} = \frac{1}{r_{\max}^2\mathcal{B}(t,r)} \sum_{j\in\{1,n\}} \left(\sum_{q=\left\lfloor c_j(t,r)\sqrt{\beta\delta}\right\rfloor}^{\left\lfloor \min(r_{\max},u(\omega,\gamma))\sqrt{\beta\delta}\right\rfloor} \mathbb{P}_j(l) \sum_{k=1}^{m_j} \binom{m_j}{k} (-1)^k \right.$$
$$\left. \cdot \left(\frac{\mathrm{d}^i f\left(k,j,(u^2+\gamma^2),s\right)}{\mathrm{d}s^i} - \frac{\mathrm{d}^i f\left(k,j,(l^2+\gamma^2),s\right)}{\mathrm{d}s^i} \right) \right), \tag{7.8}$$

where

$$f\left(k,j,b,s\right) = b\,{}_2\mathrm{F}_1\left(k, \frac{2}{\alpha_j}; 1+\frac{2}{\alpha_j}; z(j,b,s)\right), \tag{7.9}$$

and

$$z(j,b,s) = -\frac{m_j b^{\alpha_j/2}}{\eta s}. \tag{7.10}$$

The ith derivative of $f\left(k,j,b,s\right)$ with respect to s can be obtained using [103][0.430.1]:

$$\frac{\mathrm{d}^i f\left(k,j,b,s\right)}{\mathrm{d}s^i} = \sum_{p=1}^{i} \frac{U_p}{p!} \frac{\mathrm{d}^p f\left(k,j,b,s\right)}{\mathrm{d}z^p}, \tag{7.11}$$

where

$$U_p = \sum_{a=0}^{p-1} (-1)^a \binom{p}{a} z(j,b,s)^a \frac{\mathrm{d}^i z(j,b,s)^{p-a}}{\mathrm{d}s^i}, \tag{7.12}$$

$$\frac{\mathrm{d}^p f\left(k,j,b,s\right)}{\mathrm{d}z^p} =$$
$$b\frac{k_{(p)}(2/\alpha_j)_{(p)}}{(1+2/\alpha_j)_{(p)}} \left({}_2\mathrm{F}_1\left(k+p, \frac{2}{\alpha_j}+p; 1+\frac{2}{\alpha_j}+p; z(j,b,s)\right)\right), \tag{7.13}$$

and

$$\frac{\mathrm{d}^i z(j,b,s)^{p-a}}{\mathrm{d}s^i} = \sum_{e=0}^{i}\sum_{n=0}^{e}(-1)^n(-m_j b^{\alpha_j/2}/\eta)^e(-m_j b^{\alpha_j/2}/(\eta s))^{(p-a-e)} \cdot \frac{s^{(-i-e)}(1+p-a-e)_{(e)}(1+n-i-e)_{(i)}}{n!(e-n)!}, \tag{7.14}$$

where $(.)_{(a)}$ is the Pochhammer notation for the rising factorial.

Appendix C

The Laplace transform $\mathcal{L}_{I_j}(s)$, where $j \in \{\mathtt{l}, \mathtt{n}\}$, corresponds to the aggregate interference of all the UAVs in the set Φ_j. Given $T_V = t$ and $R_V = r$ this is expressed as

$$\begin{aligned}
\mathcal{L}_{I_j}(s) &= \mathbb{E}\left[\exp\left(-sI_j\right)\right] \\
&= \mathbb{E}_{\Phi_j}\left[\prod_{x\in\Phi_j}\mathbb{E}_{H_j}\left[\exp\left(-sH_j\eta l(||x||,\gamma,\alpha_j)\right)\right]\right] \\
&\overset{(a)}{=} \mathbb{E}_{\Phi_j}\left[\prod_{x\in\Phi_j} g(||x||,s,m_j,\alpha_j)\right] \\
&\overset{(b)}{=} \exp\left(-2\pi\int_{c_j(t,r)}^{u(\omega,\gamma)}(1-g(z,s,m_j,\alpha_j))\,\lambda_j(z)z\mathrm{d}z\right) \\
&\overset{(c)}{=} \exp\left(-2\pi\lambda_u\sum_{q=\left\lfloor c_j(t,r)\sqrt{\beta\delta}\right\rfloor}^{\left\lfloor u(\omega,\gamma)\sqrt{\beta\delta}\right\rfloor}\mathbb{P}_j(l)\int_l^u(1-g(z,s,m_j,\alpha_j))z\mathrm{d}z\right),
\end{aligned} \tag{7.15}$$

where (a) comes from Nakagami-m fading having a gamma distribution, (b) comes from the probability generating functional of the PPP [91] and the conversion to polar coordinates, (c) comes from the relationship $\lambda_j(z) = \mathbb{P}_j(z)\lambda_u$ and from $\mathbb{P}_j$ being a step function as in Eq. (7.6), with $g(z,s,m_j,\alpha_j)$ being given in Eq. (7.2). The integral $\int_l^u(1-g(z,s,m_j,\alpha_j))z\mathrm{d}z$ is solved similarly to the derivation process in Eq. (7.7) to give

$$\frac{1}{2}\sum_{k=1}^{m_j}\binom{m_j}{k}(-1)^{k+1}\Bigg((u^2+\gamma^2)_2\mathrm{F}_1\Big(k,\frac{2}{\alpha_j};1+\frac{2}{\alpha_j};-\frac{m_j(u^2+\gamma^2)^{\alpha_j/2}}{\eta s}\Big) - (l^2+\gamma^2)_2\mathrm{F}_1\Big(k,\frac{2}{\alpha_j};1+\frac{2}{\alpha_j};-\frac{m_j(l^2+\gamma^2)^{\alpha_j/2}}{\eta s}\Big)\Bigg). \tag{7.16}$$

This is inserted into Eq. (7.15) to give the final expression for $\mathcal{L}_{I_j}(s)$ Eq. (3.20).

Appendix D

In this appendix we present an analytical expression for a higher order derivative of $\mathcal{L}_{I_j}(s)$, where $j \in \{\mathtt{l},\mathtt{n}\}$. Following Eq. (3.20) $\mathcal{L}_{I_j}(s)$ can be expressed as a composite function

$$\mathcal{L}_{I_j}(s) = \exp\left(y(s)\right). \tag{7.17}$$

By expressing the Laplace transform as a composite function we can arrive at a generalised expression for the nth derivative of the Laplace transform. We use Faà di Bruno's formula to define the nth derivative of the composite function Eq. (7.17) with respect to s as

$$\frac{\mathrm{d}^n \exp\left(y(s)\right)}{\mathrm{d}s^n} = \sum \frac{n_k!}{g_1!g_2!...g_n!}\exp\Big(y\Big(s\Big)\Big)\prod_{i=1}^{n}\left(\left(\frac{\mathrm{d}^i y(s)}{\mathrm{d}s^i}\right)/i!\right)^{g_i}, \tag{7.18}$$

where the first sum is over all the tuples that satisfy the sum $\sum_{i=1}^{n} ig_i = n$. The ith derivative of $y\Big(s\Big)$ is given as

$$\frac{\mathrm{d}^i y(s)}{\mathrm{d}s^i} = -\pi\lambda_u \sum_{q=\left\lfloor c_j(t_\star)\sqrt{\beta\delta}\right\rfloor}^{\left\lfloor u(\omega,\gamma)\sqrt{\beta\delta}\right\rfloor} \mathbb{P}_j(l)\sum_{k=1}^{m_j}\binom{m_j}{k}(-1)^{k+1} \cdot\left(\frac{\mathrm{d}^i f\left(k,(u^2+\gamma^2),s\right)}{\mathrm{d}s^i} - \frac{\mathrm{d}^i f\left(k,(l^2+\gamma^2),s\right)}{\mathrm{d}s^i}\right), \tag{7.19}$$

where $f\left(k,b,s\right)$ follows the definition in Eq. (7.8) and Eq. (7.10). The higher-order derivative $\mathrm{d}^i y(s)/\mathrm{d}s^i$ is obtained following the methodology of Appendix B, this solution is then inserted into Eq. (7.18) to give the higher-order derivative of $\mathcal{L}_{I_j}(s)$.

Appendix E

The coverage probability expression Eq. (3.21) is derived as follows:

$$\begin{aligned}
&\mathbb{P}\Big(\text{SINR} \geq \theta\Big) \\
&= \mathbb{P}\left(\frac{S_V}{I+\sigma^2} \geq \theta\right) \\
&= \mathbb{P}\left(\frac{\eta l(R_V,\gamma,\alpha_{T_V}) H_{T_V}}{I+\sigma^2} \geq \theta\right) \\
&= \mathbb{P}\left(H_{T_V} \geq \frac{\theta(I+\sigma^2)}{\eta l(R_V,\gamma,\alpha_{T_V})}\right) \\
&\overset{(a)}{=} \mathbb{E}\left[\mathbb{E}_I\left[\frac{\Gamma(m_{T_V}, s_{R_V}(I+\sigma^2))}{\Gamma(m_{T_V})}\right]\right] \\
&\overset{(b)}{=} \mathbb{E}\left[\mathbb{E}_I\left[\exp(-s_{R_V}(I+\sigma^2)) \sum_{k=0}^{m_{T_V}-1} \frac{(s_{R_V}(I+\sigma^2))^k}{k!}\right]\right] \\
&\overset{(c)}{=} \mathbb{E}\left[\sum_{k=0}^{m_{T_V}-1} (-1)^k \frac{s_{R_V}^k}{k!} \mathbb{E}_I\left[\frac{\mathrm{d}^k \exp(-s_{R_V}(I+\sigma^2))}{\mathrm{d}s_{R_V}^k}\right]\right] \\
&\overset{(d)}{=} \mathbb{E}\left[\sum_{k=0}^{m_{T_V}-1} (-1)^k \frac{s_{R_V}^k}{k!} \frac{\mathrm{d}^k \mathcal{L}_{(I+\sigma^2)}(s_{R_V})}{\mathrm{d}s_{R_V}^k}\right],
\end{aligned} \tag{7.20}$$

where (a) comes from the random fading H_{T_V} being gamma distributed with channel-dependent fading parameter m_{T_V} with $\Gamma(.)$ and $\Gamma(.,.)$ being the gamma and upper incomplete gamma functions, respectively, where $s_{R_V} = m_{T_V}\theta/(\eta l(R_V,\gamma,\alpha_{T_V}))$, (b) comes from expressing the incomplete gamma function as in [103][8.352.2], (c) arises from the substitution $\exp(-s_{R_V}(I+\sigma^2))((I+\sigma^2))^k = (-1)^k \mathrm{d}^k \exp(-s_{R_V}(I+\sigma^2))/\mathrm{d}s_{R_V}^k$, (d) comes from the Leibniz integral rule.

Let

$$g(T_V, R_V) = \sum_{k=0}^{m_{T_V}-1} (-1)^k \frac{s_{R_V}^k}{k!} \frac{\mathrm{d}^k \mathcal{L}_{(I+\sigma^2)}(s_{R_V})}{\mathrm{d}s_{R_V}^k}. \tag{7.21}$$

We can express Eq. (7.20) in the final form given in Eq. (3.21) using the following procedure

$$
\begin{aligned}
&= \mathbb{E}\left[g(T_V, R_V)\right] \\
&= \mathbb{E}\Big[\mathbb{E}_V\left[g(T_V, R_V)\right]\Big] \\
&\overset{(a)}{=} \mathbb{E}[\mathbb{P}(V=0|T_0, T_i, R_0, R_i)g(T_0, R_0) \\
&+ \mathbb{P}(V=i|T_0, T_i, R_0, R_i)g(T_i, R_i)] \\
&= \mathbb{E}_{T_0,R_0}\Big[\mathbb{E}_{T_i,R_i}\left[\mathbb{P}(V=0|T_0, T_i, R_0, R_i)\right] g(T_0, R_0)\Big] \\
&+ \mathbb{E}_{T_i,R_i}\Big[\mathbb{E}_{T_0,R_0}\left[\mathbb{P}(V=i|T_0, T_i, R_0, R_i)\right] g(T_i, R_i)\Big] \\
&= \mathbb{E}_{T_0,R_0}\Big[\mathbb{P}(V=0|T_0, R_0)g(T_0, R_0)\Big] \\
&+ \mathbb{E}_{T_i,R_i}\Big[\mathbb{P}(V=i|T_i, R_i)g(T_i, R_i)\Big] \\
&\overset{(b)}{=} \int_0^{u(\omega,\gamma)} (\mathcal{A}_0(\mathtt{l}, r)g(\mathtt{l}, r)\mathbb{P}_{\mathtt{l}}(r) + \mathcal{A}_0(\mathtt{n}, r)g(\mathtt{n}, r)\mathbb{P}_{\mathtt{n}}(r))f_{R_0}(r)\mathrm{d}r \\
&+ \int_0^{u(\omega,\gamma)} (\mathcal{A}_i(\mathtt{l}, r)g(\mathtt{l}, r)f_{R_{\mathtt{l}}}(r) + \mathcal{A}_i(\mathtt{n}, r)g(\mathtt{n}, r)f_{R_{\mathtt{n}}}(r))\mathrm{d}r,
\end{aligned} \tag{7.22}
$$

where in (a) T_0 and R_0 denote the channel type and distance of the hotspot center UAV while T_i and R_i refer to the channel type and corresponding distance of another candidate serving UAV, (b) comes from $\mathbb{P}(V=v|T_v=t, R_v=r) = \mathcal{A}_j(t, r)$ defined in Subsection 3.3.2 and the expectation over R and T are found by applying the pdfs defined in Subsection 3.3.1. By rearranging the order of summation and integration we arrive at the final form given in Eq. (3.21). Note that, following the antenna gain definition in Eq. (3.2), a UAV will have a gain of 0 at the reference UE if it is further away than $u(\omega, \gamma)$; as such we consider $u(\omega, \gamma)$ to be the upper limit on the serving UAV distance in the integral above.

Bibliography

[1] "The Mobile Economy 2018," GSM Association, Tech. Rep., Feb. 2018, accessed on April 7th, 2019. [Online]. Available: https://www.gsmaintelligence.com/research/2018/02/the-mobile-economy-2018/660/

[2] "Ericsson Mobility Report," Tech. Rep., June 2018.

[3] J. Andrews, S. Buzzi, W. Choi, S. Hanly, A. Lozano, A. Soong, and J. Zhang, "What Will 5G Be?" *IEEE Journal on Selected Areas in Communications*, vol. 32, no. 6, pp. 1065–1082, June 2014.

[4] D. Lopez-Perez, Y. Yang, and F. Gunnarsson, *Heterogeneous Cellular Networks Theory, Simulation and Deployment*, X. Chu, Ed. Cambridge University Press, 2013.

[5] S. Andreev, V. Petrov, M. Dohler, and H. Yanikomeroglu, "Future of Ultra-Dense Networks Beyond 5G: Harnessing Heterogeneous Moving Cells," *ArXiv e-prints*, June 2017.

[6] ""Clarity From Above" PwC Global Report on the Commercial Applications of Drone Technology," May 2016, accessed on April 7th, 2019. [Online]. Available: https://preview.thenewsmarket.com/Previews/PWC/DocumentAssets/433056.pdf

[7] M. K. Sahi and C. Wheelock, "Consumer Drones Small Unmanned Aerial Vehicles for Aerial Imaging, Recreation, and Aerial Games: Global Market Analysis and Forecasts," Tractica, Tech. Rep., 2016, accessed on April 7th, 2019. [Online]. Available: https://www.tractica.com/download-proxy?report_id=5586&type=Executive+Summary

[8] D. Joshi, "Commercial Unmanned Aerial Vehicle (UAV) Market Analysis - Industry Trends, Companies and What You Should Know," Aug 2017, accessed on April 7th, 2019. [Online]. Available: http://uk.businessinsider.com/commercial-uav-market-analysis-2017-8

[9] A. Fitzpatrick, "The Drone Age," *Time Magazine*, June 2018, accessed on April 7th, 2019. [Online]. Available: http://time.com/longform/time-the-drone-age/

[10] O. Krauth, "AT&T Flying COW Drones Will Help Bring Cell Service Back to Puerto Rico," *Tech Republic*, Nov. 2017, accessed on April 7th,

2019. [Online]. Available: https://www.techrepublic.com/article/at-t-flying-cow-drones-will-help-bring-cell-service-back-to-puerto-rico/

[11] "Flying COW Connects Puerto Rico," Nov. 2017, accessed on April 7th, 2019. [Online]. Available: http://about.att.com/inside_connections_blog/flying_cow_puertori

[12] Google, "Expanding Internet Connectivity with Stratospheric Balloons," accessed on April 7th, 2019. [Online]. Available: https://x.company/projects/loon/

[13] N. Mattise, "Project Loon team gave Puerto Rico connectivity and assembled a helicopter," *Ars Technica*, Feb. 2018, accessed on April 7th, 2019. [Online]. Available: https://arstechnica.com/science/2018/02/project-loon-engineer-sees-a-tool-for-future-disaster-response-in-puerto-rico/

[14] "EE Pioneers 'Air Mast' Technology For Rural Mobile Coverage and Disaster Recovery," Feb. 2017, accessed on April 7th, 2019. [Online]. Available: http://newsroom.ee.co.uk/ee-pioneers-air-mast-technology-for-rural-mobile-coverage-and-disaster-recovery/

[15] M.-A. Russon, "Drones to the Rescue!" *BBC News*, May 2018, accessed on April 7th, 2019. [Online]. Available: https://www.bbc.com/news/business-43906846

[16] F. Mohammadnia, M. Fiore, and M. A. Marsan, "Adaptive Densification of Mobile Networks : Exploring Correlations in Vehicular and Telecom Traffic," *Annual Mediterranean Ad Hoc Networking Workshop (Med-Hoc-Net)*, pp. 1–8, June 2018.

[17] L. Reynaud and T. Rasheed, "Deployable Aerial Communication Networks: Challenges for Futuristic Applications," *ACM Symposium on Performance Evaluation of Wireless Ad Hoc, Sensor, and Ubiquitous Networks (PE-WASUN)*, pp. 9–16, Oct. 2012, accessed on April 7th, 2019. [Online]. Available: http://dl.acm.org/citation.cfm?id=2387030

[18] Z. Becvar, M. Vondra, P. Mach, J. Plachy, and D. Gesbert, "Performance of Mobile Networks with UAVs: Can Flying Base Stations Substitute Ultra-Dense Small Cells?" *European Wireless*, pp. 261–267, May 2017.

[19] "Telefonica Presents the First Mobile LTE Network Running in Just 40 Grams of Hardware," March 2017, accessed on April 7th, 2019. [Online]. Available: https://www.telefonica.com/en/web/press-office/-/telefonica-presents-the-first-mobile-lte-network-running-in-just-40-grams-of-hardware

[20] "DJI Matrice 200 Technical Specs," accessed on April 7th, 2019. [Online]. Available: https://www.dji.com/matrice-200-series/info#specs

[21] "Airobotics Automated Industrial Drones," accessed on April 7th, 2019. [Online]. Available: https://www.airoboticsdrones.com/

[22] A. O'Connell, "CONNECT At Globecom," Dec. 2017, accessed on April 7th, 2019. [Online]. Available: https://connectcentre.ie/news/connect-at-globecom/

[23] ""Drones as Wireless Communications Infrastructure" Youtube Video," June 2018, accessed on April 7th, 2019. [Online]. Available: https://www.youtube.com/watch?v=wUmwGAp-yaM

[24] T. Heimfarth and J. De Araujo, "Using Unmanned Aerial Vehicle to Connect Disjoint Segments of Wireless Sensor Network," *IEEE International Conference on Advanced Information Networking and Applications (AINA)*, pp. 907–914, May 2014.

[25] A. Merwaday and I. Guvenc, "UAV Assisted Heterogeneous Networks for Public Safety Communications," *IEEE Wireless Communications and Networking Conference Workshops (WCNC Workshops)*, pp. 329–334, March 2015.

[26] Y. Zeng, R. Zhang, and T. J. Lim, "Wireless Communications With Unmanned Aerial Vehicles: Opportunities and Challenges," *IEEE Communications Magazine*, vol. 54, no. 5, pp. 36–42, May 2016.

[27] I. Bor-Yaliniz and H. Yanikomeroglu, "The New Frontier in RAN Heterogeneity: Multi-Tier Drone-Cells," *IEEE Communications Magazine*, vol. 54, no. 11, pp. 48–55, Nov. 2016.

[28] M. Qutqut, H. Abou-zeid, H. Hassanein, A. Rashwan, and F. Al-Turjman, "Dynamic Small Cell Placement Strategies For LTE Heterogeneous Networks," *IEEE Symposium on Computers and Communication (ISCC)*, pp. 1–6, June 2014.

[29] M. Mozaffari, W. Saad, M. Bennis, and M. Debbah, "Drone Small Cells in the Clouds: Design, Deployment and Performance Analysis," *IEEE Global Communications Conference (GLOBECOM)*, pp. 1–6, Dec 2015.

[30] ——, "Mobile Internet of Things: Can UAVs Provide an Energy-Efficient Mobile Architecture?" *IEEE Global Communications Conference (GLOBECOM)*, pp. 1–6, Dec 2016.

[31] ——, "Efficient Deployment of Multiple Unmanned Aerial Vehicles for Optimal Wireless Coverage," *IEEE Communications Letters*, vol. 20, no. 8, pp. 1647–1650, Aug 2016.

[32] ——, "Unmanned Aerial Vehicle With Underlaid Device-to-Device Communications: Performance and Tradeoffs," *IEEE Transactions on Wireless Communications*, vol. 15, no. 6, pp. 3949–3963, June 2016.

[33] R. Irem Bor-Yaliniz, A. El-Keyi, and H. Yanikomeroglu, "Efficient 3-D Placement of an Aerial Base Station in Next Generation Cellular Networks," *IEEE International Conference on Communications (ICC)*, pp. 1–6, May 2016.

[34] S. Rohde and C. Wietfeld, "Interference Aware Positioning of Aerial Relays for Cell Overload and Outage Compensation," *IEEE Vehicular Technology Conference (VTC Fall)*, pp. 1–5, Sept. 2012.

[35] Y. Zeng, R. Zhang, and T. J. Lim, "Throughput Maximization for UAV-Enabled Mobile Relaying Systems," *IEEE Transactions on Communications*, vol. 64, no. 12, pp. 4983–4996, Dec. 2016.

[36] Y. Zeng and R. Zhang, "Energy-Efficient UAV Communication with Trajectory Optimization," *IEEE Transactions on Wireless Communications*, vol. 16, no. 6, pp. 3747 – 3760, March 2017.

[37] J. Zhang, Y. Zeng, and R. Zhang, "Spectrum and Energy Efficiency Maximization in UAV-Enabled Mobile Relaying," *IEEE International Conference on Communications (ICC)*, pp. 1–6, May 2017.

[38] J. Chen and D. Gesbert, "Optimal Positioning of Flying Relays for Wireless Networks: A LOS Map Approach," *IEEE International Conference on Communications (ICC)*, pp. 1–6, May 2017.

[39] E. Kalantari, M. Z. Shakir, H. Yanikomeroglu, and A. Yongacoglu, "Backhaul-Aware Robust 3D Drone Placement in 5G+ Wireless Networks," *IEEE International Conference on Communications Workshops (ICC Workshops)*, pp. 109–114, May 2017.

[40] E. Kalantari, I. Bor-Yaliniz, A. Yongacoglu, and H. Yanikomeroglu, "User Association and Bandwidth Allocation for Terrestrial and Aerial Base Stations with Backhaul Considerations," *IEEE International Symposium on Personal, Indoor, and Mobile Radio Communications (PIMRC)*, Oct 2017.

[41] A. Fotouhi, M. Ding, and M. Hassan, "Dynamic Base Station Repositioning to Improve Performance of Drone Small Cells," *IEEE Global Communications Conference Workshops (GLOBECOM Workshops)*, pp. 1–6, Dec 2016.

[42] ——, "Service on Demand: Drone Base Stations Cruising in the Cellular Network," *IEEE Global Communications Conference (GLOBECOM)*, pp. 1–6, Dec. 2017.

[43] J. Lu, S. Wan, X. Chen, Z. Chen, P. Fan, and K. B. Letaief, "Beyond Empirical Models: Pattern Formation Driven Placement of UAV Base Stations," *IEEE Transactions on Wireless Communications*, vol. 17, no. 6, pp. 1–15, June 2018.

[44] A. Al-Hourani, S. Kandeepan, and S. Lardner, "Optimal LAP Altitude for Maximum Coverage," *IEEE Wireless Communications Letters*, vol. 3, no. 6, pp. 569–572, Dec 2014.

[45] A. M. Hayajneh, S. A. R. Zaidi, D. C. McLernon, and M. Ghogho, "Optimal Dimensioning and Performance Analysis of Drone-Based Wireless Communications," *IEEE Global Communications Conference Workshops (GLOBECOM Workshops)*, pp. 1–6, Dec 2016.

[46] M. M. Azari, F. Rosas, K. C. Chen, and S. Pollin, "Optimal UAV Positioning for Terrestrial-Aerial Communication in Presence of Fading," *IEEE Global Communications Conference (GLOBECOM)*, pp. 1–6, Dec. 2016.

[47] ——, "Joint Sum-Rate and Power Gain Analysis of an Aerial Base Station," *IEEE Global Communications Conference Workshops (GLOBECOM Workshops)*, pp. 1–6, Dec. 2016.

[48] S. Kumar, S. Suman, and S. De, "Backhaul and Delay-aware Placement of UAV-enabled Base Station," *IEEE Conference on Computer Communications Workshops (INFOCOM Workshops)*, pp. 634–639, April 2018.

[49] M. Gruber, "Role of Altitude When Exploring Optimal Placement of UAV Access Points," *IEEE Wireless Communications and Networking Conference (WCNC)*, pp. 1–5, Sept. 2016.

[50] M. Haenggi, J. Andrews, F. Baccelli, O. Dousse, and M. Franceschetti, "Stochastic Geometry and Random Graphs for the Analysis and Design of Wireless Networks," *IEEE Journal on Selected Areas in Communications*, vol. 27, no. 7, pp. 1029–1046, Sept. 2009.

[51] J. G. Andrews, F. Baccelli, and R. K. Ganti, "A Tractable Approach To Coverage and Rate in Cellular Networks," *IEEE Transactions on Communications*, vol. 59, no. 11, pp. 3122–3134, Nov. 2011.

[52] M. D. Renzo, A. Guidotti, and G. E. Corazza, "Average Rate of Downlink Heterogeneous Cellular Networks over Generalized Fading Channels: A Stochastic Geometry Approach," *IEEE Transactions on Communications*, vol. 61, no. 7, pp. 3050–3071, July 2013.

[53] M. Afshang and H. S. Dhillon, "Fundamentals of Modeling Finite Wireless Networks Using Binomial Point Process," *IEEE Transactions on Wireless Communications*, vol. 16, no. 5, pp. 3355 – 3370, May 2017.

[54] G. P. Efthymoglou, C. Mukasa, and V. A. Aalo, "User Association to Small Cells in the Presence of Nakagami-m Fading and Co-Channel Interference," *International Conference on Telecommunications (ICT)*, pp. 1–5, May 2016.

[55] Y. J. Chun, S. L. Cotton, H. S. Dhillon, F. J. Lopez-Martinez, J. F. Paris, and S. K. Yoo, "A Comprehensive Analysis of 5G Heterogeneous Cellular Systems Operating Over Kappa-Mu Shadowed Fading Channels," *IEEE Transactions on Wireless Communications*, vol. 16, no. 11, pp. 6995 – 7010, Nov. 2017.

[56] C. Saha, M. Afshang, and H. S. Dhillon, "Enriched K-Tier HetNet Model to Enable the Analysis of User-Centric Small Cell Deployments," *IEEE Transactions on Wireless Communications*, vol. 16, no. 3, pp. 1593 – 1608, March 2017.

[57] C. Saha, M. Afshang, and H. Dhillon, "3GPP-Inspired HetNet Model using Poisson Cluster Process: Sum-product Functionals and Downlink Coverage," *IEEE Transactions on Communications*, vol. 66, no. 5, pp. 2219 – 2234, May 2018.

[58] M. D. Renzo, "Stochastic Geometry Modeling and Analysis of Multi-Tier Millimeter Wave Cellular Networks," *IEEE Transactions on Wireless Communications*, vol. 14, no. 9, pp. 5038–5057, Sept. 2015.

[59] H. Elshaer, M. N. Kulkarni, F. Boccardi, J. G. Andrews, and M. Dohler, "Downlink and Uplink Cell Association With Traditional Macrocells and Millimeter Wave Small Cells," *IEEE Transactions on Wireless Communications*, vol. 15, no. 9, pp. 6244–6258, Sept. 2016.

[60] J. G. Andrews, T. Bai, M. N. Kulkarni, A. Alkhateeb, A. K. Gupta, and R. W. Heath, "Modeling and Analyzing Millimeter Wave Cellular Systems," *IEEE Transactions on Communications*, vol. 65, no. 1, pp. 403–430, Jan 2017.

[61] V. V. C. Ravi and H. S. Dhillon, "Downlink Coverage Probability in a Finite Network of Unmanned Aerial Vehicle (UAV) Base Stations," *IEEE International Workshop on Signal Processing Advances in Wireless Communications (SPAWC)*, pp. 1–5, July 2016.

[62] V. Vardhan Chetlur and H. S. Dhillon, "Downlink Coverage Analysis for a Finite 3D Wireless Network of Unmanned Aerial Vehicles," *IEEE Transactions on Communications*, vol. 65, no. 10, pp. 4543–4558, Oct. 2017.

[63] C. Zhang and W. Zhang, "Spectrum Sharing for Drone Networks," *IEEE Journal on Selected Areas in Communications*, vol. 35, no. 1, pp. 136–144, Jan 2017.

[64] A. M. Hayajneh, S. A. R. Zaidi, D. C. McLernon, and M. Ghogho, "Drone Empowered Small Cellular Disaster Recovery Networks for Resilient Smart Cities," *IEEE International Conference on Sensing, Communication and Networking (SECON Workshops)*, pp. 1–6, June 2016.

[65] M. M. Azari, F. Rosas, A. Chiumento, and S. Pollin, "Coexistence of Terrestrial and Aerial Users in Cellular Networks," *IEEE Global Communications Conference Workshops (GLOBECOM Workshops)*, pp. 1–6, Dec. 2017.

[66] M. M. Azari, F. Rosas, and S. Pollin, "Reshaping Cellular Networks for the Sky: The Major Factors and Feasibility," *IEEE International Conference on Communications Workshops (ICC Workshops)*, pp. 1–6, May 2018.

[67] L. Zhou, Z. Yang, S. Zhou, and W. Zhang, "Coverage Probability Analysis of UAV Cellular Networks in Urban Environments," *IEEE International Conference on Communications Workshops (ICC Workshops)*, pp. 1–6, May 2018.

[68] P. K. Sharma and D. I. Kim, "Coverage Probability of 3D UAV Networks with RWP Mobility-Based Altitude Control," *IEEE International Conference on Communications Workshops (ICC Workshops)*, pp. 1–6, May 2018.

[69] X. Zhou, J. Guo, S. Durrani, and H. Yanikomeroglu, "Uplink Coverage Performance of an Underlay Drone Cell for Temporary Events," *IEEE International Conference on Communications Workshops (ICC Workshops)*, pp. 1–6, May 2018.

[70] C. Liu, M. Ding, C. Ma, Q. Li, Z. Lin, and Y.-C. Liang, "Performance Analysis for Practical Unmanned Aerial Vehicle Networks with LoS/NLoS Transmissions," *IEEE International Conference on Communications Workshops (ICC Workshops)*, pp. 1–6, May 2018.

[71] X. Wang, H. Zhang, and V. C. M. Leung, "Modeling and Performance Analysis of UAV-Assisted Cellular Networks in Isolated Regions," *IEEE International Conference on Communications Workshops (ICC Workshops)*, pp. 1–6, May 2018.

[72] U. Siddique, H. Tabassum, E. Hossain, and D. I. Kim, "Wireless Backhauling of 5G Small Cells: Challenges and Solution Approaches," *IEEE Wireless Communications*, vol. 22, no. 5, pp. 22–31, Oct. 2015.

[73] A. Mesodiakaki, A. Kassler, E. Zola, M. Ferndahl, and T. Cai, "Energy Efficient Line-of-Sight Millimeter Wave Small Cell Backhaul: 60, 70, 80 or 140 GHz?" *IEEE International Symposium on A World of Wireless, Mobile and Multimedia Networks (WoWMoM)*, pp. 1–9, June 2016.

[74] O. Semiari, W. Saad, M. Bennis, and Z. Dawy, "Inter-Operator Resource Management for Millimeter Wave Multi-Hop Backhaul Networks," *IEEE Transactions on Wireless Communications*, vol. 16, no. 8, pp. 5258–5272, Aug 2017.

[75] G. Noh, B. Hui, J. Kim, H. S. Chung, I. Kim, and A. N. Model, "DMRS Design and Evaluation for 3GPP 5G New Radio in a High Speed Train Scenario," *IEEE Global Communications Conference (GLOBECOM)*, pp. 1–6, Dec. 2017.

[76] E. Dinc, M. Vondra, and C. Cavdar, "Multi-User Beamforming and Ground Station Deployment for 5G Direct Air-to-Ground Communication," *IEEE Global Communications Conference (GLOBECOM)*, pp. 1–6, Dec. 2017.

[77] Z. Xiao, P. Xia, and X. Xia, "Enabling UAV Cellular With Millimeter-Wave Communication: Potentials and Approaches," *IEEE Communications Magazine*, vol. 54, no. 5, pp. 66–73, May 2016.

[78] M. Alzenad, M. Z. Shakir, H. Yanikomeroglu, and M. S. Alouini, "FSO-Based Vertical Backhaul/Fronthaul Framework for 5G+ Wireless Networks," *IEEE Communications Magazine*, vol. 56, no. 1, pp. 218–224, Jan. 2018.

[79] M. Najafi, H. Ajam, V. Jamali, P. D. Diamantoulakis, G. K. Karagiannidis, and R. Schober, "Statistical Modeling of FSO Fronthaul Channel for Drone-based Networks," *IEEE International Conference on Communications (ICC)*, pp. 1–6, May 2018.

[80] U. Challita and W. Saad, "Network Formation in the Sky: Unmanned Aerial Vehicles for Multi-hop Wireless Backhauling," *IEEE Global Communications Conference (GLOBECOM)*, Dec. 2017.

[81] X. Lin, V. Yajnanarayana, S. D. Muruganathan, S. Gao, H. Asplund, H.-L. Maattanen, M. B. A, S. Euler, and Y.-P. E. Wang, "The Sky Is Not the Limit: LTE for Unmanned Aerial Vehicles," *IEEE Communications Magazine*, vol. 56, no. 4, pp. 204 – 210, April 2018.

[82] "TR 36.777: Technical Specification Group Radio Access Network; Study on Enhanced LTE Support for Aerial Vehicles (Release 15)," 3GPP, Tech. Rep., Jan. 2018.

[83] G. Geraci, A. Garcia-Rodriguez, L. G. Giordano, D. Lopez-Perez, and E. Bjoernson, "Supporting UAV Cellular Communications through Massive MIMO," *IEEE International Conference on Communications Workshops (ICC Workshops)*, pp. 1–6, May 2018.

[84] M. Lu, M. Bagheri, A. P. James, and T. Phung, "Wireless Charging Techniques for UAVs: A Review, Reconceptualization, and Extension," *IEEE Access*, vol. 6, pp. 29 865 – 29 884, May 2018.

[85] N. H. Motlagh, M. Bagaa, and T. Taleb, "UAV Selection for a UAV-Based Integrative IoT Platform," *IEEE Global Communications Conference (GLOBECOM)*, pp. 1–6, Dec. 2016.

[86] F. Khelifi, A. Bradai, K. Singh, and M. Atri, "Localization and Energy-Efficient Data Routing for Unmanned Aerial Vehicles: Fuzzy-Logic-Based Approach," *IEEE Communications Magazine*, vol. 56, no. 4, pp. 129–133, April 2018.

[87] S. Ahmed, A. Mohamed, K. Harras, M. Kholief, and S. Mesbah, "Energy Efficient Path Planning Techniques for UAV-Based Systems With Space Discretization," *IEEE Wireless Communications and Networking Conference (WCNC)*, pp. 1–6, April 2016.

[88] R. Gangula, D. Gesbert, D. F. Külzer, and J. M. Franceschi, "A Landing Spot Approach for Enhancing the Performance of UAV-Aided Wireless Networks," *IEEE International Conference on Communications Workshops (ICC Workshops)*, pp. 1–6, May 2018.

[89] H. Ghazzai, H. Menouar, and A. Kadri, "On the Placement of UAV Docking Stations for Future Intelligent Transportation Systems," *IEEE Vehicular Technology Conference (VTC Spring)*, pp. 0–5, June 2017.

[90] A. Trotta, M. Di Felice, K. R. Chowdhury, and L. Bononi, "Fly and Recharge: Achieving Persistent Coverage Using Small Unmanned Aerial Vehicles (SUAVs)," *IEEE International Conference on Communications (ICC)*, pp. 1–6, May 2017.

[91] M. Haenggi, *Stochastic Geometry for Wireless Networks*. Cambridge University Press, 2013.

[92] M. Leonard, "FAA to Sort Out Drone Spectrum-Use Strategy," *GCN*, Oct. 2018, accessed on April 7th, 2019. [Online]. Available: https://gcn.com/articles/2018/10/08/faa-drone-spectrum.aspx

[93] "5G Spectrum, GSMA Public Policy Position," GSMA, Tech. Rep., Nov. 2018.

[94] "Recommendation P.1410-5 "Propagation Data and Prediction Methods Required for the Design of Terrestrial Broadband Radio Access Systems Operating in a Frequency Range From 3 to 60 GHz"," ITU-R, Tech. Rep., 2012.

[95] C. A. Balanis, *Antenna Theory: Analysis and Design*. Wiley-Interscience, 2005.

[96] A. F. Molisch, *Wireless Communications*. Wiley IEEE Press, 2011.

[97] W. Khawaja, I. Guvenc, D. Matolak, U.-C. Fiebig, and N. Schneckenberger, "A Survey of Air-to-Ground Propagation Channel Modeling for Unmanned Aerial Vehicles," *ArXiv e-prints*, Jan. 2018.

[98] A. A. Khuwaja, Y. Chen, N. Zhao, M. S. Alouini, and P. Dobbins, "A Survey of Channel Modeling for UAV Communications," *IEEE Communications Surveys and Tutorials*, vol. 20, no. 4, pp. 2804 – 2821, July 2018.

[99] T. M. Clover and J. A. Thomas, *Elements of Information Theory.* John Wiley & Sons, 2006.

[100] J. A. Hartigan and M. A. Wong, "A K-Means Clustering Algorithm," *Applied Statistics*, vol. 28, pp. 100–108, March 1979.

[101] W. Newhall, R. Mostafa, C. Dietrich, C. Anderson, K. Dietze, G. Joshi, and J. H. Reed, "Wideband Air-to-ground Radio Channel Measurements Using an Antenna Array at 2 GHz for Low-Altitude Operations," *IEEE Military Communications Conference (MILCOM)*, Oct. 2003.

[102] "TR 36.814: Further Advancements for E-UTRA Physical Layer Aspects (Release 9)," 3GPP, Tech. Rep., 2010.

[103] I. Gradshteyn and I. Ryzhik, *Table of Integrals, Series, and Products.* Academic Press, 2007.

[104] A. Ghosh, T. A. Thomas, M. C. Cudak, R. Ratasuk, P. Moorut, F. W. Vook, T. S. Rappaport, G. R. MacCartney, S. Sun, and S. Nie, "Millimeter-Wave Enhanced Local Area Systems: A High-Data-Rate Approach for Future Wireless Networks," *IEEE Journal on Selected Areas in Communications*, vol. 32, no. 6, pp. 1152–1163, June 2014.

[105] S. Suman, S. Kumar, and S. De, "UAV-Assisted RF Energy Transfer," *IEEE International Conference on Communications (ICC)*, May 2018.

[106] D. Lee, J. Zhou, and W. T. Lin, "Autonomous Battery Swapping System for Quadcopter," *2015 International Conference on Unmanned Aircraft Systems, ICUAS 2015*, pp. 118–124, 2015.

[107] N. Kingry, L. Towers, Y.-c. Liu, Y. Zu, Y. Wang, B. Staheli, Y. Katagiri, S. Cook, and R. Dai, "Design, Modeling and Control of a Solar-Powered Quadcopter," *IEEE International Conference on Robotics and Automation (ICRA)*, pp. 1–8, May 2018.

[108] B. Read, "Fly By Light," *Royal Aeronautical Society*, Feb. 2017, accessed on April 7th, 2019. [Online]. Available: https://www.aerosociety.com/news/fly-by-light/

[109] J. Ouyang, Y. Che, J. Xu, and K. Wu, "Throughput Maximization for Laser-Powered UAV Wireless Communication Systems," *ArXiv e-prints*, March 2018.

[110] C.-X. Zu and H. Li, "Thermodynamic Analysis on Energy Densities of Batteries," *Energy & Environmental Science*, vol. 4, no. 8, p. 2614, 2011, accessed on April 7th, 2019. [Online]. Available: http://xlink.rsc.org/?DOI=c0ee00777c

[111] T. Nozawa, "New Battery Technologies Still Years Away," Nikkei Asian Review, April 2018, accessed on April 7th, 2019. [Online]. Available: https://asia.nikkei.com/Tech-Science/Tech/New-battery-technologies-still-years-away?page=2

[112] C. Vaalma, D. Buchholz, M. Weil, and S. Passerini, "A Cost and Resource Analysis of Sodium-ion Batteries," *Nature Reviews Materials*, vol. 3, 2018.

[113] J. Plaza, "Will Hydrogen Fuel Cells Help Drones Stay in the Air?" June 2017, accessed on April 7th, 2019. [Online]. Available: https://www.expouav.com/news/latest/hydrogen-fuel-cells-drones/

[114] R. F. Service, "Lithium-sulfur Batteries Poised for Leap," *Science*, vol. 359, no. 6380, pp. 1080–1081, March 2018, accessed on April 7th, 2019. [Online]. Available: http://science.sciencemag.org/content/359/6380/1080

[115] M. A. Rahman, X. Wang, and C. Wen, "A Review of High Energy Density Lithium-air Battery Technology," *Journal of Applied Electrochemistry*, vol. 44, no. 1, pp. 5–22, Jan 2014, accessed on April 7th, 2019. [Online]. Available: https://link.springer.com/article/10.1007/s10800-013-0620-8

[116] "Global Drone Regulations Database," accessed on April 7th, 2019. [Online]. Available: https://www.droneregulations.info/

[117] O. Rudgard, "Drone Near-Misses Triple in Two Years," The Telegraph, March 2018, accessed on April 7th, 2019. [Online]. Available: https://www.telegraph.co.uk/news/2018/03/19/drone-near-misses-triple-two-years/

[118] Federal Aviation Administration; Office of the Secretary of Transportation; Department of Transportation, "Operation and Certification of Small Unmanned Aircraft Systems," *14 CFR Parts 21, 43, 61, 91, 101, 107, 119, 133, and 183*, pp. 1–624, 2016, accessed on April 7th, 2019. [Online]. Available: https://www.faa.gov/uas/media/RIN_2120-AJ60_Clean_Signed.pdf

[119] Irish Aviation Authority (IAA), "Irish Aviation Authority Small Unmanned Aircraft (Drones) and Rockets Order, 2015," no. 563, 2015, accessed on April 7th, 2019. [Online]. Available: https://www.iaa.ie/general-aviation/drones/drone-regulations-guidance

[120] "Amazon Prime Air," accessed on April 7th, 2019. [Online]. Available: https://www.amazon.com/Amazon-Prime-Air/b?ie=UTF8&node=8037720011

[121] "Classes of Airspace," Federal Aviation Administration, accessed on April 7th, 2019. [Online]. Available: https://www.faasafety.gov/gslac/ALC/course_content.aspx?cID=42&sID=505

[122] European Aviation Safety Agency (EASA), "NPA 2017-05 (A): Introduction of a Regulatory Framework for the Operation of Drones," 2017, accessed on April 7th, 2019. [Online]. Available: https://www.easa.europa.eu/document-library/notices-of-proposed-amendment/npa-2017-05

[123] "A Buyer's Guide to Fixed-Wing Drones for Professional Use," SmartPlanes White Paper, accessed on April 7th, 2019. [Online]. Available: https://www.army-technology.com/downloads/whitepapers/surveillance/buyers-guide-fixed-wing-drones-professional-use/

[124] M. Giles, "Zipline Launches the World's Fastest Commercial Delivery Drone," MIT Technology Review, April 2018, accessed on April 7th, 2019. [Online]. Available: https://www.technologyreview.com/s/610735/zipline-launches-the-worlds-fastest-commercial-delivery-drone/

[125] K. Vasudeva, M. Simsek, D. Lopez-Perez, and I. Guvenc, "Analysis of Handover Failures in Heterogeneous Networks with Fading," *IEEE Transactions on Vehicular Technology*, vol. 66, no. 7, pp. 6060–6074, July 2017.

[126] X. Xu, Z. Sun, X. Dai, T. Svensson, and X. Tao, "Modeling and Analyzing the Cross-Tier Handover in Heterogeneous Networks," *IEEE Transactions on Wireless Communications*, vol. 16, no. 12, pp. 7859–7869, Dec. 2017.

[127] A. Mahbas, H. Zhu, and J. Wang, "Mobility Management in Small Cell Networks," *IEEE Global Communications Conference (GLOBECOM)*, pp. 1–6, Dec. 2017.

[128] A. Antonopoulos, E. Kartsakli, A. Bousia, L. Alonso, and C. Verikoukis, "Energy-Efficient Infrastructure Sharing in Multi-Operator Mobile Networks," *IEEE Communications Magazine*, vol. 53, no. 5, pp. 242–249, May 2015.

[129] J. Kibiłda, N. J. Kaminski, and L. A. DaSilva, "Radio Access Network and Spectrum Sharing in Mobile Networks: A Stochastic Geometry Perspective," *IEEE Transactions on Wireless Communications*, vol. 16, no. 4, pp. 2562–2575, April 2017.

[130] L. Doyle, J. Kibiłda, T. Forde, and L. A. DaSilva, "Spectrum without Bounds, Networks without Borders," *Proceedings of the IEEE*, vol. 102, no. 3, pp. 351–365, March 2014.